Joana Abreu Luís da Silva Santos

FE/S CLUSTER BIOGENESIS REGULATION BY THE JANUS-FACED REGULATOR, ISCR: AN UNFORESEEN MECHANISM OF DNA RECOGNITION AND DISCRIMINATION

Tese de Candidatura ao grau de Doutor em Ciências Biomédicas submetida ao Instituto de Ciências Biomédicas Abel Salazar da Universidade do Porto:

Orientador – Doutor Pedro Pereira
Categoria – Investigador Principal
Afiliação – IBMC - Instituto de Biologia Molecular e Celular
Co-orientadora – Doutora Sandra Macedo-Ribeiro
Categoria – Investigadora Principal
Afiliação – IBMC - Instituto de Biologia Molecular e Celular
Co-Orientadora – Professora Doutora Ana Margarida Damas
Categoria – Professora Catedrática
Afiliação – ICBAS - Instituto de Ciências Biomédicas Abel Salazar da Universidade do Porto

IV

V

Preceitos Legais

De acordo com o disposto no nº 2 do artigo 8º do Decreto-lei nº 388/70, nesta dissertação foram utilizados os resultados de trabalhos publicados abaixo indicados.

No cumprimento do disposto referido Decreto-Lei, a autora desta dissertação declara que interveio na conceção e execução do trabalho experimental, na interpretação e redação dos resultados publicados sob o nome Santos, J. A.:

Santos, J.A., Alonso-García, N., Macedo-Ribeiro, S., Pereira, P.J.B. (2014). "The unique regulation of iron-sulfur cluster biogenesis in a Gram-positive bacterium." *Proc Natl Acad Sci U S A*. 111(22): E2251-E2260.

"When one door of happiness closes, another opens; but often we look so long at the closed door that we do not see the one which has been opened for us."
— Helen Keller

IX

Agradecimentos

Estas são as primeiras palavras que escrevi para a minha tese. As primeiras palavras devem pertencer às pessoas que me ajudaram a chegar até aqui, às pessoas que caminharam comigo e tornaram o sucesso desta etapa, uma realidade.

Gostaria de agradecer aos meus supervisores Pedro Pereira e Sandra Macedo-Ribeiro por terem acreditado em mim e por me terem dado a oportunidade de realizar este trabalho. O caminho que traçámos fez-me crescer tanto a nível profissional, como pessoal. Obrigada por terem confiado em mim e no meu trabalho. Agradeço também à Professora Ana Margarida Damas por ter aceite co-orientar a minha tese, assim como à Annalisa Pastore e a todos os elementos do seu grupo por me terem recebido no seu laboratório de braços abertos e me terem ajudado em tudo o que precisei. Ainda que a minha visita tenha sido tão curta, consegui adquirir um conhecimento preponderante para o desenvolvimento do trabalho aqui apresentado.

A minha família foi e sempre será a minha âncora, o meu mais adorado porto de abrigo. A minha mãe sempre me fez ver a realidade, sempre me ajudou a chegar mais longe e sempre reconheceu o meu melhor, mesmo quando as palavras permaneciam escondidas, teve sempre um sorriso do coração para me dar. O meu pai sempre me ensinou a sonhar, a acreditar no possível do impossível e sempre teve enormes demonstrações de alegria e carinho para as minhas vitórias, por mais pequenas que fossem. Para os meus pais guardo o pedaço mais caloroso do meu coração. A minha avó, essa mulher de mãos fortes e coração alegre, sempre me ensinou isso mesmo: a ser forte e alegre e a não desistir. A ela devo muito mais do que a minha educação. Devo uma imensidão de bons momentos que fizeram de mim uma criança, uma adolescente, uma mulher feliz. Minha mana, minha companheira de uma vida, tu que estás sempre lá para tudo, ensinaste-me que há sempre um lado bom em tudo e que a fé é algo que devemos ter em nós, nas pessoas que amamos e em Deus. Não há batalhas que não possamos ganhar se acreditarmos. Os meus queridos tios, Lina e Fernando, que acompanharam a minha infância, me ajudaram a crescer e a tornar-me uma pessoa melhor, ensinaram-me que por mais que a vida mude,

podemos sempre continuar iguais a nós mesmos. Os meus sogros são um verdadeiro exemplo para mim, receberam-me de coração aberto e em tão pouco tempo ensinaram-me mais do que muita gente numa vida inteira: o amor e a amizade pode perdurar no tempo e ajudar a ultrapassar tudo o que o destino nos reserve. Acima de tudo, devemos valorizar o que temos e não o que não temos ou o que não podemos ter. À minha restante família, agradeço todo o amor e carinho incondicional ao longo de todos estes anos. O meu querido avô não pôde testemunhar esta caminhada, mas sei que acreditava fervorosamente no meu potencial e esteja onde estiver rezo para que esteja orgulhoso de mim.

E como poderia eu ter chegado aqui sem os meus amigos? Esses que partilharam tantos e bons momentos comigo? Vocês sabem quem são, mas não posso deixar de escrever umas palavras de apreço a alguns que por razões impossíveis de definir, me fizeram ser maior e chegar mais longe. Rita, tudo o que passámos juntas enriqueceu-me e faz-me saber que nunca poderei estar sozinha contigo por perto. Sofia, obrigada por tudo o que me deste ao longo destes 12 anos, contigo partilhei alguns dos momentos mais sorridentes da minha vida. Sílvia, minha "bina", tu és tudo aquilo que sempre desejei para melhor amiga: sorridente, bondosa, carinhosa e muito muito especial. Joaninha, sem ti não me teria mantido minimamente sã durante a escrita desta tese (assim como em tantos outros momentos do doutoramento!), essa é a mais pura das verdades. Tu cativaste-me e continuas a cativar-me todos os dias e, com isto, ambas sabemos que digo tudo o que há por dizer. Ana, João e Margarida, a vossa família é a minha família, estou grata por vos ter na minha vida, pois a nossa ligação nunca poderá esmorecer. Gabriela, Isabel, Sara, Iliona, Bebiana, e Rosa: vocês ajudaram-me a crescer, fizeram parte deste caminho, deram-me a mão sempre que precisei e, por isso, sei que a nossa amizade perdurará no tempo. Vilaça Babe, ainda bem que estás por perto, ajudas-me mais do que imaginas. Para voçês, estarei sempre aqui. Aos meus amigos mais recentes, mas pelos quais nutro uma amizade incondicional: Aida, Alexandre, Ana, Tiago, Rute, Bruno e Luís voçês são verdadeiramente os melhores companheiros para todos os momentos. A minha vida é muito mais colorida por vos ter como amigos.

Nada disto teria sido possível sem a ajuda, paciência e companheirismo dos meus colegas e amigos de laboratório, por quem nutro um carinho especial.

Vivemos todo o tipo de momentos, mas levo comigo os risos, as palermices, as demonstrações de carinho e os bons conselhos. Sem vocês não teria chegado onde cheguei. Desejo-vos o melhor deste mundo, porque pessoas especiais não merecem menos do que isso!

Um especial agradecimento à Noélia Alonso, ao Frederico Silva e ao Paulo Oliveira. À Noélia pela contribuição preponderante para a publicação do artigo e por me ter acompanhado em todo o processo, sem nunca me deixar desanimar. Ao Frederico, pela amizade, acompanhamento e inestimável ajuda ao longo dos últimos anos. Ao Paulo, por estar sempre disponível para discutir ciência e por me ter ajudado sempre que precisei. Agradeço aos três, por sentir que ficam genuinamente felizes com as minhas vitórias.

Rodrigo, meu mais que tudo, tu mostraste-me a melhor face do amor: aquela em que posso ser amada, aceite e valorizada por tudo aquilo que sou, sem medos e sem restrições. Ensinaste-me que o amor é caminhar de mão dada: nunca à frente, nunca atrás, sempre lado a lado. Não poderia ter pedido melhor dádiva do que amar e ser amada por alguém como tu: forte, honesto e essencialmente único. És o meu melhor amigo e todos os dias anseio pelo nosso futuro juntos.

Um obrigado honesto e eterno a todos,

Joana

XII

Abstract

Iron-sulfur clusters (Fe/S) are ubiquitous cofactors of proteins intervening in vital biological processes. Therefore, Fe/S cluster biosynthesis pathways are tightly regulated in a wide range of organisms. The iron-sulfur cluster regulator, IscR, harbors a [2Fe-2S] cluster and enables the crosstalk between the iron-sulfur cluster (ISC) and sulfur assimilation (SUF) biosynthetic pathways to coordinate the utilization of iron and cysteine for Fe/S cluster assembly. Depending on its ligation status, IscR binds to distinct sets of promoters, thereby modulating cluster biosynthesis, as well as its own expression. IscR ability to recognize different types of promoters was unexpected since it contains a single predicted helix-turn-helix (HTH) DNA-binding domain. Although Fe/S cluster biogenesis is a well characterized process in Gram-negative bacteria, in Gram-positive microorganisms this process remains relatively unexploited. Gram-positive bacteria were thought to rely exclusively on the SUF machinery for Fe/S cluster biosynthesis and IscR was therefore considered restricted to Gram-negative bacteria. However, we identified the ISC and the SUF operons, as well as a functional IscR, in the unique Gram-positive bacterium *Thermincola potens*. Structural and functional analysis of *T. potens* and *Escherichia coli* IscR identified a key residue, Glu43, serving as negative filter against promoters that are controlled by IscR under anaerobiosis. Our findings suggest that cluster ligation is responsible for the remodeling of the protein-DNA interactions, eliminating unfavorable contacts between Glu43 and type-1 promoters and allowing productive binding. This work unveils a conserved mechanism of promoter discrimination, along with subtle structural differences that modify DNA sequence recognition specificity.

Resumo

Centros de ferro-enxofre são cofatores ubíquos de proteínas envolvidas em diversos processos biológicos. Em bactérias Gram-negativas, a biossíntese de centros de ferro-enxofre é regulada pelo factor de transcrição IscR (iron-sulfur cluster regulator) que contém um centro [2Fe-2S]. Dependendo da presença ou ausência do seu centro de ferro-enxofre, a IscR reconhece diferentes promotores, o que permite a sua autoregulação, assim como a regulação da biossíntese de centros ferro-enxofre. A proteína IscR permite a comunicação entre os sistemas de biogénese de centros ferro-enxofre ISC (iron-sulfur cluster) e SUF (sulfur formation) para coordenar a utilização de ferro e cisteína para a produção de centros de ferro-enxofre. A capacidade de distinção entre diferentes sequências de DNA é inesperada, uma vez que que a proteína IscR contém apenas um domínio de ligação ao DNA. Apesar de ser um processo bastante caracterizado em bactérias Gram-negativas, a biogénese de centros de ferro-enxofre em organismos Gram-positivos é ainda um campo relativamente inexplorado. Até agora, considerava-se que as bactérias Gram-positivas dependiam apenas da via SUF para a biossíntese de centros ferro-enxofre e, desta forma, a proteína IscR seria expressa exclusivamente em bactérias Gram-negativas. No entanto, foi possível identificar as vias ISC e SUF, assim como uma IscR funcional, na bactéria Gram-positiva *Thermincola potens*. A análise estrutural e funcional da proteína IscR de *T. potens* e *Escherichia coli* demonstra que o resíduo Glu43 é preponderante para a discriminação da sequência de um grupo de promotores controlado por este regulador em condições anaeróbias. Os resultados apresentados sugerem que a inserção de um centro de ferro-enxofre na proteína induz a remodelação as interacções entre a IscR e a sequência de DNA, eliminando o contacto desfavorável do resíduo Glu43 com promotores do tipo-1 e permitindo o reconhecimento dos mesmos. Este estudo descreve um mecanismo conservado de discriminação entre grupos de promotores, assim como evidencia diferenças estruturais subtis que explicam a diferente especificidade no reconhecimento de sequências de DNA.

Table of Contents

List of Figures

XVIII

List of Tables

Abbreviations

ATC – A-type carrier

CD – Circular dichroism

DMRB – Dissimilatory metal reducing bacteria

EMSA – Electrophoretic mobility shift assay

ENDOR – Electron-nuclear double resonance

EPR – Electron paramagnetic ressonance

DTT – Dithiothreitol

DNA – Deoxyribonucleic acid

DNIC – Di-nitrosyl iron complex

FAD – flavin adenosine nucleotide

FADH2 – reduced flavin adenosine nucleotide

Fdx – Ferredoxin

FNR – Fumarate nitrate regulator

GPR – Gram-positive region

Hmp – Haemoglobin

H_2O_2 – Hydrogen peroxide

IAV – Influenza A virus

IHF – Integration host factor

IMAC – Immobilized metal affinity chromatography

IPTG – Isopropyl β-D-1-thiogalactopyranoside

ISC – Iron-sulfur cluster

IscR – Iron-sulfur cluster regulator

MST – Microscale thermophoresis

MFC – Microbial fuel cell

MHC – Multiheme c-type cytochromes

Mtb – *Mycobacterium tuberculosis*

NDSB-201 – 3-(1-pyridino)-1-propane sulfonate

NIF – Nitrogen fixation

NMR – Nuclear magnetic ressonance

NO – Nitric oxide

O_2 – Molecular oxygen

O^{2-} – Superoxide

OH^- – Hydroxyl anion

OH – Hydroxyl

ORE – Oxidant-responsive element

PLP – Pyridoxal-5'-phosphate

RNAP – Ribonucleic acid polymerase

RNS – Reactive nitrogen species

RRE – Roussin's red ester

ROS – Reactive oxygen species

S^0 – Sulfane sulfur

S^{2-} – Sulfide

SOD – Superoxide

TEV – Tobacco etch virus

UVRR – Ultraviolet resonance raman

Uv/Vis – Ultraviolet/Visible

UP – Upstream promoter

XXII

Chapter 1

General Introduction

1.1 - Fe/S clusters as ubiquitous and multipurpose cofactors in Nature

Iron is an essential biological cofactor playing a major role in multiple cellular processes, such as nitrogen fixation and respiration, and can be incorporated in proteins in several ways: as mono or di-iron reaction centers or combined with elemental sulfur in the form of Fe/S clusters (1-3). Iron-sulfur (Fe/S) clusters are ubiquitous and complex protein cofactors consisting of iron and elemental sulfur that are involved in processes as diverse as DNA replication and photosynthesis (4, 5). Due to their stability at multiple oxidation states and their physiologically relevant redox potentials (ranging from -500 to -150mV), Fe/S clusters confer to many enzymes the ability to participate in electron transfer and redox catalysis, as well as to function as sensors that modulate gene expression according to the cellular redox balance (4, 6). Thanks to their redox properties, Fe/S clusters are versatile prosthetic groups and the high abundance of Fe/S cluster-containing proteins is proof of the evolutionary success of Fe/S chemistry (7, 8). Fe/S clusters in rubredoxins are composed by one iron atom coordinated by four cysteinyl residues, whereas in rhombic [2Fe–2S] clusters each iron atom is ligated by two protein ligands (Fig. 1) (7). The combination of rhombic centers leads to the formation of [4Fe–4S] and more complex structures (5). Once incorporated into proteins, iron in Fe/S clusters is commonly coordinated by cysteine or histidine residues; but aspartate and serine side chains or backbone amides were also shown to function as cluster ligands (9). Several different protein folds have been found to coordinate these simple Fe/S clusters. Of the nearly 50 folds identified, over 90% harbor $[2Fe-2S]^{2+,+}$ or $[4Fe-4S]^{2+,+}$ clusters, being the latter three times more abundant, which is consistent with the higher chemical stability of tetranuclear clusters (10). Nevertheless, it remains difficult to infer the presence of Fe/S clusters directly from protein sequences.

During the past decades, considerable progress has been made towards the quantitative and qualitative characterization of iron-sulfur centers of proteins (11). The properties of iron-sulfur clusters are determined by their electronic arrangement and ability to electron delocalization (12). Iron-sulfur proteins display a wide range of midpoint potentials, resulting from several factors, such as the

nature of the cluster ligands (13). Electron paramagnetic resonance (EPR) and Mössbauer spectroscopies are the techniques most commonly used to detect iron-sulfur clusters in proteins and investigate their properties, but complementary techniques are also widely applied, namely Nuclear magnetic resonance (NMR) spectroscopy, X-ray crystallography, Electron-nuclear double resonance (ENDOR), Magnetic circular dichroism and Ultraviolet-visible (UV/Vis) absorption (14, 15). Information obtained from EPR analysis includes electronic structure, metal coordination-sphere composition and geometry, whereas Mössbauer spectroscopy provides detailed information of the chemical state of the iron atoms, as well as the electron distribution in various redox states of distinct iron-sulfur cluster types (16). Studies of hyperfine-shifted resonances by NMR provides relevant information about their structures in solution, their electron distribution from iron ions onto protein atoms, and the electron-transfer reactions in which they participate (17). The combination of these different techniques provides full characterization of the protein active center.
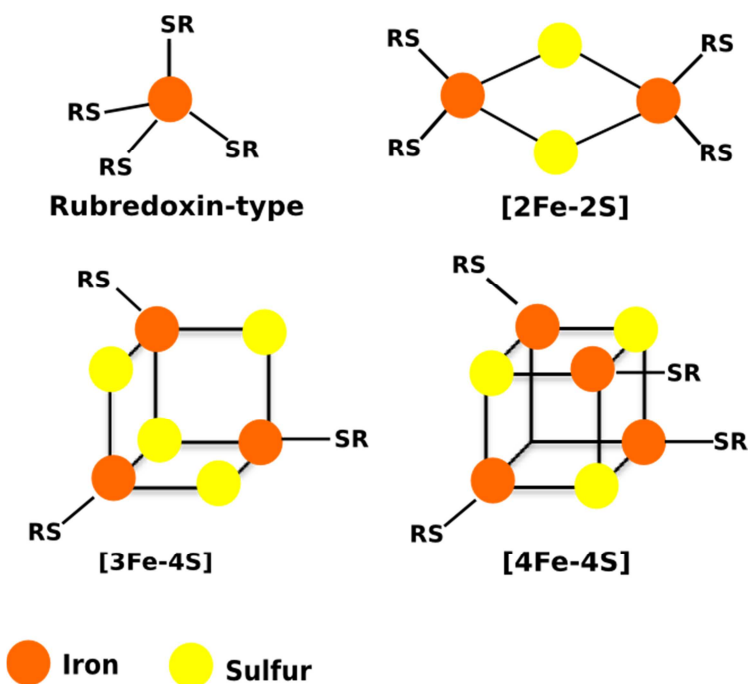
Fig. 1 - Common types of iron–sulfur clusters. Structural rearrangements of rubredoxin type, [2Fe-2S], [3Fe-4S], and [4Fe-4S] iron–sulfur clusters. Iron is colored in yellow, sulfide in orange and coordinating residues (SR) are indicated.

1.1.1. *Fe/S clusters as oxidative stress targets*

Reactive oxygen species

Although Fe/S incorporation into proteins proved to be highly beneficial during evolution, due to their intrinsic chemical reactivity, Fe/S clusters can be very fragile and become hazardous elements for the cell (18, 19). Oxygen species convert exposed Fe/S clusters to unstable forms that quickly decompose, ultimately interfering with several cellular processes in which they play essential roles. Moreover, degradation of Fe/S clusters can trigger the formation of reactive oxygen species (ROS, Box 1, equations 1-2) that are detrimental to lipids, proteins and DNA (20). Fe/S-containing proteins can react with superoxide (ROS; Box 1, equations 3-6) through their exposed clusters, producing the hydroxyl anion and often leading to loss of protein activity. Therefore, Fe/S clusters can be both targets and generators of ROS, and both events can potentially inhibit pivotal metabolic pathways (18, 19).

Nitric oxide (NO) stress

Nitric oxide (NO) is a signaling and defense molecule of major importance (21). In eukaryotes and at nanomolar concentrations, NO functions as signal *via* reversible coordination with the heme group in soluble guanylate cyclase to facilitate vasodilatation, while at micromolar concentrations within mammalian macrophages it is used as an effector molecule in the defense against pathogenic invasion (22, 21). Although for some bacteria (e.g. soil bacteria) NO is a natural metabolite, its ability to react with several key biomolecules including DNA, metalloproteins, thiol groups of proteins and low molecular weight thiols (e.g. glutathione and homocysteine), means that NO is also cytotoxic and can pose a potential threat to bacterial survival (23). Thus, it is crucial for bacteria to sense increased environmental NO levels and trigger specific adaptive responses to neutralize its poisonous effect (24).

Box 1 – Oxidative Stress (adapted from (25))

Oxidative stress results from an imbalance between reactive oxygen species (free radicals) and antioxidant defenses (26). This imbalance can be the consequence of exposure to increased levels of ROS: superoxide (O^{2-}), hydrogen peroxide (H_2O_2) and the hydroxyl radical (OH^-), which are products of the stepwise reduction of molecular oxygen (Equation 1)

$$O_2 \xrightarrow{e^-} O^{2-} + 2H^+ \xrightarrow{e^-} H_2O_2 \xrightarrow{e^-} HO^{\bullet} + H^+ \to H_2O \qquad (1)$$
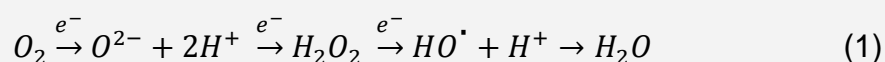
During aerobic growth, both superoxide and hydrogen peroxide are endogenously generated upon auto-oxidation of flavin cofactors of redox enzymes (27). Reaction between Fe^{2+} and hydrogen peroxide yields the highly reactive hydroxyl anion (Fenton reaction, equation 1), linking the cellular iron levels to oxidative stress.

$$Fe^{2+} + H_2O_2 + H^+ \to Fe^{3+} + HO^{\bullet} + H_2O \qquad (2)$$
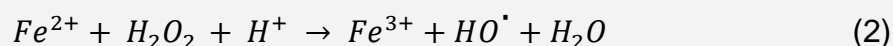
The highly detrimental reaction of superoxide with protein Fe/S clusters produces hydroxyl anion (OH) and results in additional oxidative stress (equations 3-6). The hydroxyl anion is the strongest oxidant that exists in aqueous environments and is able to cause severe and sometimes lethal DNA lesions (26)

$$[4Fe - 4S]^{2+} + O^{2-} + 2H^+ \to [4Fe - 4S]^{3+} + H_2O_2 \qquad (3)$$

$$[4Fe - 4S]^{3+} \to [3Fe - 4S]^{1+} + Fe^{2+} \qquad (4)$$

$$Fe^{2+} + H_2O_2 + H^+ \to Fe^{3+} + HO^{\bullet} + H_2O \qquad (5)$$

$$HO^{\bullet} + DNA \to H_2O + DNA\ lesion \qquad (6)$$
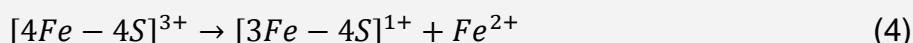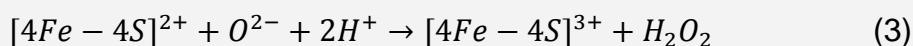
Several NO-responsive regulatory proteins contain iron-sulfur clusters as their sensory unit and NO-mediated modification of Fe/S proteins is well documented in both bacteria and mammalian cells (28-31). The reaction of iron-sulfur clusters in regulatory proteins was shown to produce at least two distinct iron-nitrosyl species: dinitrosyl iron complex (DNIC) and Roussin's Res Ester (RRE) (32). The condensation of two RRE species yields a novel, tetranuclear octonitrosyl cluster. Insights into the mechanisms of cluster nitrosylation were provided by recent studies on the WhiD protein from *Streptomyces coelicolor* and the WhiB-like proteins from *Mycobacterium tuberculosis* (28). Since reversible modification of iron-sulfur clusters by nitric oxide can serve as genetic switch in a

group of regulatory proteins, such as SoxR and FNR (30, 31), the repair of DNIC to [2Fe-2S] cluster is crucial for the correct functioning of the signaling mechanism. Additionally, iron–sulfur proteins are broadly distributed and vital for many important cellular functions (5) and modification of iron–sulfur clusters by NO is expected to impair multiple metabolic processes. While DNIC formation has been widely characterized, the reverse process remains poorly understood. It is known that repair of the NO-modified iron-sulfur proteins requires at least two steps: decomposition of the protein-bound DNICs and re-assembly of new iron-sulfur clusters in the proteins (33). Hence, bacterial survival highly depends on fine-tuned response mechanisms to fluctuations of NO concentrations that enable its function as a signaling molecule, its elimination when cytotoxic levels are reached, and the repair of NO-modified Fe/S clusters.

1.2. Role of Fe/S cluster proteins as sensors

Equilibrium of the cellular redox state is crucial for both bacterial metabolism and cellular integrity. Oxidative stress has the potential to highly impact this balance, having a deleterious effect on essential cellular components. Although molecular oxygen is used for aerobic respiration it is also a source of damaging reactive oxygen species (ROS, Box 1) and the onset of O_2 in the atmosphere posed a real threat to anaerobic bacteria partly due to the inherent sensitivity of Fe/S clusters, present in proteins with pivotal metabolic and regulatory roles (18). To counteract oxidative stress, bacteria use sensitive and specific sensors that monitor diverse environment signals, such as oxygen availability, cellular redox state and levels of ROS (34, 35). These sensors are responsible for detecting specific redox signals, triggering adequate regulatory outputs that confer the organism the ability to adapt to environmental conditions. The sensing mechanism occurs either *via* altered DNA binding affinity of the sensory protein or the concerted action of a two-component signaling cascade (35). Fe/S cluster regulatory proteins enable organisms to sense stressful conditions and respond accordingly at the level of transcription. The reactivity of Fe/S clusters makes them perfectly designed cofactors to function as sensors of diverse stresses (36).

1.2.1. *Fumarate nitrate reductase (FNR), a sensor of environmental oxygen*

Molecular oxygen allows aerobic respiration and thereby its use is energetically beneficial to bacteria. Facultative anaerobes such as *E. coli* have a sufficiently flexible metabolism to use O_2 metabolism as the terminal electron acceptor for aerobic respiration and alternative electron acceptors, such as nitrate and fumarate, when O_2 levels are low (37). Such metabolic flexibility heavily relies on the ability of bacteria to sense both oxygen availability and respond accordingly by modulating transcription of target genes (35).

Regulation of FNR activity through its Fe/S cluster

In *Escherichia coli*, the transcription factor FNR acts primarily during the transition from aerobic to anaerobic respiration regulating over 300 genes implicated in diverse pathways. FNR functions span from the activation of genes encoding components of alternative electron transport chains to the repression of genes with aerobic roles during anaerobic growth (38, 39). FNR is part of the cAMP receptor protein (CRP)/fumarate and nitrate reduction regulatory protein (FNR) superfamily of regulators, consisting of two domains: an N-terminal sensory domain harboring the binding site for either a $[4Fe-4S]^{2+}$ or a $[2Fe-2S]^{2+}$ cluster and a C-terminal DNA binding domain which contains a helix-turn-helix motif and recognizes specific DNA-binding sites within target promoters (40-42). Under anaerobic conditions, *E. coli* FNR is activated through the insertion of an O_2-labile [4Fe-4S] cluster by the ISC biosynthetic machinery (43). Cofactor incorporation on FNR leads to conformational changes that alleviate inter-subunit repulsion and enable dimerization of the ≈30kDa monomer. The FNR homodimer is then able to recognize specific DNA promoter sequences and to regulate transcription of target genes (44).

FNR's $[4Fe-4S]^{2+}$ cluster is coordinated by four cysteine residues in the N-terminal domain and spectroscopic studies showed that it acts as a direct O_2 sensor (Fig. 2). The sensing mechanism involves the conversion of the $[4Fe-4S]^{2+}$ cluster to a $[2Fe-2S]^{2+}$ cluster via an unstable [3Fe-4S] intermediate with the concomitant production of one Fe(III) and two sulfide ions (S^{2-}). This reaction that is initiated with the binding of O_2 to the $[4Fe-4S]^{2+}$ cluster leading to a one-electron

oxidation, not only enables O_2 detection, but also amplifies the signal by recycling the initial product of O_2 reduction, superoxide, back to O_2 (45). Exposure to O_2 and consequent conversion of the cubic $[4Fe-4S]^{2+}$ clusters into planar $[2Fe-2S]^{2+}$ clusters results in FNR dimer dissociation into transcriptionally inactive monomers, in which interactions with the DNA and the transcription machinery are no longer favored (44). If oxygen levels in the environment remain high, the $[2Fe-2S]^{2+}$ clusters are gradually degraded to yield the cluster-free (apo-) form of FNR. Such cluster degradation was observed *in vitro* and is enhanced by superoxide (46, 47). Reversion to $[4Fe-4S]^{2+}$-FNR was observed upon addition of dithionite to air-exposed $[2Fe-2S]^{2+}$-FNR (48), whereas apo-FNR was shown to act as a scaffold to regenerate the FNR active homodimer both *in vitro* and *in vivo* (49). In *E. coli*, FNR is expressed under both aerobic and anaerobic conditions involving a continuous cycling between active $[4Fe-4S]^{2+}$-FNR, inactive $[2Fe-2S]^{2+}$-FNR and apo-forms, with the O_2 levels modulating the relative predominance of each one and thereby regulating the expression of FNR target genes (35). During aerobic growth and assuming that cluster degradation is faster then the rate of cluster synthesis and repair, the inactive monomeric form of FNR predominates, while anaerobiosis leads to accumulation of the dimeric $[4Fe-4S]^{2+}$-loaded FNR form.

FNR response to nitric oxide (NO)

Besides being responsive to O_2 environmental levels, FNR was also shown to sense NO levels. The flavohaemoglobin (Hmp) of *Escherichia coli* is implicated on the defense mechanisms against the detrimental effects of NO and is repressed by FNR (50). NO is able to react with the Fe/S cluster of purified FNR under anaerobic conditions with the concomitant production of a dinitrosyl☐iron–cysteine complex (DNIC-FNR). Up☐regulation of *hmp* promoter *in vivo* by pathophysiologicaly relevant NO concentrations was shown to be dose-dependent and abolished by *fnr* mutation. Moreover, NO also regulates expression of model FNR☐controlled promoters (30).
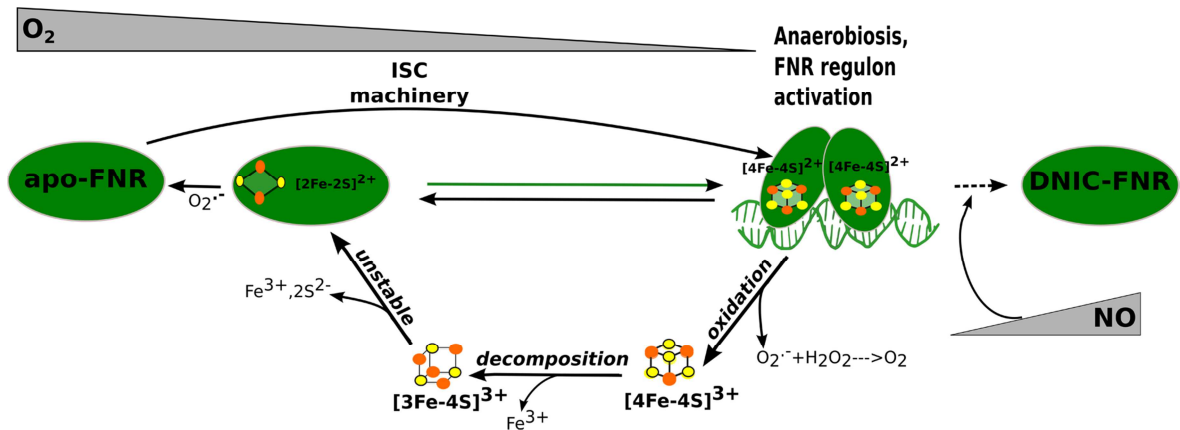
Fig. 2 - Schematic representation of the mechanism of action of *E. coli* FNR. Under anaerobic conditions, monomeric and inactive apo-FNR is matured by the ISC biosynthetic machinery producing [4Fe–4S]$^{2+}$-FNR. Cluster assembly promotes FNR dimerization and binding to specific DNA sequences at target promoters to activate the FNR regulon. In the presence of oxygen (O$_2$), the [4Fe-4S]$^{2+}$ cluster is converted to a planar [2Fe-2S]$^{2+}$ cluster via an unstable [3Fe-4S] intermediate (black arrows). This is accompanied by conversion of FNR from the DNA-binding competent dimeric form to the transcriptionally inactive monomer. Further exposure of FNR to oxygen results in [2Fe-2S]$^{2+}$-FNR degradation and apo-FNR formation. The active dimeric FNR [4Fe–4S]$^{2+}$ is also sensitive to NO to form a DNIC–FNR complex, which leads to its monomerization and dissociation from DNA. [2Fe-2S]$^{2+}$-FNR could be converted back to [4Fe–4S]$^{2+}$-FNR *in vitro* through addition of dithionite (green arrow).

1.2.2. *SoxR, a redox sensor*

SoxR in *Escherichia coli*

In enteric bacteria, such as *E. coli*, the SoxRS system is a two-component regulatory system that modulates gene transcription in response to oxidative stress by activating the expression of several defense genes, such as the antioxidant protein superoxide dismutase (SOD) (51-53). The transcription factor SoxR, named after its superoxide-sensing role, is a constitutively expressed protein that belongs to the MerR family of transcription factors (54), whose activity is crucial for transcription regulation in response to oxidative stress (55, 56). *E. coli* SoxR is a homodimer, with each 17kDa subunit containing a [2Fe-2S] cluster coordinated by four cysteine residues (Cys$^{119, 122, 124, 130}$). Although both holo- and apo-SoxR were shown to be dimeric and bind to the *soxS* promoter with similar affinity, loss of the [2Fe-2S] yields a transcriptional inactive protein (57). Under redox stress conditions, the [2Fe-2S] cluster becomes oxidized and SoxR activates the expression of the *soxS* gene (58). SoxS is itself a transcription factor that activates the expression of the SoxRS regulon (>100 genes), encoding proteins that reestablish redox balance and repair oxidant-induced damage (59). To guarantee that the regulatory loop continues dependent on the external redox

signal, SoxS is subsequently degraded by proteolysis (60). Thus, SoxR transcriptional activity, but not DNA binding or structural integrity, is completely dependent of its [2Fe-2S] clusters

SoxR is present in a wide range of bacteria, but SoxS is found exclusively in enteric bacteria. Extensive bioinformatic analysis of genomes lacking the *soxS* gene predicted that, in non-enteric bacteria, SoxR directly regulates a rather small set of genes coding for putative oxygenases, oxidoreductases and transporters (61). Unlike most iron-sulfur regulators, whose function is essentially modulated through assembly/disassembly of their Fe/S clusters, the regulatory switch controlling transcriptional activity of SoxR consists on the reversible one electron oxidation–reduction of its [2Fe-2S] clusters (Fig. 3A). The [2Fe-2S] cluster of SoxR can exist in both +1 and +2 oxidation states and both forms bind the *soxS* promoter region with similar affinities, but only the $[2Fe-2S]^{2+}$-SoxR form is transcriptionally active (57, 62). The reduction potential of the SoxR $[2Fe-2S]^{2+/1+}$ couple is -285mV (vs standard hydrogen electrodes at pH 7.6), which makes it prone to oxidation by a wide range of redox-active species (62). However, electrochemical measurements on DNA-modified electrodes revealed that binding of SoxR to its cognate DNA results in a substantial shift in the reduction potential to +200mV, indicating that oxidation of the cluster to a +2 state can only take place through the action of strong oxidizing molecules (63). This specific feature enables SoxR to act as a sensor: it is only transcriptionally active under oxidative stress conditions and does not respond to minor imbalances in the cellular redox status.

Structure of *E. coli* SoxR

The crystal structures of *E. coli* SoxR and of its complex with the *soxS* promoter in the oxidized state have been solved at resolutions of 3.2 Å and 2.8 Å, respectively (64). The X-ray structure of [2Fe-2S]-SoxR displays an overall similarity to other transcription factors belonging to the MerR family (aligns with several Mer or Mer-like regulators with a r.m.s.d ≈ 3. Structure-based sequence alignment, as calculated by Dali server; (65)). The SoxR protein consists of an N-terminal winged helix DNA-binding domain, a dimerization domain and a C-terminal sensor domain where the [2Fe-2S] clusters are coordinated (Fig. 3B). The SoxR dimer is stabilized through extensive interactions of the α5 helices of both monomers, forming an antiparallel-coiled coil. The α5 helix makes additional

hydrophobic contacts with the α3 and α4-helices of the same subunit. The C-terminal sensor domain encompasses the Fe/S-cluster binding region (residues 119 to 130) and is stabilized through interactions with the α3′, α4′ and α5′-helices of the other subunit. Notably, the [2Fe-2S] cluster of SoxR is solvent-exposed in an asymmetric charge environment and is partially stabilized through interactions with residues from the other monomer of the functional homodimer, some of which belonging to the DNA-binding domain (64).
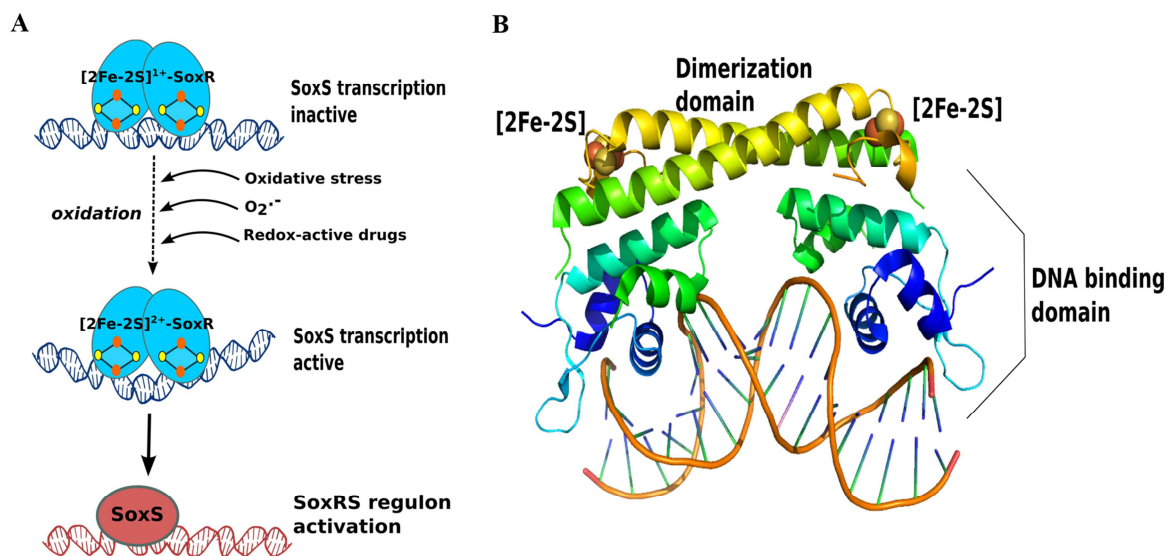
Fig. 3 - Structure of [2Fe-2S]-SoxR and its regulatory mechanism. A) Schematic representation of the SoxRS system in *E. coli*. SoxR exists as a transcriptionally inactive [2Fe–2S]$^{1+}$-homodimer. [2Fe–2S]$^{1+}$-SoxR is capable of sensing and responding to oxidative stress, as well as to redox-active and superoxide-generating compounds. Upon exposure to such environmental stresses, oxidation of [2Fe–2S]$^{1+}$-SoxR enables the recognition of the *soxS* promoter sequence. SoxR binding induces structural changes on the DNA and activates expression of its downstream signaling protein, SoxS, which in turn activates the SoxRS regulon. B) Structure of SoxR bound to DNA (PDB entry 2ZHG, (64)). SoxR secondary structure is represented as ribbons with chain colored with a gradient from blue (N-terminal) to orange (C-terminal).The [2Fe-2S] cluster is represented as orange and yellow spheres and DNA is in sticks representation**.**

In the complex SoxR-DNA structure, both the DNA-binding and Fe/S cluster domains of SoxR are rotated outwards, which results in an increased distance between the α2- and α2′-helices (64). Ultraviolet Resonance Raman (UVRR) spectroscopy of Trp98 and Trp91 in SoxR have shown that these tryptophan residues undergo small environmental changes upon DNA binding (66), implying that the structure of the individual domains of free and DNA bound SoxR suffer only minor conformational changes. However, the abrupt alteration in the redox

potential of SoxR upon DNA binding suggests that the solvent-exposed environment and electronic structures of the [2Fe–2S] cluster in SoxR may be altered when the protein is bound to its cognate DNA (63). The direct interaction between the sensory-domain of SoxR and the DNA-binding region provides a direct way for communication of the oxidative signal. Redox-induced changes in the [2Fe–2S] cluster of SoxR are transmitted to the DNA-binding domain and produce distortions in target promoters, allowing transcription activation (64).

The SoxR–DNA structure suggests a reasonable mechanism by which reversible oxidation of the [2Fe–2S] cluster leads to an interdomain structural rearrangement required for the remodeling of the -35 and -10 promoter elements, so they are optimally positioned to interact with the RNAP (Ribonucleic Acid Polymerase) (67). However, a high-resolution structure of the transcriptionally inactive [2Fe–2S]$^{+}$ form of SoxR bound to DNA is essential to further understand how the redox signal may be propagated from the [2Fe-2S] cluster to the cognate DNA.

Redox and nitrosative stress sensing by SoxR

Recent studies in different bacteria challenged the generally accepted view that SoxR responded to superoxide and suggested that this regulator has a much broader sensorial capacity, mediating the oxidative stress response to redox-cycling drugs, such as viologens, phenazines and quinones (68-70). In fact, as mentioned previously, the [2Fe-2S] cluster of SoxR is solvent-exposed and poses as a readily available platform for the reduction of redox-active drugs (64). Interestingly, in enteric bacteria, SoxR senses a broader range of compounds than in non-enteric bacteria, such as *Pseudomonas aeruginosa* and *Streptomyces coelicolor (69)*. Such differences in SoxR sensitivity are fully consistent with its role in the general stress response in enterobacteria and with a more restricted regulon in other bacteria that lack the *soxS* gene. More recently, it was demonstrated that the residues in the vicinity of the [2Fe-2S] cluster are responsible for fine-tuning SoxR sensitivity. In fact, a hypervariable motif of three residues within the highly conserved Fe/S binding site region (69) was shown to be the primary modulator of SoxR proteins sensitivity towards different redox compounds (69).

The SoxRS regulon can also be activated by NO, through direct nitrosylation of the [2Fe-2S] cluster of SoxR. The reaction between NO and

SoxR is irreversible, with the concomitant formation of a protein-bound DNIC. Although relatively stable *in vitro*, nitrosylated iron-sulfur centers in SoxR rapidly disappear *in vivo*, probably meaning that such proteins are scavenged through specific protective mechanisms dedicated to counteract nitrosative stress (71).

1.3. Bacterial Fe/S cluster biogenesis machineries

In striking contrast to the chemical and structural simplicity of Fe/S clusters, their synthesis and assembly into apoproteins is a highly complex and orchestrated cellular process (reviewed in (72)). In the past decade, different machineries in both bacteria and eukaryotes were shown to be dedicated to Fe/S-proteins maturation, namely the NIF, ISC and SUF systems (73, 72, 74).

The NIF system, first identified in *Azotobacter vinelandii*, is mostly dedicated to the maturation of the nitrogenase enzyme under nitrogen fixation conditions (75), but it has also been found to mature other (non-nitrogenase) Fe/S-containing proteins in organisms that, such as *Helicobacter pylori*, do not fix nitrogen (76). In contrast, both ISC and SUF machineries guarantee the maturation of the remaining cellular Fe/S proteins. Homologous ISC proteins are found in mitochondria (77) and SUF homologues are found in chloroplasts (78).

Despite the obvious differences among the various systems, synthesis of Fe/S clusters and their transfer into apo-targets is underlined by the same basic principles and has common molecular players (Fig. 4) (72). The overall biosynthetic process can be divided into two steps: (i) the *de novo* assembly of the Fe/S clusters on a recipient protein, known as scaffold, and (ii) its subsequent transfer into an apo-protein. Briefly, L-cysteine is converted into L-alanine by a cysteine desulfurase (named IscS, NifS or SufS) with the concomitant release of sulfur (79), which is transferred to the scaffold protein that provides the molecular platform for Fe/S cluster assembly (80, 81). The transient Fe/S cluster is subsequently transferred to final acceptors (82, 83).
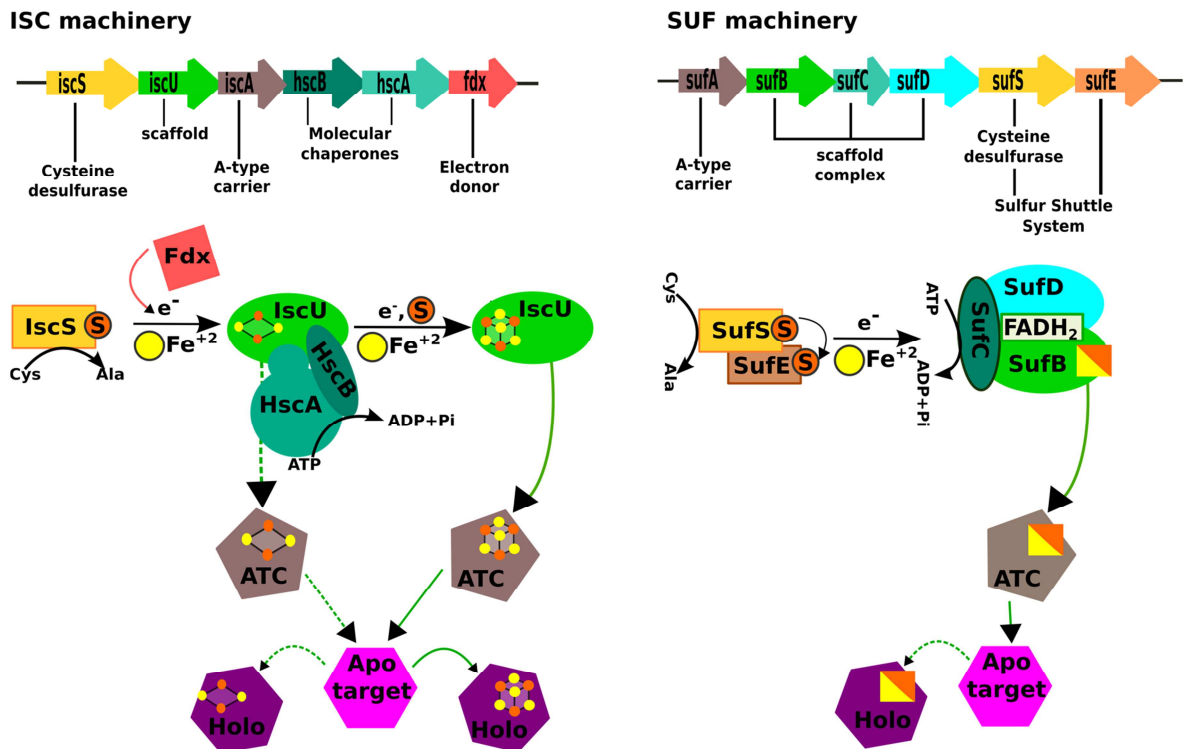
Fig. 4 - Biogenesis of Fe/S clusters by the ISC and SUF machineries. A) The ISC system is encoded by the *iscRSUA-hscBA-fdx* operon. IscS converts L-cysteine into alanine with the concomitant release of sulfur to IscU, the scaffold protein onto which Fe and S are transiently assembled as Fe/S clusters (depicted as yellow and orange spheres, respectively). Delivery of labile [2Fe-2S] clusters from IscU to A-type Fe/S carriers (ATCs) is facilitated through interaction with the HscBA co-chaperone duo, whereas [4Fe-4S] cluster release from the scaffold to an ATC is not stimulated by the presence of these chaperones (84) and transfer to an ATC can occur directly. From the ATC, the Fe/S cluster is delivered to apo-targets. The identity of the Fe^{2+} (yellow sphere) donor remains elusive although experimental evidence strongly supports a role for CyaY, a frataxin homologue. Electrons required for cluster assembly are most probably donated by ferredoxin (Fdx). B) The SUF system is encoded by the *sufABCDSE* operon. SufS and SufE form a heterodimeric cysteine desulfurase complex, in which sulfur is transferred from SufS to SufE, and subsequently to the scaffold SufB onto which the Fe/S cluster is assembled. SufB binds a $FADH_2$ cofactor and is part of a $SufBC_2D$ complex, wherein SufC is an ATPase and SufD is presumably involved in iron acquisition. Regardless of the type of Fe/S cluster (yellow and orange square) assembled on SufB, the cluster is directly delivered from the scaffold to an ATC that subsequently matures final apo-targets.

1.3.1. *The ISC system*

The *Escherichia coli* ISC system, encoded by the *iscRSUA-hscBA-fdx* (*isc*) operon, catalyzes the maturation of the majority of Fe/S cluster proteins under non-stress conditions (Fig. 4). The ISC machinery exists in both prokaryotes and eukaryotes and its considered the housekeeping system for Fe/S cluster biogenesis in prokaryotes, including *E. coli* and *A. vinelandii* (85).

E. coli IscS, a PLP (pyridoxal-5'-phosphate) dependent enzyme, is a homodimer of 90kDa in solution (86). IscS catalyzes the conversion of cysteine to

alanine with the concomitant production of sulfur, via the formation of a persulfide on a conserved Cys residue (Cys328). The enzyme-bound persulfide can then be transferred to Cys residues on the scaffold protein (87). Deletion of IscS is lethal in *A. vinelandii* and leads to severe growth defects in *E. coli* (79, 88). Many of these defects are a direct consequence of the reduced activity of Fe/S enzymes (79).

IscU sequence is highly homologous to the N-terminal domain of NifU, the scaffold of the NIF system and contains the three conserved Cys residues known to be involved in cluster coordination (89). Extensive biochemical studies led to the confirmation that IscU serves as the scaffold component for the ISC machinery: it incorporates both iron and sulfur, stimulates the assembly of the Fe/S cluster, and its transfer to apotargets (89, 90, 84, 91). Analysis of the enzymatic IscS-directed cluster assembly on IscU revealed the sequential formation of two $[2Fe-2S]^{2+}$ clusters, followed by the slow formation of a single $[4Fe-4S]^{2+}$ cluster on each IscU homodimer (89). Importantly, formation of the $[4Fe-4S]^{2+}$ cluster-containing form was accompanied by a loss of the $2[2Fe-2S]^{2+}$ cluster species, suggesting that the $[4Fe-4S]^{2+}$ species is formed by reductive coupling of the two $[2Fe-2S]^{2+}$ clusters (89). Additionally, pre-formed clusters on IscU were shown to be efficiently transferred to apo-proteins, such as acotinase (84), ferredoxin (92), NsrR (93), and IscR (93).

During Fe/S cluster assembly, IscS interacts with and directly transfers sulfur to the IscU scaffold protein (80). Sulfur transfer was shown to occur between Cys328 of IscS and Cys63 of IscU involving the formation of a disulfide bridge in a covalently bound IscS-IscU complex (87). The crystal structure of the IscS-IscU complex showed that one monomer of IscU interacts with one subunit of the IscS homodimer leading to a 2:2 stoichiometry (94). Following cluster assembly, *E. coli* IscU was shown to interact with both HscA and HscB for cluster transfer to apo-proteins (95). A conserved motif in IscU, LPPVK, was identified as the primary HscA recognition site (95) and the co-chaperone HscB was shown to stimulate HscA-IscU interaction (96), contacting with IscU through a conserved patch of hydrophobic residues (97, 98). The rate of cluster transfer from IscU to apo-targets is greatly enhanced (>20-fold) when HscA and HscB are present, an effect that was shown to be ATP-dependent (99).

In summary, Fe/S cluster assembly and subsequent deliver to apo-proteins is an intricate process, involving a concerted action and conformational changes of the scaffold, chaperones and final targets.

1.3.2. *The SUF system*

In *E. coli*, deletion of the entire *isc* operon produces growth defects and simultaneously leads to reduced activity of Fe/S enzymes (100). The fact that such strains remained viable raised the possibility of functional compensation and led to the identification of the SUF system (101). The *E. coli* SUF system is composed by six genes forming the sufABCDSE (*suf*) operon and its function in Fe/S clusters biogenesis was assigned after the analysis of diverse combinations of both ISC and SUF *E. coli* mutant strains (101). Suppression of either the *isc* or *suf* operons is not lethal in *E. coli* (for synthetic lethality both systems have to be inactivated) and *suf* mutations have only a mild effect on the activity of Fe/S proteins. However, absence of the SUF system increases *E. coli* sensitivity to iron starvation (85), whereas in strains lacking the ISC pathway and under anaerobic conditions, *suf* operon expression fully restored the activity of FNR (fumarate and nitrate reduction regulatory protein) (43). Although there is some redundancy between the two systems, the ISC system functions as the housekeeping Fe/S cluster assembly system in *E. coli*, whereas the *suf* operon is specifically triggered to synthesize Fe/S clusters in conditions that lead to the disruption of iron or sulfur metabolism, such as iron starvation or oxidative stress (Fig. 4) (102, 85).

The SUF machinery for Fe/S cluster assembly relies on the formation of two separate complexes of *suf* encoded proteins: the SufBCD and the SufSE complexes. The SufBCD complex was shown to function as a scaffold that is able to bind and transfer a [4Fe-4S] cluster to apoproteins, including SufA (83, 103, 81). In the SufBCD complex, SufB is regarded as the scaffold containing the Cys residues to coordinate nascent Fe/S clusters; SufC is an ATPase resembling those associated with ABC transporters (104) and SufD was suggested to be involved in iron entry into the scaffold complex (105). The SufSE complex poses as a sulfur donor for Fe/S cluster formation. SufS is cysteine desulfurase homologous to IscS, whose activity is greatly enhanced through interaction with SufE (106, 107). *In vitro* experiments showed that the cysteine desulfurase activity

of the SufS-SufE complex is substantially stimulated in presence of the SufBCD complex and SufE in turn interacts with SufB, leading to the proposal that sulfur transfer from SufS to SufB is mediated by SufE (108).

The SufBCD complex exists predominantly as a $SufBC_2D$ stable form, which is the most efficient complex in Fdx maturation and therefore is proposed to serve as the terminal scaffold (109). A worth noticing feature of the $SufBC_2D$ complex is its ability to bind one equivalent of flavin adenosine nucleotide (FAD) only in its reduced state ($FADH_2$) (81). This cofactor can eventually provide the electrons to mobilize the ferric iron required for Fe/S cluster assembly from ferric citrate, ferritins or CyaY.

1.3.3. *The delivery step – A-type proteins*

Once a cluster is assembled on a scaffold, it must be delivered to an apo-target. In *E. coli*, the total number of Fe/S-containing proteins is predicted to be close to 150 (8) and experimental data indicates that A-type proteins mediate the Fe/S clusters delivery process (Fig. 4) (110, 111). *E. coli* possesses three A-type proteins, namely IscA, SufA and ErpA that share 30% sequence identity. IscA and SufA belong to the *isc* and *suf* operon, respectively, whereas ErpA is located elsewhere in the chromosome (111). A-type proteins were initially proposed to act as complementary scaffolds given the presence of three highly conserved cysteine residues on their C-terminal region, as it was observed for the IscU scaffold (112, 113). This proposal was underscored by the observation that the pre-formed cluster could be transferred to apo-targets (113, 114). However, this view was profoundly challenged by several observations. First, A-type proteins are not able to interact with cysteine desulfurase enzymes, an essential step for sulfur transfer and subsequent cluster assembly on a scaffold (94). Second, while mutations on IscA or SufA were found to be almost neutral, an *erpA* mutation was found to be lethal under respiratory growth conditions and neither of these proteins was able to compensate for a mutation on IscU (115, 100). Finally, both IscU and SufBCD were able to mature IscA and SufA, respectively, but the reverse reaction was not possible (83, 114). Taken together, these results established A-type proteins as "Fe/S clusters carriers" (ATCs, A-Type Carriers) rather than scaffolds (109, 116). Moreover, function of A-type proteins was shown to require functional SufB or

IscU, further proving that ATCs are unlikely to have a scaffold function (111). Under this perspective, nascent clusters would be transferred from their scaffolds to ATCs that would deliver them to apo-proteins. However, phylogenomic and genetic analyses suggest that ATCs function enables multiple routes for Fe/S clusters trafficking and that the choice of maturation route is modulated by growth conditions, such as oxygen levels (111).

1.3.4.   *CyaY as an iron donor for Fe/S cluster biogenesis*

CyaY, the bacterial homolog of eukaryotic frataxin, is the primary candidate as iron donor for Fe/S cluster biosynthesis (117). In humans, reduced levels of frataxin were linked to the neurodegenerative disease Friedreich's ataxia (118). This pathology is a consequence of Fe/S cluster biogenesis disruption, mitochondrial iron accumulation and oxidative stress, which are known contributors for reduced activity of Fe/S proteins (119). In contrast to frataxin deletion in eukaryotes organisms, suppression of CyaY, the bacterial homolog of frataxin, does not alter iron content or sensitivity to oxidative stress (120). Nonetheless, the CyaY *E. coli* mutant had reduced amounts of Fe/S cluster-containing respiratory Complex I and Complex II, which is probably a consequence of decreased maturation of Fe/S proteins (121, 122). *In vitro* studies provided further insights into CyaY function: CyaY can bind iron specifically forming a stable complex, albeit with some distinct properties from other iron-binding proteins (123).

CyaY interacts strongly with the IscU-IscS complex, forming a heterotrimeric assembly (124) and was able to donate iron for Fe/S cluster assembly on IscU in the presence of both IscS and cysteine (125). Further biochemical studies, suggested that CyaY can act as an iron-dependent inhibitor of cluster formation, whose function is exerted through interaction with IscS and modulated by iron bioavailability to adapt Fe/S cluster biogenesis to the pool of Fe/S acceptor proteins (126). Very recently, ferredoxin (Fdx) was shown to bind to IscS (127, 128), while supplying electrons to reduce sulfane sulfur (S^0) to sulfide (S^{2-}) following the enzymatic conversion of cysteine (127). Moreover, Fdx and CyaY compete for overlapping binding sites on IscS and holo-Fdx binding to IscS does not perturb the affinity of IscS for IscU (127, 128). These results reinforce the

proposal of Fdx and CyaY acting, in a stepwise fashion, as electrons and iron donors for Fe/S cluster biosynthesis, respectively,.

1.3.5. *ISC and SUF systems under stress conditions*

Fe/S proteins are easily damaged by oxidative stress due to the inherent reactivity of their Fe/S clusters (18, 129). Hence, such environmental stress conditions are expected to influence the function of protein machineries responsible for the *de novo* synthesis and delivery of Fe/S clusters to apo-proteins. Although the ISC and the SUF systems share the same basic principles, combined genetic and biochemical studies pinpointed several differences in the ability to function under stress conditions (102, 85). The ISC system is sensitive to oxidative stress, being fully inactivated by ROS (102). Indeed, the Fe/S cluster assembled on IscU is exposed and thus intrinsically prone to oxidation (89, 130). Such cluster accessibility promotes copper or cobalt attack that, due to their thiophilicity (i.e ability to bind sulfur), can replace iron and form mixed clusters. Although this was true for cooper (131), cobalt reacts preferentially with degraded or transiently synthetized clusters, rather than attack them directly in Fe/S proteins. Indeed, a transient iron-cobalt-sulfur complex built on IscU could be transferred to an apo-protein (129). Thus cobalt toxicity is intimately linked to the poisoning of the entire Fe/S cluster biogenesis pathway.

In *E. coli*, submicromolar concentrations of H_2O_2 were detrimental to the ISC machinery and, under such conditions, the *suf* operon was activated to compensate the lack of Fe/S cluster biosynthesis (102). Likewise, *suf* operon expression was triggered under iron starvation conditions (85). These results made evident that organisms exposed to oxidants rely on the SUF system to mediate Fe/S cluster biogenesis rather than the ISC pathway. Additionally, the fact that SufB has $FADH_2$ as a cofactor may be indicative that the SUF system is better equipped for iron mobilization when iron is scarce, given that this cofactor can probably provide the necessary reducing power to mobilize iron from diverse sources (105, 81). Moreover, the *E. coli* SufS-SufE complex is more resistant to oxidative stress than the IscS-IscU complex (132) and the SUF system efficiently repaired damaged clusters (102). Finally, transcriptomic analysis showed that

cobalt induced *suf* operon expression, linking cobalt toxicity to the impairment of Fe/S cluster biosynthesis, iron bioavailability and oxidative stress (133).

1.3.6. *Diversity of ISC and SUF systems*

Homologs of *E. coli* ISC and SUF proteins are found in a wide range of organisms, but some species contain distinct patterns of Fe/S cluster biosynthesis systems. For instance, in contrast to *E. coli* and most Gram-negative bacteria, cyanobacteria (*e.g Synechocystis spp.*) possess only an incomplete SUF system and no ISC system (134) and *Mycobacterium tuberculosis* (Mtb), the causative agent of tuberculosis, contains a simplified SufBCDS operon (135). A similar scenario is encountered in most Gram-positive bacteria that carry only a *suf* operon (136), a particular case that will be described in more detail in the following section.

Fe/S cluster biogenesis in Gram-positive bacteria

Fe/S cluster biogenesis systems have been under intensive scrutiny in Gram-negative bacteria, such as *E. coli* (reviewed in (137)), but are poorly understood in Gram-positive bacteria. *In silico* analyses identified a highly conserved SUF machinery in Gram-positive bacteria that is relatively different from the *E. coli* SUF system (138). Bioinformatic characterization identified *cis*-acting elements on the *suf* promoter region similar to those located upstream of the *suf* operon in *E. coli*. Similar to what was observed in *E. coli*, the Fur and OxyR regulators, as well as the DNA-bending protein IHF (integration host factor), probably recognize these regions (136). However, in contrast to *E. coli*, no orthologs of IscR, SufE or SufA were found in the Gram-positive bacterium *Enterococcus faecalis* (138).

Furthermore, Gram-positive bacteria code for an IscU-like protein, named SufU, that lacks the conserved HscA recognition motif LPPVK (138). Such feature is fully consistent with the absence of a HscA in Gram-positive organisms. SufU is essential in *Bacillus subtilis* and was shown to interact with SufS, from which it receives sulfur, to subsequently maturate apo-targets (139). Moreover, SufU is highly homologous to the N-terminal domain of *A. vinelandii* NifU, including the residues known to coordinate the cluster. Besides lacking the specific LPPKV

motif, SufU also contains a characteristic 19 amino acid insertion that is apparently restricted to SufU homologues from Gram-positive bacteria. This insertion was named Gram-positive region (GPR) and may be involved in the interaction of SufU with other macromolecules (136). However, considering that SufB lacks some of the cysteine residues that were found to coordinate the Fe/S cluster in its *E. coli* homolog (81), additional experiments are required to establish if SufBCD is indeed a scaffold in Gram-positive bacteria and, if so, understand the presence of two scaffold proteins. In fact, it is possible that there is no scaffold redundancy, given that SufU was shown to act as desulfurase activator in *B. subtilis* (140). SufC and SufB are highly similar to their *E. coli* orthologues, but functional and biochemical data is required to fully understand the SufBCD complex role in Fe/S cluster biogenesis in Gram-positive bacteria.

1.4. IscR, the Fe/S cluster biogenesis regulator

1.4.1. _Concerted regulation of ISC and SUF systems by IscR_

Fe/S proteins are widely distributed in Nature and essential for many cellular processes (8). The synthesis of many of these proteins is regulated to accommodate changes in environmental conditions that can be detrimental to Fe/S clusters (141). Consistent with this notion, both Fe/S cluster biogenesis machineries, ISC and SUF, are tightly regulated by the [2Fe-2S] cluster-containing transcription factor IscR (142). IscR, encoded by the first gene of the *iscRSUA-hscBA-fdx* (*isc*) operon, acts as a repressor of the Isc pathway and was shown to coordinate a $[2Fe-2S]^{+1}$ cluster upon anaerobic isolation (142). Mutations on either *iscA* or *hscA* genes significantly reduced the activity of IscR, showing that repression by IscR is dependent of functional ISC machinery and is closely linked to its Fe/S cluster (142). Biochemical characterization of purified holo-IscR ([2Fe-2S]-IscR) provided insights into the mechanism by which IscR is able to sense the cellular Fe/S cluster status. Mössbauer experiments using whole cell extracts revealed that $[2Fe-2S]^{+1}$-IscR is the predominant form *in vivo*, which becomes further oxidized even upon anaerobic isolation (143). However, cluster oxidation did not affect the binding affinity of IscR towards the *isc* promoter (143). Site-specific mutagenesis revealed that the three highly conserved cysteine residues

(Cys[92, 98, 104]) (144, 145) are essential for cluster coordination and, since both apo and holo-forms of IscR are homodimers in solution (144), full cysteinyl cluster coordination was unlikely. Indeed, His107 was subsequently identified as the fourth residue crucial for the formation of the holo-protein, giving rise to a (Cys)$_3$(His)$_1$ cluster binding scheme (143).

Extensive functional and biochemical studies on the regulation of the ISC pathway further contributed to understanding the feedback mechanism by which IscR adapts the expression of ISC proteins to cellular Fe/S cluster demand (146). Binding of holo-IscR to two upstream binding sites (site A and site B) in the *isc* promoter (P$_{isc}$) is essential for full IscR-mediated repression of the ISC pathway (147). IscR binding is expected to prevent attachment of the RNAP, since sites A and B coincide with the sequences of the conserved −10 and −35 hexamers of P$_{isc}$ required for σ^{70} recognition (148), and a potential consensus upstream promoter (UP) element (149). Mutation of the third binding site (site C) identified on the P$_{iscr}$ region had no effect on its expression *in vivo* and a functional role remains to be assigned to this sequence (146). Inhibition of cluster formation through substitution of either of the cysteine residues on IscR prevented *isc* repression by IscR under both aerobic and anaerobic conditions. Consistent with this observation, holo-IscR has a much higher affinity for sites A and B than apo-IscR, further demonstrating that the Fe/S cluster is crucial for IscR function as repressor of the ISC pathway (146). The link between the Fe/S cluster of IscR and its function raised the question of which Fe/S cluster biogenesis machinery is the primary system responsible for formation of holo-IscR. In strains where the *iscSUA-hscBA-fdx* operon was deleted, P$_{isc}$ repression is substantially alleviated, suggesting that maturation of IscR is achieved mainly through the ISC pathway (146). However, further *in vitro* and *in vivo* studies showed that IscR can receive its Fe/S cluster from different sources, namely ErpA under normal growth conditions and SufBCD under stress conditions (93).

IscR was shown to sense Fe/S cluster homeostasis through its own Fe/S cluster (Fig. 5) (146). Under aerobic conditions, overexpression of FNR amplified the overall cellular Fe/S cluster requirements and led to decreased repression of the *isc* operon, showing that IscR was unable to compete with other recipient proteins of the ISC machinery. Maturation of other Fe/S proteins is probably priviledged as a consequence of the unusual coordination of the Fe/S cluster of

IscR. Thus, IscR probably constitutes a poor substrate for the ISC machinery and it is matured only when the levels of Fe/S clusters are restored (143, 146). The finding that IscR is more sensitive to changes in Fe/S levels under aerobic conditions is physiologically reasonable. During aerobic growth, it is likely that Fe/S clusters are continuously being damaged or destroyed, thereby increasing the demand for Fe/S cluster biogenesis and/or repair. This imbalance would be translated in more competition between IscR and other substrate proteins of the ISC machinery under aerobic conditions than under anaerobic conditions. Hence, transcriptional control of *iscRSUA-hscBA-fdx* by [2Fe-2S]-IscR is part of a negative feedback regulation mechanism where the demand for the maturation of Fe/S proteins modulates the expression of genes whose products are necessary for Fe/S cluster biosynthesis (150).
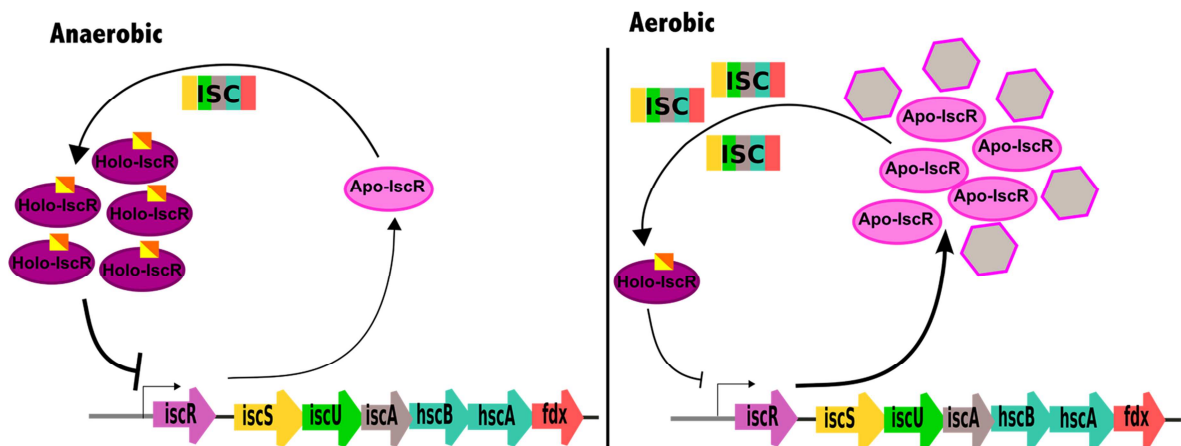
Fig. 5 – Schematic model of the regulation of Fe/S cluster biosynthesis by the ISC pathway in aerobic and anaerobic growth conditions. Under aerobic growth the demand for Fe/S clusters is predicted to be high due to elevated levels of apo-protein substrates (grey hexagons), which would compete with IscR (light mangenta ovals) for Fe/S clusters from the ISC pathway (rainbow rectangles). Given the lower affinity of apo-IscR towards Fe/S cluster ligation, such competition would culminate in low levels of [2Fe–2S]-IscR (holo-IscR. dark mangenta ovals) and less repression of *iscRSUA–hscBA–fdx*. Under anaerobiosis, maturation of Fe/S enzymes by the ISC machinery is satisfied. The low demand for Fe/S biosynthesis results in higher levels of [2Fe–2S]-IscR and increased repression of the *isc* operon.

Following its assignment as the repressor of the *isc* operon, IscR was further implicated in the regulation of the *suf* operon, coding for the additional Fe/S cluster biogenesis system specifically activated under stress conditions (Fig. 6). (85, 145). The regulation of the SUF machinery relies on the action of IscR and of two additional transcription factors: the peroxide responsive regulator OxyR and the ferric uptake regulator Fur, and the host-integration factor IHF (151, 85, 145).
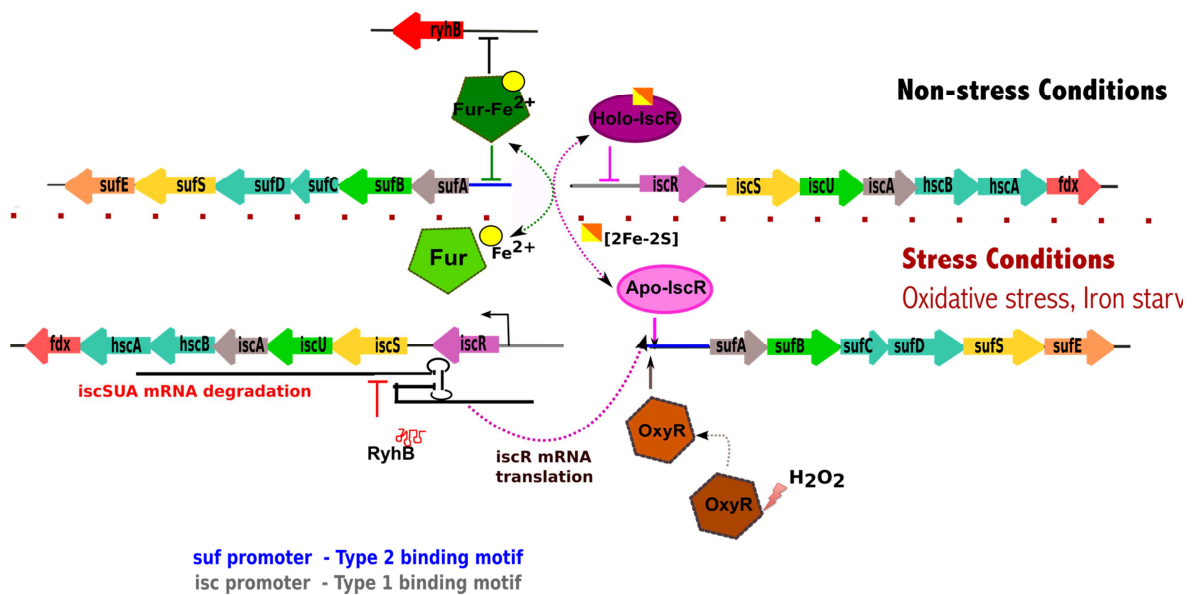
Fig. 6 - Regulation of Fe/S homeostasis in *E. coli*. The *suf* and *isc* operons are depicted. The expression of the *suf* operon is regulated by the transcription factors Fur (green), OxyR (brown) and IscR (mangenta). The *isc* operon expression is controlled by holo-IscR and by the small non-coding RNA, RyhB (red). Under non-stress conditions (top), IscR is matured by the ISC machinery and represses its expression, creating an autoregulatory loop modulated by the Fe/S cellular state. Under such conditions, Fur-Fe^{2+} (dark green) represses the ryhB gene expression. Under iron starvation (bottom left), the *suf* operon is activated in two ways: (i) Repression by Fur is alleviated, and (ii) there is expression of the *ryhB* gene. The *IscSUA* mRNA is degraded, the IscSUA proteins are not synthesized, whereas the apo-form of IscR (apo-IscR) accumulates and activates the expression of the *suf* operon. Under oxidative stress (bottom right), OxyR and apo-IscR activate the expression of the *suf* operon, whereas the IscSUA system is predicted to be non-functional and apo-IscR formation favored. As the SUF system was reported to enable IscR maturation, under stress conditions the ISC system may be completely shut down.

Both OxyR and Fur are very well characterized global sensor regulators in *E. coli*: OxyR senses oxidants by means of the reversible oxidation of specific cysteine residues (152), while Fur utilizes Fe^{2+} as a corepressor and blocks transcription of target genes according to environmental iron levels (1). Three *cis*-acting oxidant-responsive elements (OREs) were identified on the *E. coli suf* promoter region. ORE-I is the binding site of OxyR that contacts RNA polymerase through a loop, whose formation is facilitated by IHF bound at ORE-II. IscR recognizes the third ORE (ORE-III) and, together with OxyR, induces the *suf* operon (145). Low levels of *suf* expression under non-oxidant conditions are the result of repression by Fur, binding to a putative Fur box located upstream the *suf* operon and that partially coincides with ORE-III (153). Indeed, analysis of the *suf*

promoter region by DNase I footprinting revealed that Fur and IscR recognize overlapping sequences and further biochemical analysis showed that Fur and IscR binding is mutually exclusive. Moreover, given the higher affinity of Fur towards the *suf* promoter, binding of IscR is only possible in the absence of Fur (154). Hydrogen peroxide exposure impairs the function of the Fur regulatory protein, apparently through oxidation of its iron cofactor, leading to the disruption of iron homeostatic mechanisms (155). Expression of the SUF machinery is therefore kept at basal levels during normal growth conditions, whereas under iron starvation and oxidative stress, Fur derepresses the *suf* operon and both IscR and OxyR activate its expression (154). The combined action of IscR and Fur explains why constitutively active IscR variants, having single cysteine to alanine substitutions, retained their ability to activate *suf* expression *in vivo* but still required oxidant treatment (145). Moreover, IscR is able to recognize the IHF binding site *in vitro*, but the IHF binding affinity greatly exceeds that of apo-IscR, remaining probably unaffected by IscR *in vivo* (154).

Additionally, ISC proteins synthesis is post-transcriptionally controlled by a small regulatory RNA (sRNA), RyhB that binds to target mRNAs encoding iron-binding proteins to induce their degradation (156). This Fur-regulated sRNA binds to the *iscS* Shine-Delgarno sequence of the polycistronic mRNA, iscRSUA, promoting the cleavage of the downstream *iscSUA* transcript, while the IscR-containing part of the transcript is stabilized and efficiently transcribed (157). As a result, apo-IscR synthesis is favored and *suf* expression is subsequently stimulated, allowing the switch between the ISC and SUF systems to be modulated when iron becomes scarce (157). Thus, in Gram-negative bacteria, *suf* genes are negatively regulated by Fur in response to iron bioavailability and positively regulated by both OxyR and apo-IscR in response to oxidative stress, whereas *isc* is controlled by IscR and indirectly regulated by Fur/RyhB (102, 154) (Fig. 6). In summary, usually IscR derepresses the ISC pathway during aerobic growth in a feedback mechanism modulated by Fe/S clusters levels, whereas under stress conditions, IscR upregulates the SUF system to compensate for Fe/S-protein degradation and/or damage. Under stress conditions, the ISC system is expressed but may be nonetheless shut down due to higher sensitivity of IscU to ROS and metal stress (129).

1.4.2. *IscR regulon in E. coli*

Genome-wide transcription profiling data in strains containing or lacking IscR, either in anaerobic or aerobic conditions, linked IscR function to the expression of more than 40 genes of 20 predicted operons in *E. coli* (Table 1). Besides the regulation of ISC and SUF machineries, IscR was shown to directly contribute for the regulation of a set of operons coding for anaerobic Fe/S proteins (158). Seven new promoters under IscR control were identified, including *hyaA* (*hyaABCDEF*) and *hybO* (*hybOABCDFG*) coding for hydrogenases-1 and -2, respectively; and the *napF* (*napFDAGHBC*) encoding the periplasmic nitrate reductase (147). All three enzymes coordinate Fe/S clusters and are induced in response to anaerobiosis (63, 158). Under aerobic conditions, IscR was shown to directly repress the expression of *hyaA*, *hybO* and *napF* operons, which is consistent with their upregulation during anaerobic respiration (147).

Table 1 - IscR regulon in *E. coli*. Operons under IscR control code for proteins involved in multiple biological pathways and other transcription factors are required for the regulation of some of these operons

Operons	Function	IscR function	Additional Transcription Factors	Comments	Ref
iscR		Repressor	None	Two binding sites	(147, 142)
sufA	Fe/S biogenesis	Activator	Fur, OxyR	Binding site overlaps with Fur	(153, 154)
erpA		Repressor	Unknown	A-type carrier	(147)
nfuA		Activator	Unknown	A-type carrier	(147)
hyaA	Hydrogen production	Repressor	ArcA, AppY	Binding site overlaps with ArcA	(147, 159)
hybO		Repressor	FNR, ArcA	----	(147)
napF	Nitrate reduction	Repressor	FNR, NarP, ModE	Binding site overlaps with ModE	(147)
ydiU	Unknow	Activator	Unknown	Unknown function	(147)

Binding sites for IscR were identified within the *hyaA* and *napF* promoters and interestingly the sequences recognized by IscR overlap those recognized by other transcription factors, namely ModE and ArcA, known regulators of *napF* and *hyaA* expression, respectively (147). The *napF* operon is activated by ModE in response to molybdate (binding at the upstream promoter) and by FNR and NarP in response to anaerobiosis (binding at the downstream promoter) (160). The impact of IscR in the *hyaA* operon expression was more thoroughly investigated revealing a novel mechanism for O_2 modulation of gene expression in *E. coli* (159). During anaerobic respiration, the operon *hyaABCDEF* is controlled by two transcription factors, ArcA and AppY that were shown to antagonize IscR repression (159). Binding of IscR and ArcA is mutually exclusive and apo-IscR was a stronger repressor of the *hya* operon than its holo-form. Induction of *hyaA* expression during anaerobic growth required override of IscR repression by both ArcA and AppY, low amounts of IscR and weak repression by holo-IscR (159). Repression of these particular set of genes (*hyaABCDEF* and *napFDAGHBC*) suggests that repression by IscR is required to prevent the expression of the encoded anaerobic Fe/S proteins, whose degradation upon exposure to oxygen would by itself generate oxidative stress (18), and explains the need for an aerobic repressor (IscR) in addition to two anaerobic activators (ArcA and AppY) (159). Thus, IscR is a transcriptional regulator contributing to the control of the expression of anaerobic Fe/S proteins, as well as the expression of proteins responsible for Fe/S cluster biogenesis.

1.4.3. *DNA recognition by IscR*

Phylogenetic and DNase I footprinting of promoters controlled by IscR revealed a high degree of conservation of IscR-binding sites in related bacteria (147). This analysis identified two types of conserved motifs recognized by IscR, named type-1 (*iscR*, *yadR* and *yhgI*) and type-2 (*hyaA*, *sufA*, *napF*) motifs (Fig. 7). For both types of promoters, IscR was found to protect a region of ≈28-30bp that comprises one single binding site, except for the *iscR* promoter that encompasses three binding sites (A, B and C). Contrary to sites A and B, the downstream site C does not possess the compiled type-1 sequence and is not well conserved in other bacteria (147).

The ability of IscR to recognize different binding motifs was unexpected, given that the IscR monomer contains a single DNA binding domain (142). Regulation of type-2 promoters by IscR, such as the *hyaA* promoter, was subsequently characterized and provided insights into the differential DNA recognition by IscR (159). Surprisingly, binding of IscR to type-2 promoters does not require the [2Fe-2S] cluster, a feature that is not linked to whether IscR acts as an activator or as a repressor (144). Further characterization of the interaction between IscR and its targets, demonstrated that presence of the Fe/S cluster greatly enhances the affinity of IscR towards type-1 promoters and is essential for their regulation *in vivo* (147, 144, 142), whereas both apo-IscR and holo-IscR bind with similar affinities to type-2 promoters both *in vitro* and *in vivo (144)*. Extensive analysis of the type-2 sequences allowed the identification of an imperfect palindrome motif, containing several bases at conserved positions, including a CC dinucleotide (Fig. 7). Although the position of the binding sites within the *hyaA*, *sufA* and *ydiU* promoters is nearly the same relative to their predicted -35 elements, IscR repressed the *hya* operon expression, but induced the expression of both *suf* and *ydiU* operons. This observation may result from minor differences in the spacer regions to the -35 hexamer and/or the strong interaction of IscR with the *hyaA* promoter in comparison to other IscR-target promoters (144).

Fig. 7 - Comparison between IscR-binding sites and the IscR binding motifs proposed from phylogenetic sequence conservation. Sites recognized exclusively by [2Fe-2S]-IscR (*iscb*, *yadR* and *yhgI*) were compiled as type-1 promoters, whereas recognition of type-2 promoter sequences was shown to be independent of IscR cluster occupancy. Strictly conserved bases are highlighted in red and residues conserved between at least two sequences are colored in yellow. In the binding motifs: R and Y are puRine and pYrimidine, respectively; S is G or C; W is A or T; K is T or G; M is A or C and n is any nucleotide (147). Alignment prepared with ClustalW (161) and colored with Aline (162).

Given that both holo- and apo-forms were shown to interact similarly with type-2 promoters, holo-IscR binding to these promoters under anaerobiosis is probably prevented through the presence of other transcription factors that compete with IscR for the same binding site. This was found to be the case for both *sufA* and *hyaA* promoters, where the IscR binding site overlaps with the binding sequence of Fur and ArcA, respectively (154, 159). This interplay between IscR and other transcription factors represents a mechanism by which these promoters are tightly regulated in response to environmental conditions.

Thus, in contrast to other well characterized Fe/S-containing regulators that have only one transcriptionally active protein form, both apo- and holo-IscR enroll in specific regulatory roles, being able to differentially recognize two types of DNA sequences according to its cluster occupancy (146, 144).

1.4.4. *The Rrf2 family of regulators*

IscR belongs to the widespread Rrf2 family of regulators (PF02082, Pfam database). Rrf2 members are relatively small proteins (12-18 kDa) with a characteristic helix-turn-helix (HTH) domain next to their N-terminus. Besides IscR, this family contains the global cysteine regulator, CymR (163); the NO-sensing repressor, NsrR (164); and the rhizobial iron regulator A, RirA (165). With the exception of CymR, all Rrf2 members with an assigned function were shown to coordinate a Fe/S cluster (142, 165, 166).

In *B. subtilis*, CymR is the regulator of the cysteine biosynthesis pathway (167) and its activity is positively regulated by the interaction with the o-acetylserine (OAS)-thiol-lyase, CysK (168). Complex formation (CymR-CysK) stabilizes binding of CymR to DNA. Through binding to its OAS substrate, a direct percursor of cysteine, CysK is able to act as an indirect sensor of the cellular cysteine concentration and transmit this information to CymR. When cysteine is present, OAS concentrations are low and formation of the CymR-CysK complex is favored, which in turn leads to repression of cysteine biosynthesis (168). In *Staphylococcus aureus*, CymR was shown to indirectly regulate biofilm formation and stress response, playing a key role in virulence (169-171). The crystal structure of both CymR from *B. subtilis* and *S. aureus* reveals a biologically active dimer, where each monomer folds into two tightly packed domains: a DNA-binding

domain, harboring the characteristic winged helix–turn–helix (wHTH) motif; and a long dimerization domain, which places the wHTH motifs at the extremes, opposing each other (Fig. 8A). This architecture explains how these small regulators can recognize DNA targets encompassing 23 to 27 bp (169, 163). Notably, RirA, IscR and NsrR contain three conserved C-terminal cysteine residues (Fig. 8B), but these conserved residues are not found in all Rrf2 family proteins. Some Rrf2 family members comprise two, one or no cysteines and, with the exception of IscR, NsrR and CymR (146, 169, 172), the ligands and sensing mechanisms that activate or inactivate these proteins are unknown.

NsrR is a relatively well-characterized Rrf2 regulator, particularly in *B. subtilis*, where it was shown to control the transcription of genes involved in NO detoxification (172). For NO detoxification, *B. subtilis* makes use of both flavohemoglobin (*hmp*) and nitrite reductase (encoded by the *nasDEF* operon) proteins (173). NsrR is a master regulator of NO metabolism in both Gram-negative and Gram-positive bacteria, repressing the transcription of the *nasDEF* operon and *hmp* gene under anaerobic fermentative growth conditions (174). Transcription of these genes is controlled by the membrane-bound histidine kinase ResE and the cytoplasmic ResD regulator (172). NsrR recognizes the -35 element of the *nasD* promoter, leading to the disruption of the RNA polymerase-ResD-DNA complex (172). Under NO-exposure, both *nasD* and *hmp* are derepressed due to the release of NsrR from the *nasD* promoter through direct nitrosylation of its [4Fe-4S] cluster (172, 175). A set of NsrR-controlled genes identified by transcriptmic analysis belongs to the Fur regulon and is involved in iron homeostasis (176). There is some controversy regarding the type of cluster bound by NsrR. Both *S. coelicolor* (166) and *Neisseria gonorrhoeae* NsrR (177) coordinate [2Fe-2S] clusters, whereas isolation of *B. subtilis* NsrR yielded a protein containing a [4Fe-4S] cluster. (175). Regardless of the type of cluster, NsrR orthologues bear a Fe/S cluster that reacts directly with NO, leading to the formation of DNIC and derepression of the nasD promoter (166, 175). NsrR binding sites compiled from the *nasD* and *hmp* promoters display an imperfect dyad symmetry that was not found in other promoter regions known to be controlled by NsrR and whose recognition by NsrR is NO insensitive (Table 2) (174, 172). Moreover, in *B. subtilis*, binding of NsrR was modulated by ResD and Fur in co-regulated promoters (174) and its Fe/S cluster was reactive towards other molecules such as cyanide,

dithiothreitol, and O_2 (175). Thus, NsrR serves as a sensor of environmental NO concentrations and is involved in the global stress response to nitrosative stress (173).

IscR and NsrR share low sequence similarity within the helix-turn-helix domain, having only three identical amino acids (underlined, 28-LADISER-QGIS-LSYLEQLFSRLRK-51), and therefore recognize very distinct DNA binding motifs (Table 2) (147, 178). Although it is predicted that Rrf2 regulators contain a common strutural signature characterized by a N-terminal helix–turn–helix DNA-binding domain, members of this family display different DNA-binding properties that are translated in distinct cellular functions.

Fig. 8 - Structure of the Rrf2 family regulator CymR and the Fe/S cluster binding region in other Rrf2 regulators. A) Structure of the *B. subtilis* CymR monomer, showing the dimerization helix and the typical HTH DNA-binding domain [PDB entry 2Y75 (163)]. The predicted location of the cluster-coordinating cysteine residues found in homologous Fe/S cluster-containing Rrf2 proteins (e.g., IscR, NsrR, and RirA) is delimited by lines. B) Amino acid sequence alignment of *B. subtilis* CymR with Fe/S-containing Rrf2-type regulators. The sequences of IscR and NsrR of *E. coli*, RirA of *Rhizobium leguminosarum* (*R. leguminosarum*) and CymR of *B. subtilis*, are aligned. Strictly conserved amino acids are highlighted in red, and increasing residue conservation is represented by a color gradient from green to red. Alignment prepared with ClustalW (162). The three cysteines assigned as cluster ligands in IscR, NsrR, RirA are denoted with open triangles**.**

Table 2 – Sequence motifs compiled from IscR and NsrR DNA-binding sites

Protein	DNA-binding motif*	Ref.
IscR	ATASYYGACTRwwwYAGTCRRSTAT or AWARCCCYTSnGTTTGMnGKKKTKWA	(147)
NsrR	gATGyATTTxAAATrCAtc	(178)

*R and Y are puRine and pYrimidine, respectively; S is G or C; W is A or T; K is T or G; M is A or C and n is any nucleotide

1.4.5. *Implications of IscR in host-pathogen interactions*

The interaction between pathogenic microbes and their hosts is determined by survival strategies on both sides (179). Due to its redox properties, iron holds a central position at the host-pathogen interface, being vital for the growth of virtually all organisms, including pathogenic bacteria. Iron utilization by pathogens requires specific mechanisms that allow the interaction with and the acquisition of iron from iron-binding proteins (180). However, high concentrations of iron lead to oxidative stress, while low concentrations substantially affect bacterial growth. Hence, to guarantee their survival, pathogens have to tightly regulate both iron acquisition and transport (180). Additionally, to counteract bacterial invasion, the host innate immune system generates ROS and reactive nitrogen species (RNS) responsible for oxidative stress (179). Both iron starvation and oxidative stress have a detrimental effect on the function and biogenesis of Fe/S enzymes (18). Thus, the ability to adapt to changes in O_2 and iron bioavailability is vital for many bacterial pathogens, as many niches within a host are hypoxic (181) and iron depleted (180). Pathogenic bacteria have evolved transcriptional regulatory systems that perceive such hostile conditions and respond by reprogramming gene expression (182, 183). For this reason, defensive mechanisms that detoxify ROS and RNS and repair damaged cell components essential for the intracellular survival of the pathogen during infection are strictly regulated in pathogens (179, 182).

Given the role of IscR is as a sensor of the cellular Fe/S clusters pool that directly modulates the expression of a diverse set of genes, it is not surprising that IscR function directly affects the ability of some microbial pathogens to maintain iron homeostasis and resist oxidative stress during host infection (184-187). The plant pathogen *Erwinia chrysanthemi* faces both iron starvation and oxidative stress at the onset of infection and consequently both oxidative-stress resistant and Fe/S biogenesis systems are essential for virulence (186). *Arabidopsis thaliana* produces ROS to counteract infection, which are detrimental to Fe/S clusters. The degradation of Fe/S clusters is sensed by *E. chrysanthemi* IscR, whose activity is essential to maintain the appropriate levels of Fe/S cluster biogenesis in such adverse environments (186). Moreover, IscR was required for peroxide resistance in *Pseudomonas aeruginosa* PA14, an opportunistic human pathogen responsible for lethal infections in immunocompromised individuals

(188). *P. aeruginosa iscR* mutant was shown to be hypersensitive to H_2O_2 and paraquat, due to decreased catalase A (KatA) enzyme activity (184). Recently, it was shown that IscR regulated the *P. aeruginosa isc* operon under both physiological and stress conditions, conferring resistance to oxidative stress and contributing to iron homeostasis (184). In *Shigella flexneri*, a facultative intracellular pathogen and the causative agent of bacterial dysentery, the expression of both *suf* and *isc* promoters increased when the pathogen was living intracellularlly due to iron scarcity. IscR was found to be a positive regulator of *suf* expression under oxidant conditions and a negative regulator of *isc* expression in the absence of hydrogen peroxide, protecting *S. flexneri* against oxidative stress (187). IscR was also found to modulate sensitivity to oxidative stress through repression of Fe/S cluster biogenesis during host coinfection with the bacterium *Haemophilus influenza* and influenza A virus (IAV) (189). Furthermore, IscR function on *Vibrio vulnificus* highly impacted the motility and adhesion to host cells, its hemolytic activity, and the survival of this pathogen under oxidative stress during infection (185). Thus, *V. vulnificus* IscR, whose expression is upregulated by the transcriptional regulator Aph, functions as a global regulator contributing to the overall efficiency of pathogenesis by regulating not only the Fe/S cluster biogenesis genes but also the expression of a wide range of virulence and survival related genes (185, 190).

Very recently, IscR was also linked to the virulence of food-borne pathogen *Yersinia pseudotuberculosis* possibly through the control of the Type III secretion systems (T3SS), an injectisome that delivers bacterial effector proteins directly into the host cell cytoplasm (191).

In conclusion, apart from its evident biological importance in the regulation of both ISC and SUF machineries, IscR may be of pharmacological interest. In plants, regulation of Fe/S cluster biogenesis is proposed to be achieved by glutaredoxins that could act as Fe/S cluster☐containing sensor of the SUF machinery (192), whereas in mammals, IRP1 and IRP2 proteins act post-transcriptionally to adjust the cellular requirements for iron (193). Hence, since IscR structural homologs can be found in the pathogens mentioned above, but are absent in their hosts of choice, IscR is a potential target for novel antimicrobial agents.

Chapter 2

Methods

Protein Expression and Purification

A synthetic *iscr* gene, encoding the same amino acid sequence as *TherJR_1914* from the *T. potens* genome, except for a Gly-Leu insertion immediately downstream from the N-terminal methionine and containing the *Nco*I and *Acc65*I restriction sites, was ordered from Eurofins MWG Operon. The *E. coli iscr* gene (b2531) fragment spanning nucleotides +4 to +489 of the IscR ORF was amplified from an *E. coli* K12 colony using specific primers (see Table A.1 in Appendix). IscR^{Tp}-wt ORF was cloned into the *Nde*I and *Xho*I sites of the expression vector pET30a or into the *Acc65*I and *Nco*I sites of the expression vector pETZ2_1a, whereas IscR^{Ec}-wt ORF was cloned into *Hind*III and *Nco*I sites of the expression vector pETZ2_1a (194). The latter constructs were used to obtain the triple mutants (C92/101/107S for *T. potens* or C92/98/104S for *E. coli*) corresponding to the clusterless forms of the proteins (apo-IscR^{Tp} and apo-IscR^{Ec}) by site-directed mutagenesis (see Table A.2 in Appendix). All constructs were verified by DNA sequencing. The N-terminal His$_6$-tagged apo-IscR^{Tp} was overexpressed in *E. coli* BL21 (DE3) cells and the *E. coli* protein in *E. coli* BL21 Star (DE3) (Life Technologies). Briefly, cells were grown in LB medium at 37 °C until OD$_{600}$ = 0.7. At this point, the temperature was decreased to either 25 °C (apo-IscR^{Ec}) or 30 °C (apo-IscR^{Tp}), and the expression was induced with the addition of 0.5 mM isopropyl β-D-1-thiogalactopyranoside (IPTG). Cells were harvested by centrifugation after 4 h and lysed by incubation (60 min on ice with shaking) with 25 µg/mL chicken egg white lysozyme (Sigma). Clarified protein extracts in 20 mM sodium phosphate (pH 7.5), 0.5 M NaCl, 10 mM imidazole, 5% (vol/vol) glycerol, 150 mM arginine, and 2.5 mM β-mercaptoethanol (buffer A) were loaded onto a HisTrap HP column (GE Healthcare) preequilibrated in the same buffer, and bound proteins were eluted with buffer A containing 125 mM imidazole. The IscR-containing fractions were pooled, and the His6 and the solubility tags were removed by incubation with tobacco etch virus (TEV) protease at 4 °C concomitantly to an overnight dialysis against 20 mM sodium phosphate (pH 7.5), 0.2 M NaCl, 10 mM imidazole, 5% (vol/vol) glycerol, 150 mM arginine, and 2.5 mM β-mercaptoethanol. After overnight dialysis, the NaCl was restituted to approximately 0,5M by adding the necessary volume of a 5M NaCl solution and pure recombinant IscR was separated from the expression tag and noncleaved

material by a second immobilized-metal affinity chromatography (IMAC) step, in the same conditions as described above. The buffer was further exchanged for 10 mM Hepes (pH 7.5), 800 mM KCl, and 5% (vol/vol) glycerol using a HiPrep 26/10 (GE Healthcare) desalting column. Following concentration in a centrifugal device, the protein was either used immediately or flash-frozen in liquid nitrogen and stored at –80 °C until needed. Final protein concentrations were estimated by measuring the absorbance of the samples at 280 nm. Point mutants apo-IscR^{Tp}-E43A, apo-IscR^{Ec} E43A, and apo-IscR^{Tp}-P40S were generated by site-directed mutagenesis of the pETZ2_1a constructs (see Table A.2 in Appendix). All IscR protein variants used for biochemical and crystallization experiments were expressed and purified as described for apo-IscR^{Tp}, except for selenomethionyl apo-IscR^{Tp} that was produced in a methionine auxotroph strain (*E. coli* B834, Stratagene), using SelenoMet medium (Molecular Dimensions) following manufacturer's instructions and for apo-IscR^{Tp}-wt that was purified by a single IMAC step followed by desalting on a HiPrep 26/10 column (GE Healthcare). The *E. coli* cysteine desulfurase IscS used in reconstitution assays was expressed and purified as described previously (195).

Electrophoretic Mobility-Shift Assay

Complementary oligonucleotides (Sigma) containing the sequence of the *E. coli hya* or of the *T. potens isc* promoter (Table 3) were annealed into double-stranded DNA by heating a 50 µM solution to 95 °C for 5 min in a water bath, followed by slowly (overnight) cooling to room temperature. For electrophoretic mobility-shift assay (EMSA) analysis using the complete sequence of the *T. potens suf* promoter region (Table 3), the sequence upstream of the *sufC* gene (TherJR_0923) was amplified by PCR using a synthetic template (Eurofins). DNA solutions (1 µM) were incubated with 7.5–10 µM purified protein at room temperature for 20 min in binding buffer [40 mM Tris·HCl (pH 8.0), 100–150 mM KCl, 5% (vol/vol) glycerol, and 1 mM DTT (Dithiothreitol)], and the resulting complexes were resolved on 8% (wt/vol) nondenaturing polyacrylamide gels using 1× TAE (40 mM Tris·HCl, 20 mM acetic acid, and 1 mM EDTA) as running buffer. DNA was detected by either ethidium bromide staining or chemiluminescent detection. For chemiluminescent detection, annealed DNA probes were end-

labeled with digoxigenin using recombinant ter- minal transferase (Roche). The labeled probes (1.5 µmol) were mixed with 11.25 µmol purified IscR in 15 µL of binding buffer [40 mM Tris·HCl (pH 8.0), 10% (vol/vol) glycerol, 1 mM DTT, and 50 mM KCl]. For competition reactions, labeled probe was added after incubating the protein for 10 min with 100-fold molar excess competitor DNA. The samples were separated in 8% (wt/vol) nondenaturing polyacrylamide gels and electroblotted onto positively charged nylon membrane (GE Healthcare), and the digoxigenin-labeled probes were detected with anti-digoxigenin-AP antibody and the chemiluminescent substrate disodium 2-chloro-5-(4-methoxyspiro [1,2-dioxetane-3,2′-(5′-chloro)tricycle [3.3.1.1(3,7)]decan]-4-yl)-1-phenyl phosphate (CDP-Star; Roche).

Table 3 - Oligonucleotides used in binding and crystallization assays

Name	Sequence
hyaEc	5'-AAATCCACAC AGTTTGTATT GTTTTG-3'
hya_bend	5'- CTAGCATAAA TCCACACAGT TTGTATTGTT TTGTGA-3'
iscbEc	5'-TAAATAGTTG ACCAATTTAC TCGGGAATGT CAGACT-3'
C5G	5'-AAATGCACAC AGTTTGTATT GTTTTG-3'
C5A	5'-AAATACACAC AGTTTGTATT GTTTTG-3'
C5T	5'-AAATTCACAC AGTTTGTATT GTTTTG-3'
C6G	5'-AAATCGACAC AGTTTGTATT GTTTTG-3'
C6A	5'-AAATCAACAC AGTTTGTATT GTTTTG-3'
C6T	5'-AAATCTACAC AGTTTGTATT GTTTTG-3'
iscTp_1	5'-TAAAAAATCT TAGTATTTTA GTTGGAATTT TTCTTGACCA GAAAATAACT GTATGC-3'
iscTp_2	5'-TAAAAAATCT TAGTATTTTA GTTGGAATTT TTCTTGACC-3'
iscTp_3	5'-TAAAAAATCT TAGTATTTTA GTTGGAATT-3'
iscTp_4	5'-TTTTTCTTGA CCAGAAAATA ACTGTATGC-3'
iscTp_5	5'-TAAAAAATCT TAGTATTTTA GTTGGAA-3'
hya_26_OH	5'-GAAATCCACA CAGTTTGTAT TGTTTTG-3'
suf	5'- CGCTTTATAT TTAGGAAAGA TGCAGCGCCG GCTATAAAAT AGCCGGCTTT TTCTAAGCTC TTAATCAATA GCCGGATCCA ATTATTGTAG AATCCTGCCC AAAATTATTT GTACTTTTTT ATCCCGGCAG GAGGATAAAT GTGGGTGGAC AAAGAAAAAT ACCCCTGTAG TTTTTGGATT TAAACCAGGA ATCCGTCAGG AGGGAATATT GCGCTTTATA TTTAGGAAAG ATGCAGCGCC GGCTATAAAA TAGCCGGCTT TTTCTAAGCT CTTAATCAAT AGCCGGATCC AATTATTGTA GAATCCTGCC CAAAATTATT TGTACTTTTT TATCCCGGCA GGAGGATAAA TGTGGGTGGA CAAAGAAAAA TACCCCTGTA GTTTTTGGAT TTAAACCAGG AATCCGTCAG GAGGGAATAT TG-3'

Bending assay

Oligonucleotides containing the *E. coli hya* promoter sequence (*hya_bend*, Table 3) flanked by *Xba*I and *Sal*I restriction sites (Sigma) were prepared as

described in Electrophoretic Mobility-Shift Assay. The resulting double-stranded fragment was subsequently cloned into the *Xba*I and *Sal*I sites of the pBend5 vector (ATCC® 87123™), and confirmed by DNA sequencing and restriction analysis with *EcoR*I and *Hind*III. Fragments of identical size (121bp) containing the *hya* sequence (Table 3) at one of six locations were obtained after digestion with *Mlu*I, *Spe*I, *Xho*I, *EcoR*V, *Stu*I, or *BamH*I, and purified using a PCR purification kit (NZYTech) according to the manufacturer's instructions. Each fragment (1µM) was incubated with apo-IscR^{Ec} (5 µM) in binding buffer [40 mM Tris·HCl (pH 8.0), 100–150 mM KCl, 5% (vol/vol) glycerol, and 1 mM DTT] at room temperature for 30 min and resolved on a 8% (wt/vol) non-denaturing polyacrylamide gel. DNA fragments were detected by ethidium bromide staining. The bending angle of the *hya* promoter upon apo-IscR^{Ec} binding was infered by plotting the mobility ratio of each protein-bound complex over the free DNA fragment *versus* the relative position of the apo-IscR^{Ec} binding site within the fragment. A quadratic equation was derived from each experiment and the first- and second-order polynomial coefficients were used to estimate the DNA bending angle (196). The angle induced by apo-IscR^{Ec} on the *hya* promoter was calculated from three experiments with a derived quadratic equation with $r^2 > 0.86$.

Fe/S Cluster Reconstitution

Reconstitution of the Fe/S cluster of apo-IscR^{Tp}-wt was performed under oxygen-depleted atmosphere (<3 ppm O2) in an anaerobic chamber (Belle Technology). All buffers used were sparged with nitrogen gas for 20 min and kept in the anaerobic chamber for at least 12 h before use. Small volumes of aerobically purified proteins (apo-IscR^{Tp}-wt and *E. coli* IscS), as well as sodium dithionite, cysteine, and iron (II) sources were equilibrated in the same low-oxygen conditions for 1 h. An apo-IscR^{Tp}-wt solution (25 µM) was mixed with ammonium iron (II) sulfate (Sigma) and L-cysteine (Sigma) in 20-fold and eightfold molar excess, respectively. The reaction [in 50 mM Tris (pH 8), 150 mM NaCl, 5 mM DTT] was started after 10 min by addition of 2 µM *E. coli* IscS, and Fe/S cluster formation was followed by monitoring absorbance at 420 nm. Upon reaction completion, R-IscR^{Tp}-wt (reconstituted IscR^{Tp}-wt) was purified by IMAC (His-Buster Nickel spin columns; Amocol). Absorption spectra (250–750 nm) were

recorded immediately after purification and upon sample reduction with 2 mM sodium dithionite. Control reactions were performed omitting L-cysteine (non-reconstituted IscR^{Tp}-wt; NR-IscR^{Tp}-wt).

Circular Dichroism Measurements

Binding of IscR^{Ec} variants to target promoters was monitored by circular dichroism (CD) spectroscopy (197). CD spectra were recorded at 20 °C in 1-nm steps on a temperature-controlled Jasco J-815 spectropolarimeter, continuously purged with nitrogen gas. For each sample, the smoothed average of four spectra was considered. Briefly, concentrated protein (either 235 µM apo-IscR^{Ec} or apo-IscR^{Ec} E43A) was added to a 1.0-mm-path quartz cuvette containing DNA (either 1.66 µM *hyaEc* or *iscbEc*, Table 3) and CD spectra (230-360 nm) were recorded following each addition. A CD spectrum of each protein over the same range was also recorded and confirmed that the contribution attributable to apo-IscR variants was restricted to the region below 250 nm.

Binding of wild-type IscR^{Tp} to DNA was monitored using the same instrument settings as above. Either anaerobically reconstituted (R-IscR^{Tp}-wt) or non-reconstituted (NR-IscR^{Tp}-wt) purified apo-IscR^{Tp}-wt was added incrementally to a sealed 10-mm-path quartz cuvette containing the *iscTp_1* sequence (Table 3) in binding buffer, and CD spectra (260–320 nm) were recorded.

Microscale Thermophoresis Assays

Interactions between IscR variants (apo-IscR^{Tp}, apo-IscR^{Tp} E43A, apo-IscR^{Tp} P40S, and apo-IscR^{Ec} E43A) and the different DNA sequences (*iscTp_3*, *iscTp_4*, *iscTp_5*, *hyaEc*, and *iscbEc*) (Table 3) were assessed using microscale thermophoresis (MST) (198) with a Monolith NT.115 instrument (NanoTemper Technologies). Purified proteins (20 µM) were labeled using the Monolith NT.115 Protein Labeling Kit RED-NHS (NanoTemper Technologies) according to the manufacturer's instructions. Labeled proteins were diluted to 50 nM in assay buffer [40 mM Tris·HCl (pH 7.9), 150 mM KCl, 5% (vol/vol) glycerol, 1 mM DTT, 0.1% (vol/vol) Tween 20]. Ligand dilutions were prepared in assay buffer without Tween 20 and mixed with each protein sample at a volume ratio of 1:1. Measurements with apo-IscR^{Tp}, apo-IscR^{Tp} P40S, and apo-IscR^{Tp} E43A were performed in

standard capillaries whereas hydrophilic capillaries were used for measurements with apo-IscR^{Ec} E43A. For each interaction, data from at least two independent runs were averaged, and the average curve was fitted with NTAnalysis software (NanoTemper Technologies). Microscale thermophoresis data collection was carried out at the Campus Science Support Facilities Protein Technologies Facility (www.csf.ac.at).

Crystallization of apo-IscR^{Tp} and apo-IscR^{Ec}:hya complex

Initial crystallization conditions for apo-IscR^{Tp} were screened at 20 °C using the sitting-drop method with commercial sparse-matrix crystallization screens. Drops consisting of equal volumes (1 µL) of protein (at 20 mg/mL) and precipitant solution were equilibrated against a 300-µL reservoir. Crystals were obtained after 2 d using 0.1 M Bis-Tris (pH 6.5) and 3 M NaCl as precipitant. Before data collection, crystals were cryoprotected by immersing them briefly in a 1:1 mixture of precipitant solution and 60% (vol/vol) of 500 mg/mL NDSB-201 (3-(1-pyridino)-1-propane sulfonate) solution in ethylene glycol and flashcooled in liquid nitrogen (46). Selenomethionyl apo-IscR^{Tp} crystallized in the same conditions and was cryoprotected following the procedure described above.

A 3.8-fold molar excess of apo-IscR^{Ec} was mixed with double-stranded oligonucleotide (prepared as described in Electrophoretic Mobility-Shift Assay) comprising region −30 to −55 of the *E. coli hya* promoter sequence with a single-base 5′ overhang (*hya_26_OH*) (Table 3) and incubated at room temperature for 30 min. The complex was either used immediately or flash frozen in liquid nitrogen and stored at −80 °C. Initial crystallization conditions were established at the High Throughput Crystallization Laboratory of the European Molecular Biology Laboratory, using the sitting-drop method. Crystals were obtained at 20 °C, from 0.2-µL drops composed of identical volumes of complex solution [350 µM protein and 92 µM oligonucleotide in 40 mM Tris·HCl (pH 8.0), 150 mM KCl, 10% (vol/vol) glycerol, 1 mM DTT] and of precipitant [0.1 M citric acid (pH 4.0 or 6.0), 1 M lithium chloride, 20% (wt/vol) PEG 6000]. Better and larger crystals could be obtained from the condition at pH 4.0 using the hanging-drop vapor diffusion method. The optimized crystals were cryoprotected in the same conditions as the apo-IscR^{Tp} crystals.

Data Collection and Processing

X-ray diffraction data were collected from cooled (100 K) single crystals at synchrotron beam lines ID29 (apo-IscR^{Tp} and Se-Met apo-IscR^{Tp}) (47) and ID23-EH2 (apo-IscR^{Ec}:hya complex) (199) of the European Synchrotron Radiation Facility. The apo-IscR^{Tp} data were recorded on a Pilatus 6M detector (Dectris) using a wavelength of 0.9763 Å (native dataset) or 0.9792 Å (Se-Met dataset). For the native data, 1,200 images were collected in 0.1° oscillation steps with 0.1-s exposure per frame whereas, for the Se-Met data, 3,600 images were recorded in 0.1° oscillation steps with 0.037-s exposure per frame. The apo-IscR^{Ec}:hya complex data were recorded on a MX-225 detector (Marresearch) using a wavelength of 0.8726 Å. One hundred images were collected in 0.95° oscillation steps with 5.43-s exposure per frame. Diffraction data were integrated with XDS (200), scaled with XSCALE (201), and reduced with utilities from the CCP4 program suite (202, 203). Data collection statistics are summarized in Table 4.

Structure Solution and Refinement.

The structure of apo-IscR^{Tp} was solved by single-wavelength anomalous diffraction using the anomalous signal of selenium-substituted crystals with the SHELXC/SHELXD/SHELXE pipeline (203) and the HKL2MAP GUI (204).The resulting electron density maps were readily interpretable. The structure of the apo-IscR^{Ec}:hya complex was solved by molecular replacement with PHASER (205) using a truncated version of the refined apo-IscR^{Tp} structure as search model. For both structures, alternating cycles of model building with COOT (206) and of refinement with PHENIX (207) were performed until model completion. For the apo-IscR^{Tp} structure, the final model comprises residues Gly-3 to Gly85 and Ser101 to Ile149 for subunit. A and Gly-3 to Gly85 and Ser101 to Tyr148 for subunit B whereas the apo-IscR^{Ec}:hya complex comprises residues Met0 to Asp88 and Lys103 to Ser139 for subunit A, and Gly1 to Asp84 and Gln93 to Val135 for subunit B. Model refinement statistics are summarized in Table 4.

Table 4 - Statistics of data collection, processing, and refinement

Data set	*T. potens* IscR[a]	*T. potens* IscR[a] (Se-	*E. coli* IscR-DNA[a] complex[a]
Crystallographic analysis			
Wavelength (Å)	0.9763	0.9792	0.8726
Space group	$P4_1$	$P4_1$	$P2_12_12_1$
Unit cell dimensions (Å)	a = b = 53.6; c = 118.4	a = b = 53.4; c = 118.7	a = 49.0; b = 75.8; c = 173.4
Resolution range (Å)	53.6 - 1.60 (1.69 - 1.60)	48.7 - 2.47 (2.61 - 2.47)	46.0 - 2.49 (2.62 - 2.49)
Reflections (measured / unique)	196159 / 43750 (28394 / 6325)	111297 / 11861 (13614 / 1647)	87182 / 23387 (12463 / 3244)
Completeness (%)	99.7 (98.7)	99.1 (94.1)	99.3 (96.3)
Multiplicity	4.5 (4.5)	9.4 (8.3)	3.7 (3.8)
R_{merge}[†]	0.046 (1.299)	0.190 (1.573)	0.103 (0.911)
$R_{p.i.m.}$[‡]	0.024 (0.688)	0.064 (0.555)	0.061 (0.531)
$\langle I/\sigma(I)\rangle$	14.3 (1.6)	7.3 (1.4)	8.6 (1.5)
Monomers per asymmetric unit	2	2	2
Mathews coefficient ($Å^3$ Da^{-1})	2.53	2.52	3.13
Solvent content (%)	51.4	51.2	60.7
Structure refinement			
Resolution range (Å)	48.8 - 1.60	-	46.0 - 2.49
R_{factor}[#] / Free R_{factor}[$]	0.202 / 0.220	-	0.207 / 0.251
Unique reflections (work / test set)	41642 / 1973	-	22057 / 1193
Water molecules	156	-	15
Total No. of atoms	2363	-	2999
No. of macromolecule atoms	2205	-	2984
r. m. s. d. bond lengths (Å)	0.011	-	0.008
r. m. s. d. bond angles (°)	1.09	-	1.38
Average overall B factor ($Å^2$)	38.1	-	77.7
Ramachandran favored (%)	97.5	-	96.0
Ramachandran outliers (%)	0.0	-	0.4
PDB entry	4cic	**-**	4chu

[a]Values in parenthesis correspond to the outermost resolution shell. Each dataset was recorded from a single crystal. [†]$R_{merge} = \sum_{hkl}\sum_i |I_i(hkl) - \langle I(hkl)\rangle|/\sum_{hkl}\sum_i I_i(hkl)$, where I_i(hkl) is the observed intensity and $\langle I(hkl)\rangle$ is the average intensity of multiple observations of symmetry-related reflections. [‡]$R_{pim} = \sum_{hkl}[1/(N-1)]^{1/2} \sum_i |I_i(hkl) - \langle I(hkl)\rangle|/\sum_{hkl}\sum_i I_i(hkl)$, where $I_i(hkl)$ is the observed intensity and $\langle I(hkl)\rangle$ is the average intensity of multiple observations of symmetry-related reflections. [#]$R_{factor} = \sum||Fo|-|Fc||/\sum|Fo|$ where |Fo| and |Fc| are observed and calculated structure factor amplitudes, respectively. [$]Free R_{factor} is the cross-validation R_{factor} computed for a randomly chosen subset of 5% of the total number of reflections, which were not used during refinement.

Chapter 3

The *E. coli* Fe/S cluster biogenesis regulator, IscR – structural fine-tuning of DNA discrimination

3.1. Summary

The ubiquitous iron-sulfur (Fe/S) cluster-containing proteins are involved in countless biological routes and play crucial roles for the functioning of both prokaryotic and eukaryotic cells. The transcription factor IscR was first implicated in the repression of the ISC (Iron Sulfur Cluster) biogenesis pathway and was shown to harbor a [2Fe–2S] cluster. Promoters controlled by IscR belong to two distinct sequence groups and the [2Fe-2S] cluster of IscR was shown to be essential for regulation of type-1 promoters (*isc, yadR, yhgI*), while apo-IscR is responsible for the regulation of type-2 promoters (*sufA*, *hyaA*, *hybO*, *napF*, *ydiU*). IscR regulation of the ISC machinery relies on a feedback mechanism fine-tuned by the cellular Fe/S cluster status, while it activates the SUF pathway to compensate for oxidative damage of Fe/S-containing proteins. Despite recent advances in understanding the regulation of *isc* and *suf* operons by environmental signals, the features of IscR modulating sequence discrimination and the structural changes associated with DNA binding specificity upon ligation of the [2Fe-2S] cluster remain poorly understood. Here we report a detailed structural and biochemical characterization of IscR suggesting that unfavorable interactions with Glu43 impair recognition of type-1 promoters by apo-IscR. Our findings suggest that binding of a Fe/S cofactor leads to the reshaping of the DNA-IscR interface for specific recognition of type-1 sites.

3.2. Introduction

Iron-sulfur (Fe/S) proteins are widely distributed in Nature and are key components in several physiological processes including respiration, photosynthesis, DNA repair, metabolism and regulation of gene expression (6, 208). Relying on their chemical versatility, Fe/S proteins can serve as regulatory sensors of diverse small molecules (36). FNR is one of the best characterized Fe/S-containing regulators, with an activation mechanism transversal to the majority of metalloregulators: the switch to a transcriptionally productive mode requires binding of a specific metal (209, 40). In contrast, the transcriptional regulator IscR has two active transcriptional forms: the clusterless (apo-IscR) and the [2Fe-2S]-bound forms that exhibit altered DNA recognition specificity and thereby control different sets of genes according to environmental conditions (146, 147, 144).

IscR belongs to the Rrf2 family of regulators, displaying the typical winged helix–turn–helix motif close to the N-terminus and a C-terminal Fe/S cluster coordinated by three cysteine and one histidine ligands (143). It is now known that the expression of ~40 genes is under the direct or indirect control of IscR, which is the key regulator of Fe/S biogenesis: the [2Fe-2S]-form of IscR represses the transcription of the *isc* operon encoding the ISC Fe/S biogenesis pathway and, under stress conditions, the apo-form activates the expression of the *suf* operon (147, 142, 145). In *E.*coli, Fe/S homeostasis is maintained through a negative feedback loop based on the ability of [2Fe-2S]-IscR to sense the cellular demand for Fe/S clusters and actively regulate the transcription of the *iscRSUA–hscBA–fdx* operon (146). Thus, due to its intrinsic sensor properties, IscR adjusts the synthesis of proteins involved in the Fe/S cluster biogenesis pathway and allows *E. coli* to cope with varying Fe/S cluster requirements.

Two distinct promoter sequences were compiled from IscR-regulated genes (147), termed type-1 and type-2 DNA-binding motifs, and whose recognition by IscR is dependent of its cluster occupancy (144). Type-1 promoters are recognized exclusively by [2Fe-2S]-IscR, whereas both [2Fe-2S]-IscR and apo-IscR interact similarly with type-2 sequences, suggesting that the Fe/S cluster is dispensable for recognition of the latter motifs (144). Given that the structure of

IscR is predicted to harbor a single wHTH DNA-binding domain, it is unexpected that it can interact and distinguish two DNA binding sites. To unveil the features underlying promoter discrimination by IscR, the three-dimensional structure of apo-IscR^{Ec} in complex with a type-2 target sequence the *hya* promoter from the hydrogenase-1 operon, was solved. This experimental model combined with biochemical studies revealed some of the molecular details involved in the unusual environmentally modulated recognition of two distinct promoter consensus sequences by IscR, using a single predicted helix–turn–helix DNA binding motif.

Our studies highlight the role of the Glu43 residue on DNA sequence discrimination by IscR and how structural changes taking place upon ligation of a [2Fe-2S] cluster contribute to broaden DNA specificity of IscR to include type-1 promoters.

3.3. Results

Apo-IscR^{Ec} induces structural changes on type-2 binding motifs

It remains unclear how cluster ligation enables IscR to recognize two very distinct DNA motifs (Fig. 7) using a single wHTH domain (146, 144). To address this question, DNA-binding assays using an IscR variant (apo-IscR^{Ec}) with the putative cluster-coordinating cysteine residues mutated to serines (C92/98/104S) were performed. Conservative replacement of the cysteine ligands ensures a minimal structural and functional impact, as well as a homogeneous apo-protein preparation lacking the Fe/S cluster. The CD spectra obtained for the *hya* binding sequence (*hyaEc*, Table 3) display the characteristic features of B-form DNA with a negative peak at ≈240nm and a positive peak centered at ≈277nm (blue line, Fig. 9A) (210). Conformational changes in the DNA can be monitored within this region because there is no ellipticity from the intrinsic Cotton effect of the protein (211). A large increase in the magnitude of the CD signal (≈85% increase in the Δε value at saturation) with a slight wavelength shift to 272 nm following sequential additions of apo-IscR^{Ec} indicative of productive binding of apo-IscR^{Ec} to the *hya* binding site. Although the shift blue shift of the signal maximum is not readily interpreted, it can be a consequence of, for example, DNA unwinding induced by protein binding (212). Both DNA and protein concentrations were kept well above the previously determined apparent K_d of apo-IscR^{Ec} binding to the *hya* sequence (≈44±3 nM) to ensure that binding would occur in a 1:1 ratio and allow stoichiometric determination (144). It is clear that the ellipticity changes (ΔΔε) increase to a plateau at approximately 2:1 molar ratio of apo-IscR^{Ec}:*hya* (Fig. 9B). Since *E. coli* IscR was shown to be a dimer in solution, this means that each *hya* duplex is recognized by one dimer of apo-IscR^{Ec}. This observation is in contrast with previous results indicating that two dimers of *E. coli* IscR (both *wild-type* IscR and IscR-C92/98/104A) bind to one *hya* site (144).

DNA bending is an important structural feature for base read-out in protein-DNA interactions and even small distortions can fine-tune sequence recognition by favoring the formation of specific contacts (213). To further investigate the features modulating DNA recognition by IscR, we performed a DNA bending assay using the pBend5 vector that contains duplicate sets of restriction sites (214). This assay

allows an empirical estimation of the magnitude of bending induced by a specific DNA-binding protein, such as IscR. Following the *hya* promoter (*hya_bend*, Table 3) cloning into the pBend5 vector, a set of DNA fragments with identical sizes but displaying distinct relative positions of the protein-binding site were generated by digestion (Fig. 9C). The electrophoretic mobility of bent DNA is dependent upon the location of the bend; migration delay is greatest when the DNA is bent at its center and smallest when near its end (215). Gel retardation analysis clearly shows that the fragment with the most centrally positioned *hya* binding sequence (*EcoRV*, Fig. 9C, 9D) has minimum mobility and that mobility increases as the binding site is placed nearer the ends of the fragment (*BamHI* and *MluI*, Fig. 9C, 9D). Fragments obtained after digestion with *Bam*HI and *Mlu*I have virtually identical mobility in the absence of apo-IscR^{Ec}, suggesting that the *hya* site did not contain significant intrinsic DNA bending prior to complex formation. Taking into consideration the mobility of each *hya* fragment in complex with apo-IscR^{Ec}, it was estimated that the *hya* sequence is distorted approximately 24º±2º from linearity (196). However, this analysis is influenced not only by protein-induced bends, but also by other distortions in DNA structure as a consequence of protein shape or DNA flexibility (212). Thus, the value obtained can reflect more than one type of DNA structural change and is better described as DNA flexure angle. Nevertheless, these results suggest that binding of one apo-IscR^{Ec} dimer to the *hya* promoter sequence is accompanied by structural deformations, though their nature could not be distinguished by the techniques used.
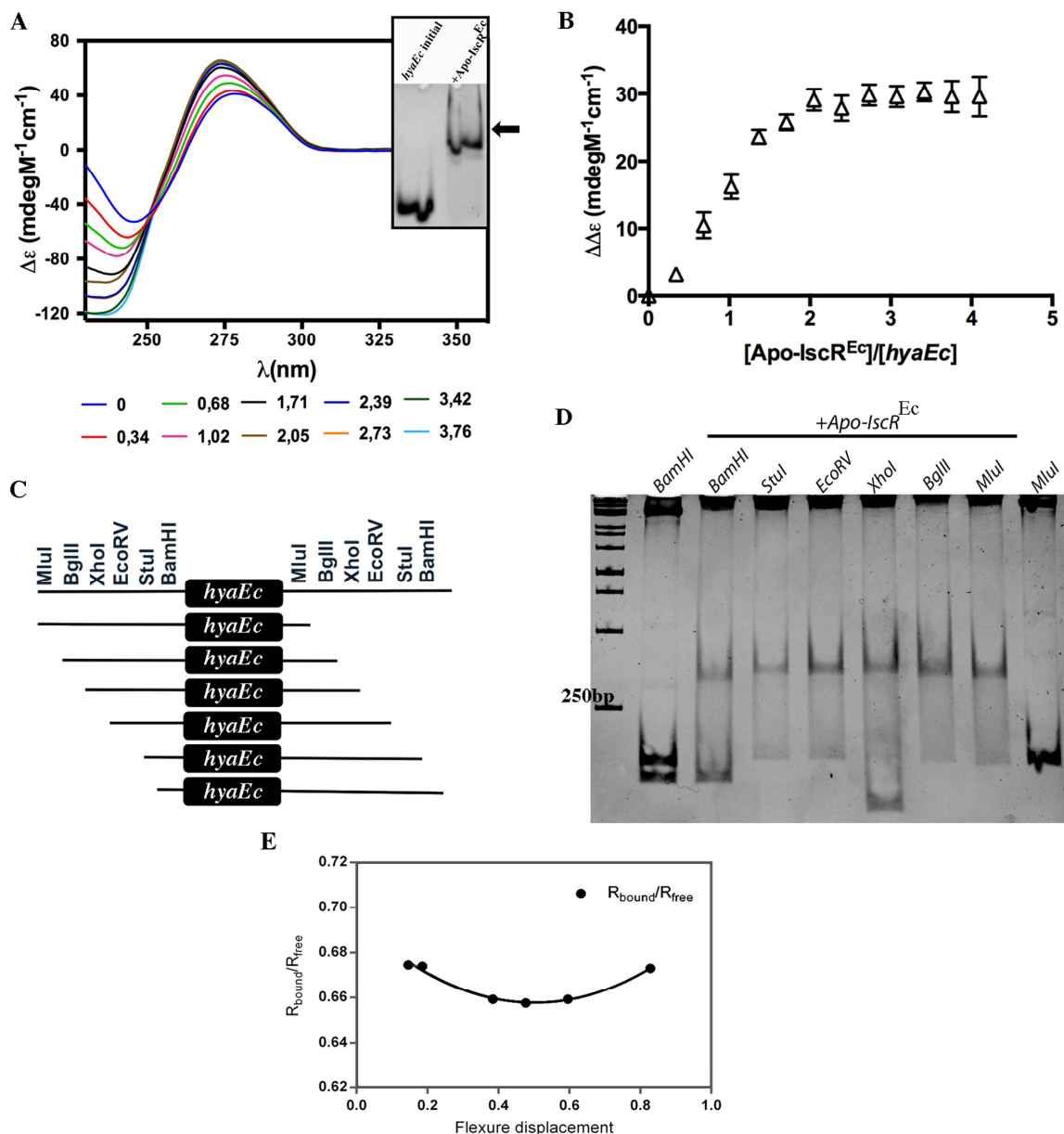
Fig. 9 - Apo-IscR^{Ec} binding to type-2 promoter sequences. (A, B) Apo-IscR^{Ec} binds as a dimer and induces structural deformations in the *hya* promoter sequence. A - CD spectra following apo-IscR^{Ec} binding to the *hyaEc* sequence (*hyaEc*, Table 3). Scans were taken from 230 to 360 nm following sequential additions of apo-IscR^{Ec} (235 μM). Representative spectra corresponding to protein:DNA ratios of 0, 0.34, 0.68, 1.02, 1.37, 1.71, 2.05, 2.39, 2.73, 3.07 3.42, 3.76, 4.10 are shown. Experiments were carried out in 40mM Tris-HCl pH 7.5, 150mM KCl, 1mM DTT, 5% glycerol (vol/vol). Inset shows an electrophoretic mobility shift assay assessing complex formation immediately after the CD titration. The band-shift corresponding to the apo-IscR^{Ec}:*hya* complex is denoted by an arrow. (B) The change in the CD spectrum of the *hyaEc* sequence following sequential additions of apo-IscR^{Ec} is indicative of a 2:1 apo-IscR^{Ec}:*hya* complex. Values of Δε were taken at the peak maxima wavelength of the CD spectra (272 nm) shown in A. (C-E) The *hya* binding site is bent by apo-IscR^{Ec}. C - Schematic representation of the *hya* site (*hya_bend*, Table 3) inserted between the *Mlu*I–*Bam*HI restriction sites of the pBend5 vector. The region delimited by the *Mlu*I–*Bam*HI recognition sequences contains restriction sites in duplicate to generate DNA fragments that are identical in length but contain the protein-binding sequence (black rectangle, *hyaEc*) at different positions. D - Gel electrophoresis of permuted fragments containing the *hyaEc* recognition site. Apo-IscR^{Ec} protein was mixed separately with 6 different fragments. The DNA fragments used were generated by digestion restriction enzymes, which, from left to right, are *Mlu*I, *Bgl*II, *Xho*I, *Eco*RV, *Stu*I, and *Bam*HI. 100-bp DNA ladders were used for comparison and the

250bp ladder band is indicated. E - Calculation of the flexure angle of the *hyaEc* sequence induced by apo-IscR^{Ec}. The mobility of the apo-IscR^{Ec}:hya complexes (R$_{bound}$) was normalized to the mobility of the corresponding free probe (R$_{free}$). Flexure displacement corresponds to the ratio between the distance from the 5' end of each fragment to the center of the *hyaEc* binding site and the full size of the probe. The plotted points were fitted with a quadratic function: $y = 0.1445x^2 - 0.1450x + 0.6941$ ($r^2 = 0.983$). The first and second order parameters of the equation are in close agreement and estimate a *hyaEc* flexure angle of 24°±2.

Structure of apo-IscR^{Ec} bound to a type-2 promoter

In order to better grasp the fine molecular details of specific promoter sequences recognition by IscR, the structure of apo-IscR^{Ec} in complex with one of its type-2 target sequences, the *hya* promoter, was determined using orthorothombic (P$_{444}$) crystals diffracting to 2,5 Å (Table 4). The asymmetric unit contained the apo-IscR^{Ec} biological dimer bound to a 26-base double stranded oligonucleotide with a single nucleotide overhang at the 5'-end of each strand (*hya_26_OH*, Table 3, Fig. 10A). This structure is highly similar to the recently reported model of apo-IscR^{Ec} (C92/98/104A mutant) in complex with DNA (PDB entry 4HF1; (216)), superposing with a r.m.s.d. of 0.5 Å for 124 aligned Cα atoms.

The apo-IscR^{Ec} monomer is mostly α-helical and encompasses two central structural features: a DNA-binding domain and a dimerization helix (Fig. 10B, 10C). Residues 88 to 103, encompassing part of the putative iron-sulfur cluster-binding region (Fig. 10B), are disordered in both monomers and could not be modeled (Fig. 10A-C). The structures of the monomers are nearly identical, superposing with an r.m.s.d. of 1,2 Å for 115 aligned Cα atoms. The characteristic wHTH domain of Rrf2 regulators involved in DNA-recognition is formed by helices α2, α3, β-strands β1 and β2 and the wing (Fig. 10B, 10C). The length of the dimerization helix allows for the placement of each DNA-binding domain at the extremes of the dimer, as well as for the DNA-recognition helix (α3) of each monomer to specifically recognize the major groove and the wing to interact with adjacent minor grooves (Fig. 10A). Such structural architecture accounts for the somehow unexpected ability of IscR to recognize DNA sequences that are relatively long imperfect palindromes (Fig. 7) (147).

A

B

C
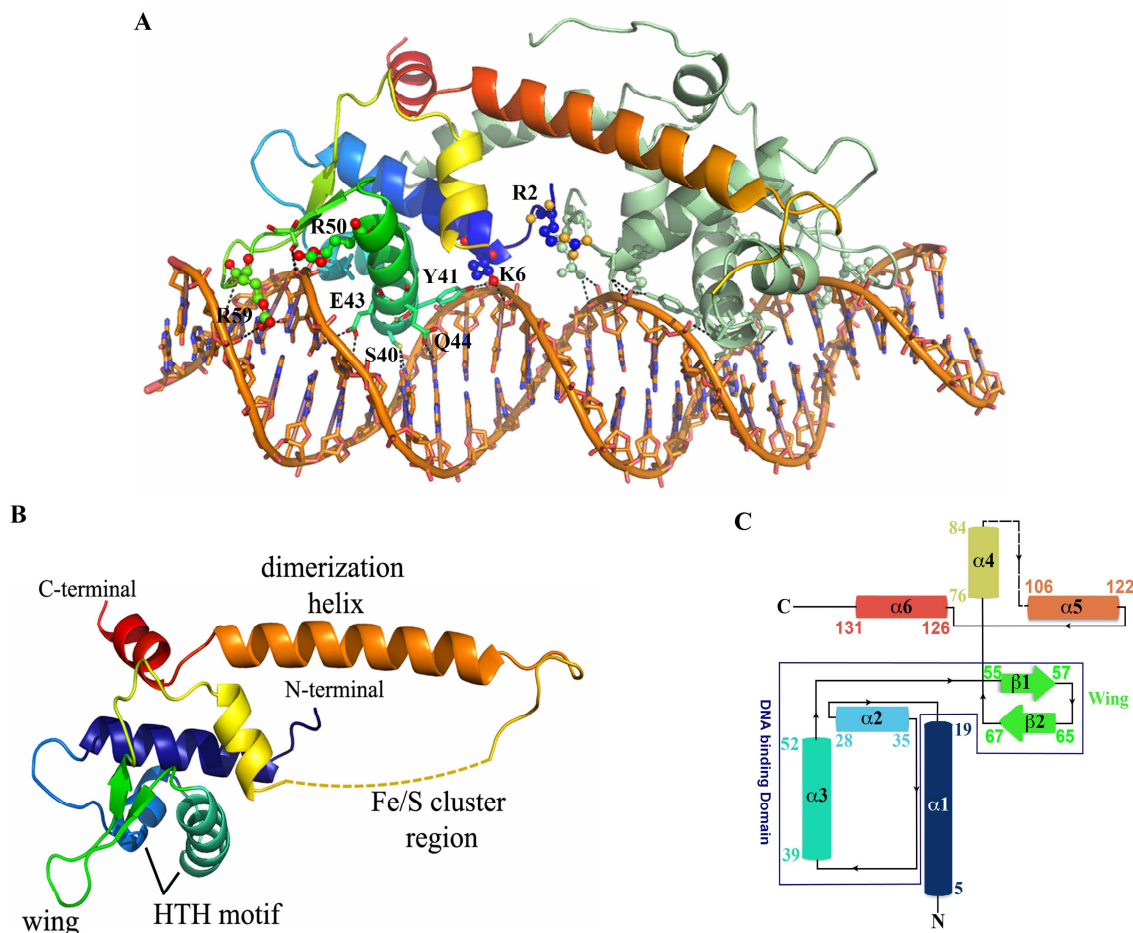
Fig. 10 – The 3D structure of apo-IscR^{Ec} bound to the *hya* promoter. (A) Interactions at the DNA-recognition interface. One of the monomers is colored from N- (blue) to C-terminal (red). Residues making contacts with the DNA are highlighted as sticks and basic residues as spheres. Hydrogen bonds between apo-IscR^{Ec} and DNA are represented as dotted lines. (B) Ribbon representation of the apo-IscR^{Ec} monomer. (C) Topology diagram of the apo-IscR^{Ec} monomer. Secondary structure element colors match those on B.

Apo-IscR^{Ec} dimer formation involves mostly interactions between residues from helix α5 of one monomer and helix α6 of the neighboring subunit, but residues from helices α1 and α2 also contribute to stabilize the homodimer (Fig. 11). Overall, 42 amino acids from monomer A and 40 amino acids from monomer B are found at the inter-subunit interface. Each monomer buries ~17% (1692 Å^2) of its total solvent accessible surface. The main chain of Arg116 crosslinks the dimerization helix α5 of one monomer with the C-terminal helix α6 of the opposing subunit (Fig. 11). Arg116 from one monomer forms a salt bridge with Glu128 OE1 and OE2, whereas Arg116 from the adjacent monomer hydrogen bonds to Asn132 OD1 and the main chain oxygens of Gln133 and Glu134. The inter-monomer association of helices α5 and α6 is further achieved by an interaction between the

side chains of Asn132 ND2 and Asp112 OD2, being locked on each side by one hydrogen bond involving Thr106 OG1 and Glu35 NE2 residues. Further polar interactions at the dimer interface are formed between the main chains of neighboring Leu3 residues.
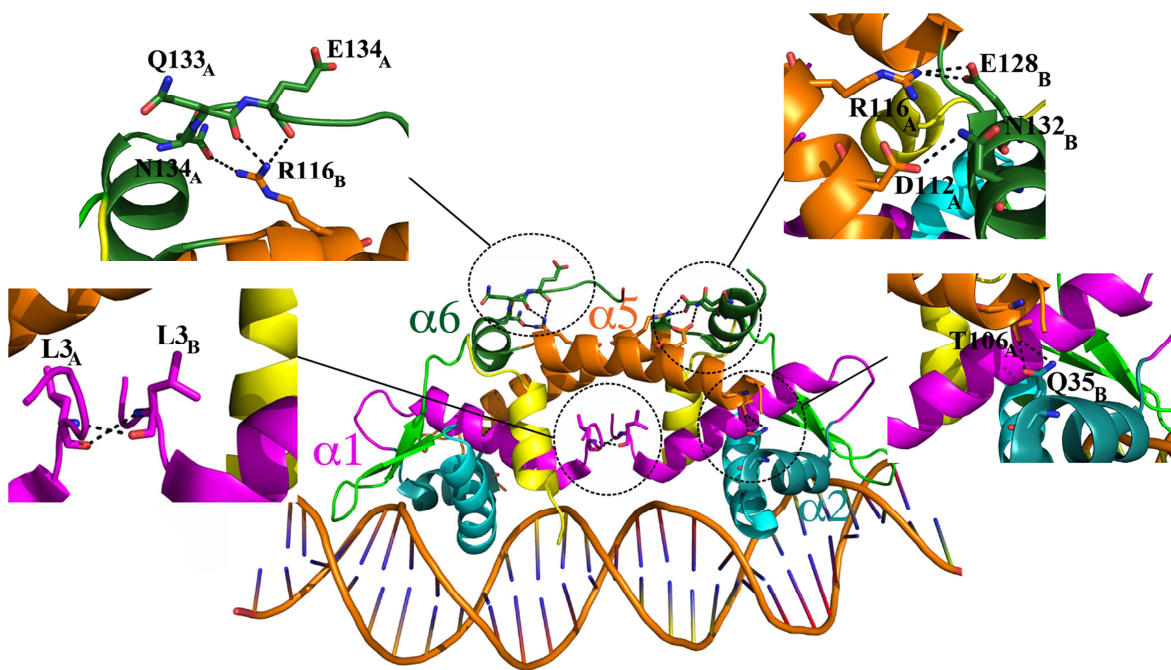
Fig. 11- Dimerization interface of apo-IscR^{Ec} in complex with the type-2 *hya* sequence. Relevant interactions for dimer formation and stabilization are highlighted. Both monomers are colored from N- (magenta) to C-terminal (green), with highlighted residues (from either monomer A or B) represented as sticks and color-coded (nitrogen blue, oxygen red) . Hydrogen bonds are represented as dashed lines.

Structural changes of apo-IscR^{Ec} upon binding to the *hya* sequence

When bound to apo-IscR^{Ec}, the *hya* sequence is bent ~10.2°±2.1 relatively to ideal B-DNA, whereas the DNA is slightly undertwisted (33°±4.0 for *hya* compared to 35–36° for the canonical B-DNA) (217). In the complex, helix α3 of the winged-helix motif from each apo-IscR^{Ec} monomer sits in the major groove of each *hya* half-site, whereas the β-hairpin folds deeply into the minor groove (Fig. 10A). Comparison with the previously reported structure of the unligated dimeric form of *E. coli* apo-IscR (C92/98/104A mutant; PDB entry 4HF0; (216)) revealed that apo-IscR^{Ec} retained the same general structure when in complex with its cognate DNA (Fig. 12A), which is evidenced by the r.m.s.d. of 1.4 Å for 120

aligned Cα atoms when superposed to free *E. coli* apo-IscR (PDB entry 4HF0, (216)).
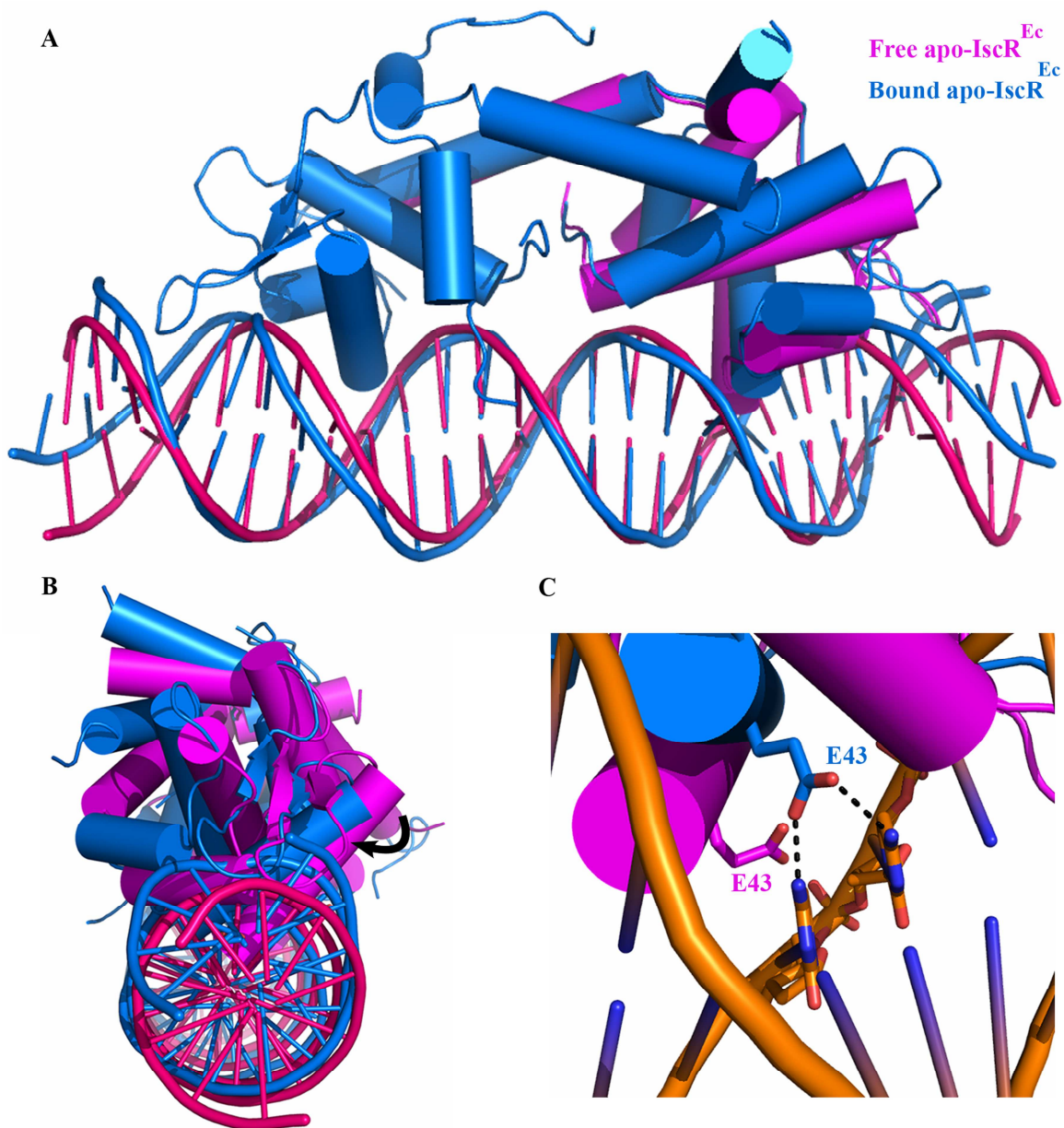
Fig. 12 – Recognition of *hya* promoter by apo-IscR^{Ec} requires only minor structural changes. (A, B) Superposition of the unligated *E. coli* apo-IscR structure (C92/98/104A, PDB entry 4HF0, (216)) with that of apo-IscR^{Ec} bound to the *hya* promoter sequence. Free and DNA-bound conformations are represented in mangenta and blue, respectively. The structure of unligated *hya* was modeled using the 3D-DART server. (218). (B) Specific contacts established within the DNA major groove require a rotation of the DNA-recognition helix α3. The molecules were rotated ~90° around y, relative the view in A and colored as in A. An arrow indicates the movement of the helix α3 upon DNA binding. (C) Close-up view of the Glu43 side chain shift upon DNA binding with the concomitant formation of a specific bidentate interaction. The Glu43 side chain is represented as sticks with carbon atoms in mangenta (unligated conformation) or blue (*hya* bound conformation) and oxygen atoms in red.

Overall, DNA binding induces a small concerted movement of the wing-helix motif within each apo-IscR^{Ec} monomer together with dimerization helix α5 of the adjacent monomer. Upon binding, the two monomers suffer a 20⁰ rotation relative to each other, which favors the interaction of the recognition helix (α3) with the DNA major groove (Fig. 12B). Particularly, the ☐helix α☐ movement allows Glu43 to come closer to the major groove and engage in a specific bidentate interaction with bases from each half-site (Fig 12C). Aside these, only subtle structural changes in the apo-IscR^{Ec} dimer were necessary for *hya* promoter recognition, namely the side chain of Arg59, whose density was missing in the unbound structure, became ordered upon interaction with the DNA minor groove AT-rich region (216).

Molecular details of apo-IscR^{Ec}-*hya* interaction

Consistent with its DNA-binding activity, the surface electrostatic potential of apo-IscR^{Ec} biological dimer is highly polarized with a patch of basic residues on the DNA-interacting surface (Fig. 13). Although the positive charge distribution might be relevant for protein orientation towards effective interaction with the DNA through non-specific contacts with the backbone phosphates, in the apo-IscR^{Ec}-DNA complex very few interactions involve lysine or arginine side chains. The side chains of Lys6 serve as placeholders by establishing a symmetric interaction with the backbone phosphodiester linking T15-T16 from one half-site and C16'-T17' from the other DNA duplex half-site, whereas the non-conserved Arg2 side chain from one of the monomers interacts with the backbone phosphate linking T15 and T16 (Fig. 10A). Although the conserved Arg50 is placed in the vicinity of the phosphate group linking T5 and C6 or A6' and C7', it is only involved in Van der Waals contacts. Additional hydrogen bonds with backbone phosphates are established by the strictly conserved side chains of Ser38, Tyr41, Tyr65 and Ser57, and by the main chain of Leu28, providing binding energy to stabilize the recognition helix at the major groove (Fig. 14A, 14B). Further stabilizing stacking interactions take place within the minor groove involving Ser5 and the conserved Tyr9 residues. The Ser5 side chain from one of the monomers also engages in a polar contact with the DNA backbone (Fig. 14B).
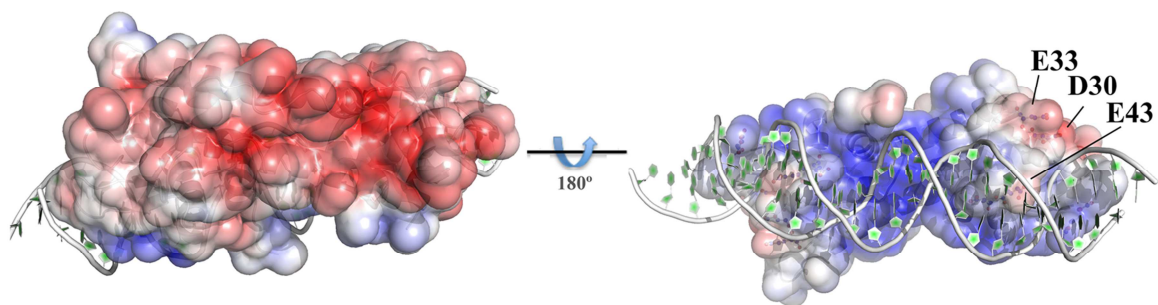
Fig. 13 – An asymmetric electrostatic surface orients the functional apo-IscR^{Ec} dimer toward its *hya* DNA target. Positive surface electrostatic potential is shown in blue and negative in red. The DNA molecule backbone is depicted as a white ribbon with bases in green.

Residue Arg59 from each monomer, in the β-hairpin wing, sits deeply in the corresponding AT-rich region of the DNA minor groove (Fig. 10A). Although minor grooves are not typically involved in base-specific hydrogen bonds, their shape enhances the electrostatic potential, especially if they encompass more negative AT-rich stretches (219, 220). The placement of the Arg59 basic side chain, equidistant to the sugar-phosphate backbones of both DNA strands, creates an optimal platform for interaction with these AT-rich segments. Additionally, Arg59 engages in base-specific hydrogen bonds to T'25 and T5 on one half site and T24 on the symmetrical site (Fig. 14A). Indeed, short runs of four to six adenine–thymine residues, known as A-tracts, are often the structural basis of narrow minor grooves and are usually recognized by arginine residues (221, 219). In line with these observations, elimination of the Arg59 side chain was shown to impair recognition of either type-1 or type-2 promoter sequences by *E. coli* apo-IscR (216). Further, highlighting the crucial role of the Arg59 side chain in DNA recognition, a GC base-pair mutation within the AT-rich region abrogated IscR binding (144). Additional Van der Waals interactions with the minor grove involve residues from the tip of the wing (Gly60-Pro61) placed between the sugar moieties of A3, A4 and T27' (A4', T26, G27 on the other half-site) (Fig. 14A).

The clustering of apo-IscR^{Ec} acidic residues contributes to the partial negative charge within the DNA-binding surface (Glu33, Asp30 and Glu43) (Fig. 13). However, only Glu43 establishes specific contacts with the DNA duplex. This negatively charged residue, together with Gln44 and Ser40, participates in the base-specific read-out of the major groove (Fig. 14B, 14C). Glu43 specifically interacts with the highly conserved C6-C7 dinucleotide and the C7'-A8' pair in the

opposite half-site, whereas Gln44 and Ser40 hydrogen bond to T19' and G20' (T18 and A19 in the opposite half-site), respectively.
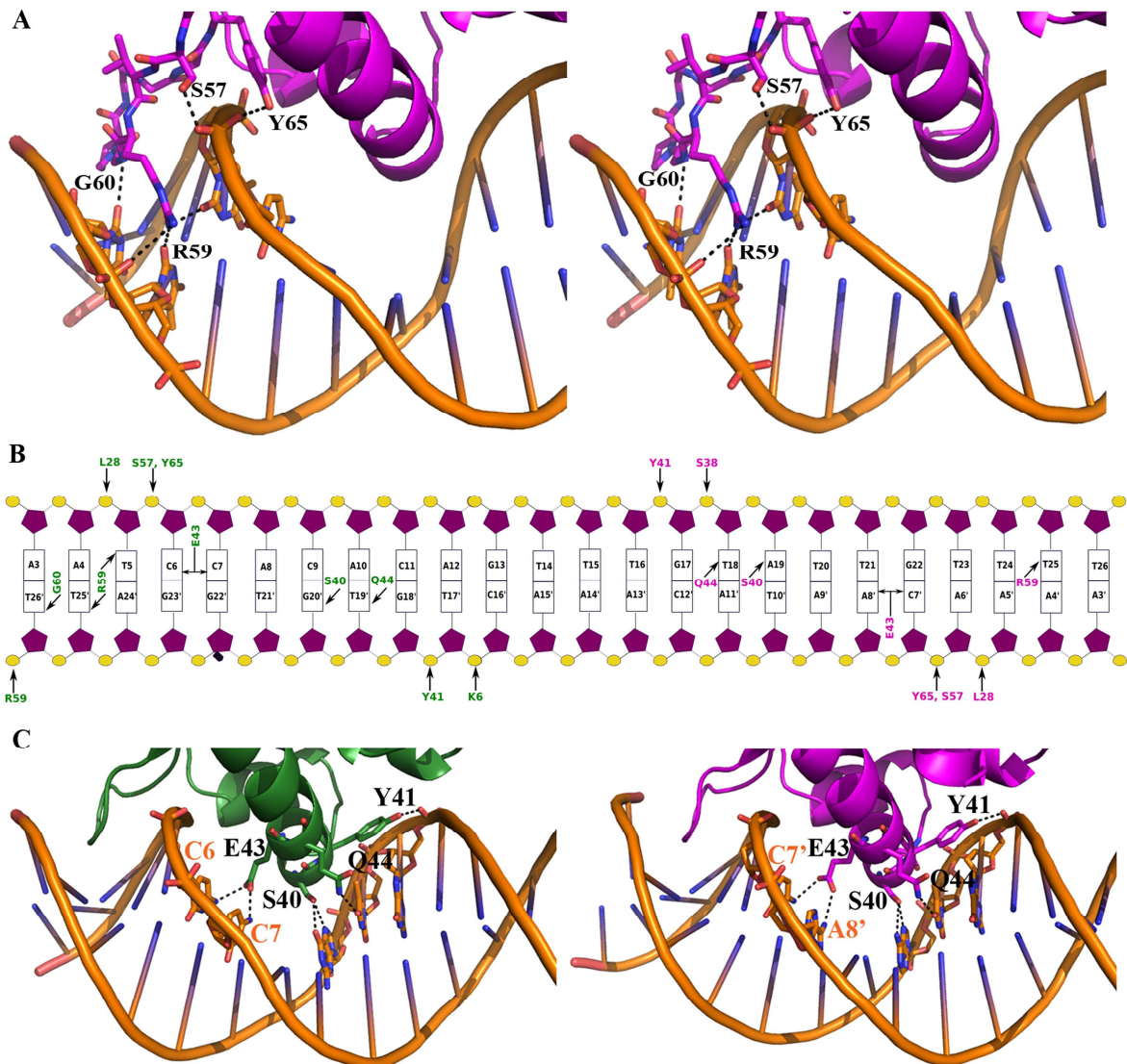
Fig. 14 – Interactions involved in the recognition of the *hya* binding site by apo-IscR[Ec]. (A) Stereoscopic view of Interaction of the residues within the wing of apo-IscR[Ec] and the DNA minor groove. DNA is represented as an orange ribbon with carbon atoms in orange, oxygen atoms in red, nitrogen atoms in blue. Wing residues are represented as sticks with carbon atoms shown in mangenta, oxygen atoms in red and nitrogen atoms in blue. (B) Schematic representation of contacts between apo-IscR[Ec] and the *hya* sequence. Contacts involving apo-IscR[Ec] monomer A and monomer B are colored in green and mangenta, respectively (C) Specific interactions between residues of the recognition helix (α□□□of each monomer of apo-IscR[Ec] and the DNA major groove. Dashed lines indicate hydrogen bonds. Monomer A is colored green (left panel) and monomer B magenta (right panel). Atom colors as in B.

Apo-IscR[Ec] E43A does not discriminate for the C6-C7 dinucleotide in the *hya* promoter sequence

Coordination of the Fe/S cluster by *E. coli* IscR was shown to involve its three cysteine residues (C[92, 98, 104]) and one histidine (H[107]) (143), discarding the proposal that the Glu43 residue could serve as the fourth cluster ligand (222). Consistent with this observation, the crystal structure of *B. subtilis* Rrf2 regulator CymR showed that the Glu43 residue did not seem to be structurally available to pose as a cluster ligand (163). From all the highly conserved residues within the recognition helix interacting with the *hya* sequence (Fig. 14C, 15A), Glu43 is the only residue making a specific bidentate interaction with a highly conserved CC dinucleotide in the type-2 DNA binding motif (Fig 7, 14B, 14C). To assess how elimination of the Glu43 side chain would affect DNA recognition by apo-IscR[Ec], we followed apo-IscR[Ec] E43A binding to the *hya* sequence by circular dichroism (Fig. 15B). Similar to what was observed with apo-IscR[Ec] (Fig. 9B), the Δε value for the *hya* sequence increases linearly with sequential additions of apo-IscR[Ec] E43A variant until a 2:1 protein-DNA ratio is reached, indicating strong stoichiometric binding. Apo-IscR[Ec] E43A retains binding specificity, being able shift the *hya* sequence (*hyaEc*, Table 3) in the presence of a randomized competitor (*random*, Table 3, Table 5, Fig. 16A).

Table 5 - Binding affinities between Apo-IscR[Ec] E43A and type-1 and type-2 promoter sequences determined by microscale thermophoresis

DNA sequence	Dissociation constant - K_d (nM)
hyaEc	180 ± 18
iscbEc	154 ± 7
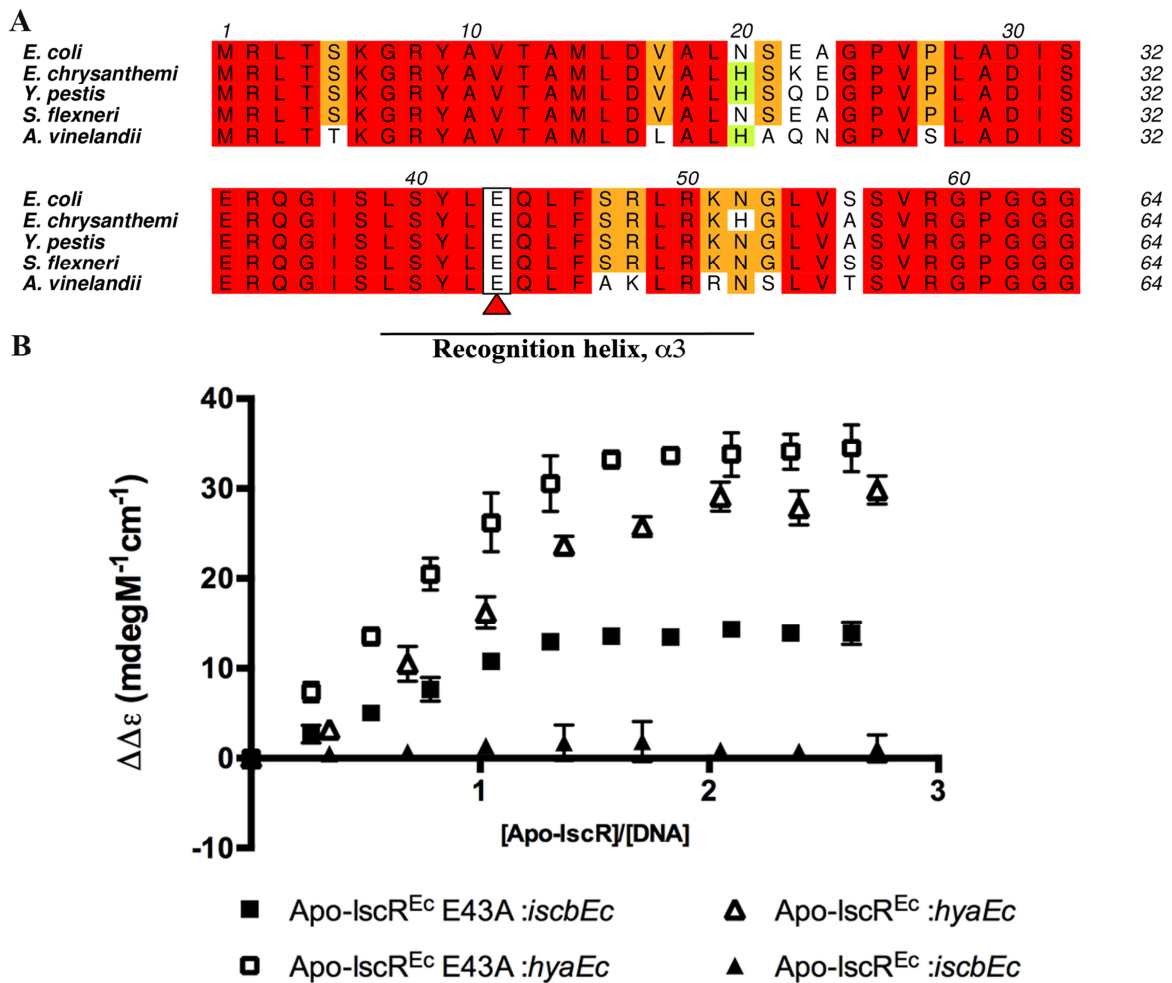
Fig. 15 – Interaction of apo-IscR^{Ec} E43A with type-1 and type-2 binding sites. (A) Glu43 is fully conserved among IscR proteins from Gram-negative bacteria. Amino acid sequence alignment of representative IscR proteins from Gram-negative bacteria: *Escherichia coli* (P08AGK), *Erwinia chrysanthemi* (E0SAX8), *Yersinia pestis* (Q0WD07), *Shigella flexneri* (P0AGL1), *Azotobacter vinelandii* (O69219). The Glu43 residue is highlighted with a red triangle, other strictly conserved amino acids are colored in red and recognition helix α□□is underlined. Increasing residue conservation is represented by a color gradient from green to red. Alignment prepared with ClustalW (161) and colored with Aline (162). (B) Apo-IscR^{Ec} E43A interacts similarly with type-2 *hyaEc* and type-1 *iscbEc* sequences. Curves correspond to titration of the *hyaEc* and *iscbEc* sequences (Table 3) with either apo-IscR^{Ec} (triangles) or apo-IscR^{Ec} E43A (squares). Values of Δε were taken at 272 nm for sequential additions of protein.

Given the specific bidentate interaction of the Glu43 residue with type-2 sequences, the fact that substitution of this amino acid by an alanine had little effect on the DNA-binding activity of IscR was unexpected. One reasonable explanation is that elimination of the Glu43 side chain influences specificity, rather than binding affinity. Indeed, the apo-IscR^{Ec} E43A bound to the *hya* site with similar affinity as the wild-type protein (216). However, it did not discriminate between nucleotide bases at positions 6 or 7, since cold sequences mutated at the C6-C7 positions (Table 3) were able to compete with the *hya* sequence for binding

to this variant but not for the apo-IscR[Ec] protein (Fig. 16B). Therefore, substitution of Glu43 for an alanine does not perturb substantially the recognition of the *hya* promoter nor the stoichiometry of the complex. During the course of this work, the structure of the IscR[Ec] E43A variant bound to the *hya* sequence (C92/C98/C104/E43A, PDB entry 4HF2, (216)) was solved and, despite losing specificity for the symmetrical CC dinucleotide, this variant was otherwise similarly bound to the *hya* site and retained all other specific interactions (216).
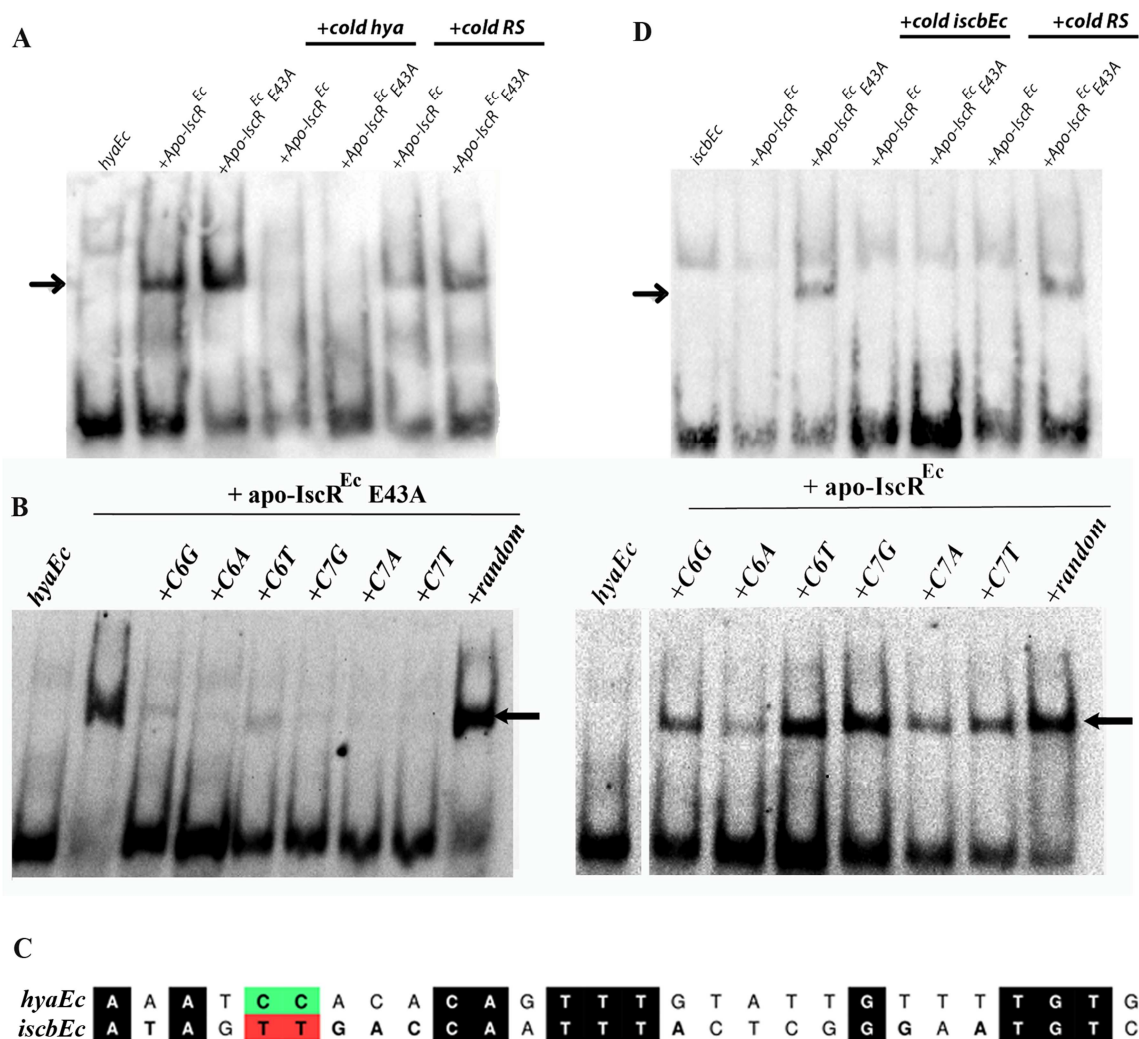
Fig. 16 - Glu43 role in the DNA sequence discrimination by *E. coli* IscR. (A) Recognition of the *hya* promoter by IscR is unaffected by elimination of the Glu43 side chain. Competition assay using a 100x fold molar excess of cold competitors, either specific (cold *hyaEc*) or non-specific (cold *random sequence*, RS). (B) Apo-IscR[Ec] E43A looses discrimination against the well-conserved CC dinucleotide in type-2 binding sites. Cold *hyaEc* sequences mutated at either the C6 (C6G, C6A or C6T, Table 3) or the C7 (C7G, C7A or C7T, Table 3) bases compete significantly with the wild type *hyaEc* sequence for binding to apo-IscR[Ec] E43A (left panel), whereas binding to apo-IscR[Ec] is mostly unaffected by the presence of cold competitors (right panel). (C) Type-2 CC dinucleotide (green) is replaced by a TT dinucleotide (red) in type-1 binding sites. Conserved nucleotides are colored in black. DNA sequence alignment was performed with ClustalW (161) and colored with Aline (162). (D) The single E43A mutation allows apo-IscR[Ec] to specifically recognize type-1 motifs.

Competition assay using a 100x fold molar excess of cold competitors, either specific (cold *iscbEc*) or unspecific (cold RS, random sequence). DNA sequences used in this group of experiments are listed in Table 3.

Glu43 discriminates against Type-1 promoters

Unlike type-2 sequences, in type-1 promoters the C6-C7 bases are replaced by a TT dinucleotide (Fig. 16C). Given that apo-IscR recognizes type-2 but not type-1 promoter sequences, a possible inhibitory interaction of Glu43 with the T6-T7 bases that could somehow prevent recognition of type-1 promoters by apo-IscR was proposed (147). Indeed, Apo-IscR^{Ec} E43A specifically recognized the type-1 *iscbEc* sequence (Table 3, Fig. 16D). These results were further substantiated by microscale thermophoresis measurements that yielded a K_d of 154 nM for Apo-IscR^{Ec} E43A binding to the *iscbEc* sequence, a value that is in close agreement with the K_d obtained for the *hyaEc* sequence (Table 3, Table 5) and is indicative that the Glu43 residue does not contribute substantially to the binding energy to either type of site. In line with previous results linking the Fe/S cluster of IscR to the recognition of type-1 promoters (147, 159, 142), apo-IscR^{Ec} was unable to recognize the *iscb* sequence (Fig. 16D).

In summary, these findings suggest that elimination of the Glu43 side chain probably lifts the unfavorable interactions with sequences containing thymine at positions 6 and 7, due to lack of suitable hydrogen-bond donors. Hence, Glu43 residue is a crucial selectivity filter that negatively affects binding of *E. coli* apo-IscR to type-1 binding motifs, thereby linking specific recognition of these sequences by *E. coli* IscR to conformational rearrangements following binding of the [2Fe-2S] cluster. These results are substantiated by the findings of other research group (216) and demonstrated the key role of Glu43 in sequence discrimination.

3.4. Discussion

In *E. coli*, IscR is a master transcriptional regulator controlling the expression of systems dedicated to the biogenesis of Fe/S clusters, as well as the O_2-dependent expression of several Fe/S-containing proteins (147). According to its cluster occupancy, which is modulated by O_2 availability *in vivo*, IscR controls the expression of two sets of target promoters containing distinct DNA motifs (146, 144). The biochemical and structural analysis of IscR variants reported here unveils determinant features underlying DNA recognition that explain how cluster ligation enables IscR to specifically discriminate between two types of binding sites through a single DNA-binding domain, an ability undescribed for any other transcription factor.

The structure of the apo-IscR[Ec]:hya complex resembles those described for other regulators of the Rrf2 family, containing a wHTH DNA-binding domain that greatly contributes to specific recognition of the type-2 binding site (169, 163). Binding to the *hya* sequence is accompanied by mild structural changes and induces a relatively small DNA bend, suggesting that apo-IscR is naturally shaped to recognize type-2 DNA motifs. The wing residue Arg59 interacts extensively with the AT-rich minor groove region and provides an anchoring point for IscR's accurate placement and concomitant DNA sequence read-out. Specific binding is strengthened by interactions between major groove cytosines (C6C7 and C7'), purines (A19 and G20') and thymines (T18 and T19') and the side chains of Glu43, Ser40 and Gln44, respectively. The contact between Glu43 and two consecutive bases is somewhat striking because bidentate interactions are normally restricted to single base positions (223). Despite the bidentate contact between the highly conserved Glu43 residue and the C6C7 and C7´A8´ dinucleotides in each *hya* half-site, this interaction contributes less than expected for the overall complex affinity. Thus, the interaction between Glu43 and the CC dinucleotide poses as a central feature in the DNA-protein interface responsible for site-specific interaction of apo-IscR[Ec] with type-2 sequences.

While involved in specific recognition of type-2 motifs, the Glu43 residue is used to discriminate against type-1 sequences. At physiological pH, this residue is expected to have hydrogen acceptor groups but not donor groups, and therefore

can only form hydrogen bonds with cytosine and adenine bases (224). Lack of energetically favourable interactions between Glu43 and the conserved T6T7 dinucleotide in one half-site of type-1 sites may negatively affect the placement of the recognition helix within the DNA major groove, thereby limiting productive binding to type-1 motifs. Consistent with this hypothesis, specific interaction of apo-IscR with the type-1 *isc* promoter sequence was possible through the replacement of the Glu43 residue by an apolar and smaller residue, such as alanine. Consequently, one can speculate that at least part of the role of Fe/S cluster binding is the removal of the Glu43 negative effect on high-affinity binding to type-1 promoters.

By using a structure-guided mutagenesis approach, a key sequence discriminatory role for Glu43 could be unveiled. Relocation of this residue upon cluster binding is crucial for type-1 promoters specific recognition, suggesting that reversible Fe/S cluster ligation enables IscR to act as a sensor of Fe/S cluster homeostasis through a switch in its target-site specificity.

.

Chapter 4

The unique regulation of Fe/S cluster biogenesis in a Gram-positive bacterium

4.1. Summary

Iron-sulfur clusters function as co-factors of a wide range of proteins, with diverse molecular roles in both prokaryotic and eukaryotic cells. Dedicated machineries assemble the clusters and deliver them to the final acceptor molecules in a tightly regulated process. In the prototypical Gram-negative bacterium *E. coli*, the two existing iron-sulfur cluster assembly systems, ISC and SUF, are closely interconnected. The ISC pathway regulator, IscR, is a transcription factor of the helix-turn-helix type that can coordinate a [2Fe-2S] cluster. Redox conditions and iron or sulfur availability modulate the ligation status of the labile IscR cluster, which in turn determines a switch in DNA sequence specificity of the regulator: cluster-containing IscR can bind to a family of gene promoters (type-1), while the cluster-less form only recognizes a second group of sequences (type-2).

However, iron-sulfur cluster biogenesis in Gram-positive bacteria is not so well characterized, and most organisms of this group display only one of the iron-sulfur cluster assembly systems. A notable exception is the unique Gram-positive dissimilatory metal reducing bacterium *Thermincola potens*, where genes from both systems could be identified, albeit with a diverging organization from that of Gram-negative bacteria. We demonstrated that one of these genes encodes a functional IscR homologue, and is likely involved in the regulation of iron-sulfur cluster biogenesis in *T. potens*. Structural and biochemical characterization of *T. potens* and *E. coli* IscR revealed a strikingly similar architecture and unveiled an unforeseen conservation of the unique mechanism of sequence discrimination characteristic of this distinctive group of transcription regulators.

4.2. Introduction

Iron-sulfur (Fe/S) proteins play crucial roles for the functioning of both prokaryotic and eukaryotic cells, being required for biological functions ranging from electron transport to redox and non-redox catalysis, and from DNA synthesis and repair to sensing in regulatory processes (7). The main role of the Fe/S cluster assembly machineries is to mobilize iron and sulfur atoms from their storage sources, assemble the two components into a Fe/S cluster, and then transfer the newly formed cluster to the final protein acceptors (73). In *Escherichia coli*, there are two of these Fe/S cluster "factories", the ISC (<u>I</u>ron <u>S</u>ulfur <u>C</u>luster) and SUF (SUlFur assimilation) systems whose corresponding genes are organized in two operons, *iscSUA-hscBA-fdx* and *sufABCDSE*, respectively (73, 225). Deletion mutants of the ISC system display a variety of growth defects due to loss of Fe/S cluster-containing enzyme activity and disruption of sulfur metabolism, whereas failure of both the ISC and SUF systems leads to synthetic lethality (226, 101).

In *E. coli*, the ISC machinery is considered the housekeeping system responsible for the maturation of a large variety of Fe/S proteins, whereas the SUF system is triggered under stress conditions, such as oxidative stress or iron starvation (85). IscR is a [2Fe-2S] cluster-containing transcription factor with a single predicted helix–turn–helix motif, first identified for its role in regulating expression of the ISC biogenesis pathway (142) and subsequently found to control the expression of more than 40 genes in *E. coli* (147, 142). According to the currently accepted model for Fe/S cluster biogenesis, under conditions unfavorable for Fe/S cluster formation the labile IscR cluster is lost and IscR-mediated repression of the *isc* operon is alleviated. At the same time, apo-IscR activates the SUF operon to further compensate for damage or loss of Fe/S clusters (154, 145). Once the demand for Fe/S biogenesis is met, higher levels of cluster-containing holo-IscR exist, causing an increased repression of the ISC pathway. Moreover, under iron limitation the ISC and SUF machineries are unable to maintain the levels of holo-IscR and therefore this feedback mechanism allows IscR to sense Fe/S demand and enables *E. coli* to respond appropriately to stress conditions (146).

There are two classes of IscR binding sites in the *E. coli* genome: a type-1

site deduced from *iscR, yadR,* and *yhgI* promoter regions, and a type-2 site compiled from the IscR sites upstream of the *hyaA, ydiU,* and *sufA* promoters (147). Interestingly, IscR binds type-1 promoters solely in its holo-form, while binding to type-2 promoters was shown to be independent of the presence of the Fe/S cluster (144). In *E. coli*, IscR mutation E43A enabled specific recognition of type-1 promoters by apo-IscR, likely mimicking the interaction mode of the cluster-bound form of the protein (see Chapter 3, (216)).

Although a molecular level understanding of the complex processes of Fe/S cluster biosynthesis in several organisms is now emerging from the combination of *in vivo* and *in vitro* approaches, these machineries are still poorly understood in Gram-positive bacteria. While homologs of the *E. coli* ISC or SUF systems are present in several organisms, some species exhibit unusual Fe/S cluster biosynthetic machineries. Most Gram-positive bacteria carry only a *suf* operon, containing genes coding for SufU and the SufBCD complex (227, 138), but no *sufE* or *sufA*-related genes, even if in some cases *sufA* can be found elsewhere in the genome (139, 138).

Thermincola potens (strain JR) is an anaerobic, thermophilic, Gram-positive dissimilatory metal reducing bacterium (DMRB), isolated from a thermophilic microbial fuel cell (MFC) (228). It is of the first Gram-positive DMRB for which there is a complete genome sequence, which revealed an unusual abundance of multiheme c-type cytochromes (228, 229). Using homology searches, we identified a series of genes with sequence similarity to both *E. coli* SUF and ISC machineries in the *T. potens* genome, including a gene *locus* coding for a putative IscR protein. Taken together, our results both identify and characterize a unique Fe/S biogenesis regulator in Gram-positive bacteria. Through structural and biochemical analysis of both *T. potens* and *E. coli* apo-IscR proteins and their E43A mutants, we were able to unveil subtle structural features important for DNA recognition and binding specificity.

4.3. Results

Unique Fe/S cluster biogenesis in *Thermincola potens*

In Gram-positive bacteria there is conservation of the *suf* operon, often present as *suf*CDSUB, which is the only machinery for Fe/S cluster biosynthesis in the majority of these organisms (136, 138). Surprisingly, homology searches on the Gram-positive DMRB *T. potens* JR genome (228) allowed identifying two gene *loci* with sequence similarity to *E. coli* SUF and ISC machineries (Fig. 17A). In *T. potens*, there are ORFs coding for homologues of the transcription factor IscR (TherJR_1914, 37% identical to the *E. coli* protein (142)), the cysteine desulfurase IscS (TherJR_1913 (226, 88)) and the scaffold IscU (TherJR_1912 (230)) from the ISC pathway. An additional *suf*-like operon in *T. potens* comprises homologues of sufC (TherJR_0923), sufB and sufD (TherJR_0924) from the *E. coli* SUF pathway, and hcsA (TherJR_0925) and hcsB (TherJR_0926) from the *E. coli isc* operon (104, 105, 96).

When compared to other Gram-positive bacteria, namely from the *Firmicutes* phylum, some unique features of the *T. potens suf* operon become evident. In *T. potens*, the *suf* operon does not code for cysteine desulfurase (SufS) homologues, although there are elsewhere in the *T. potens* genome two additional genes coding for putative cysteine desulfurases (TherJR_0460 and TherJR_3003) homologous to CsdA/SufS, which can function as complementary sulfur sources for Fe/S cluster biogenesis, possibly through the recruitment of the SUF machinery (231). The *T. potens suf* operon is also devoid of homologues of SufU, recently reported to be a zinc-dependent sulfurtransferase in *B. subtilis* (140), but encodes a sufBD protein, which together with sufC was shown to act as scaffold in Gram-negative bacteria (83, 103). Furthermore, the *suf* operon in *T. potens* includes the *hscA* and *hscB* genes coding for the chaperones responsible for transferring pre-formed clusters from the scaffold IscU to final acceptors and that, in *E. coli*, are co-transcribed with the *isc* and not with the *suf* operon (226). Additionally, genes coding for A-type carriers are absent from the *T. potens* genome.

IscU is a highly conserved protein that functions as scaffold for cluster assembly and subsequent transfer. Preserved features include the cluster ligands (three cysteines and one histidine), an aspartate residue that plays a critical role in

cluster transfer to apo-proteins and the LPPVK motif recognized by the chaperone HscA (232) (Fig. 17B). Some Gram-positive bacteria (e.g. *Enterococcus faecalis*) were shown to possess an IscU homologue, SufU, which does not contain the HscA recognition site and has a 19-residue insertion between the first two conserved cysteines (138). The *T. potens* scaffold protein displays conservation of the characteristic IscU LPPVK motif and does not contain the insertion signature specific of SufU-type proteins. Accordingly, phylogenetic analysis of IscU and SufU protein sequences places the protein encoded by the TherJR_1912 gene between the Gram-negative IscU-type and the SufU-like proteins from Gram-positive bacteria (Fig. 17C).

As previously reported for *Clostridium perfringens* (233), searches for Fe/S cluster biogenesis operons in Gram-positive bacteria with completely sequenced genomes, namely the DMRB *Desulfitobacterium hafniense* and *Desulfotomaculum reducens*, revealed that they possess a single ISC gene *locus* (*iscRSU*) but no SUF apparatus. In contrast, in other Gram-positive bacteria (e.g. *E. faecalis*) only the SUF pathway can be found. Therefore, contrary to other Gram-positive bacteria described so far, *T. potens* not only has two gene *loci* coding for the two Fe/S cluster biosynthesis machineries present in *E. coli* (ISC and SUF), but these systems display a unique organization.

The *Thermincola potens* TherJR_1914 gene codes for IscR

IscR is a [2Fe-2S] cluster-containing transcriptional regulator encoded by the first gene of the *iscRSUA-hscBA-fdx* operon that regulates both ISC and SUF systems in *E. coli* and other Gram-negative bacteria (146, 145). Apart from the sequence-unrelated SufR found in cyanobacteria (234, 134), no IscR homologue was described in Gram-positive bacteria, with the possible exception of some species of the *Clostridium* genus for which functional data is still lacking (233). In *T. potens* the TherJR_1914 gene encodes a protein of the Rrf2-family of transcriptional regulators, sharing only 37% identity with *E. coli* IscR but with full conservation of the cysteine residues known to coordinate the [2Fe-2S] cluster (Cys$^{92, 98, 104}$, *E. coli* numbering; Fig. 17D) (145).
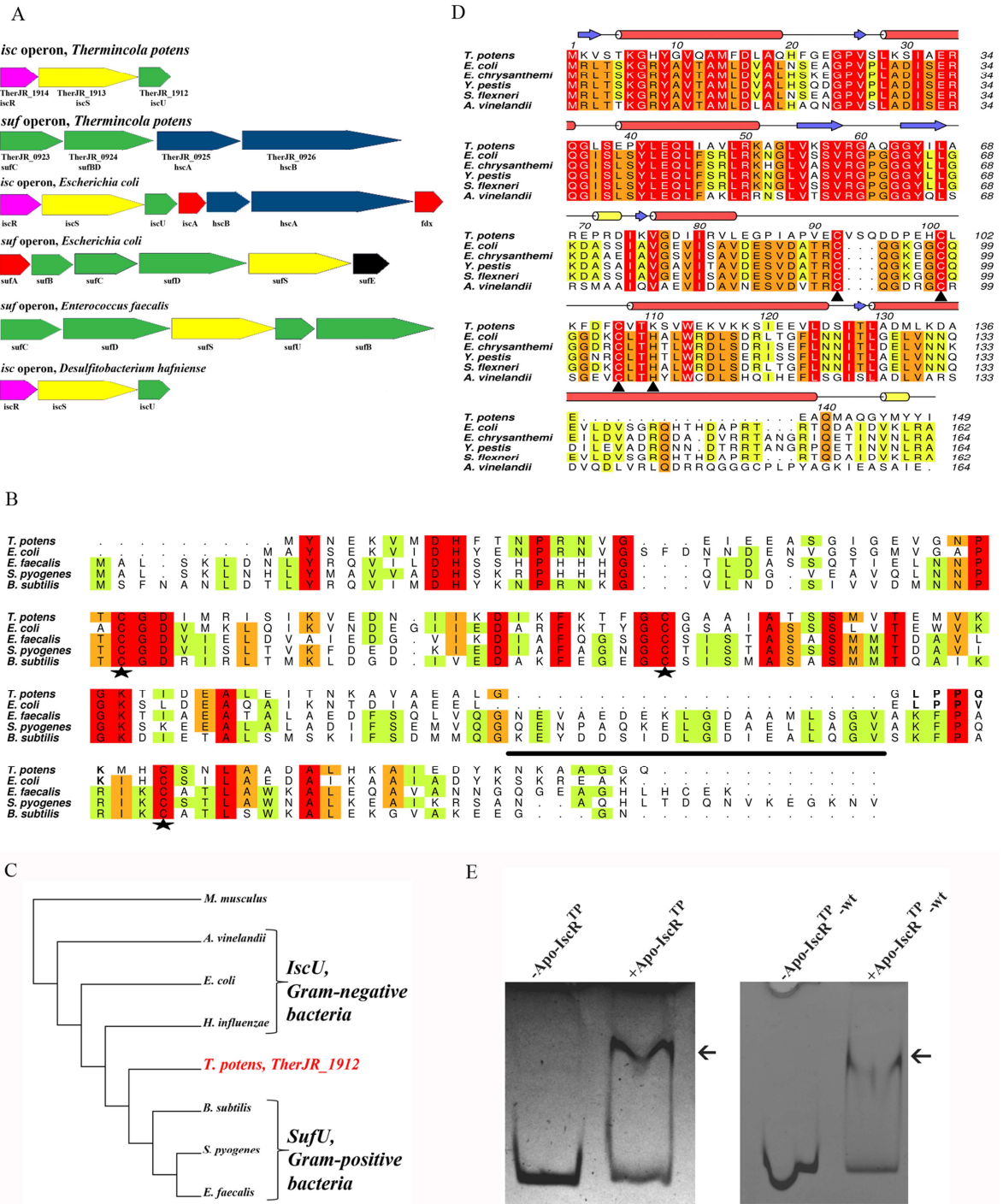
Fig. 17- Identification of an Fe/S cluster biosynthesis regulator in *T. potens*. (A) *T. potens* possesses a unique organization of genes involved in Fe/S cluster biosynthesis, with both isc and suf operons. Colors denote gene function conservation between Gram-negative (*E. coli*), Gram-positive (*E. faecalis*), and DMRB Gram-positive bacteria (*T. potens* and *D. hafniense*). (B, C) *Thermincola potens* Fe/S cluster scaffold protein displays the conserved features of IscU-type scaffolds from Gram-negative bacteria. Amino acid sequence alignment of the *T. potens* TherJR_1912 gene product and homologous proteins from both Gram-positive (*E. faecalis*, *S. pyogenes*, *B. subtilis*) and Gram-negative bacteria (*E. coli*). Strictly conserved amino acids are highlighted in red and increasing residue conservation is represented by a color gradient from green to red. Cysteine residues known to coordinate the Fe/S cluster are denoted by a star (235), the "LPPVK" HscA-binding motif is represented in bold (95) and the characteristic Gram-positive insertion is underlined (138). Numbers above the alignment refer to the *T. potens* amino acid sequence numbering. Alignment prepared with ClustalW (236) and colored with Aline (162). (C)

Neighbor-joining phylogenetic analysis of conserved protein sequences of putative IscU-type or SufU-type proteins in both Gram-positive (*T. potens*, *Streptococcus pyogenes*, *E. faecalis*, *B. subtilis*) and Gram-negative bacteria (*E. coli*, *Azotobacter vinelandii*, *Haemophilus influenza*), using *Mus musculus* as outgroup. The sequences were aligned with three distinct alignment algorithms as implemented in ADOPS (237). The resulting cladogram places the *T. potens* scaffold protein between IscU proteins from Gram-negative bacteria and SufU proteins from other Gram-positive bacteria. (D) The *T. potens* TherJR_1914 gene codes for a protein that is highly homologous to IscR from Gram-negative bacteria. Strictly conserved amino acids are highlighted in red, and increasing residue conservation is represented by a color gradient from green to red. Alignment prepared with ClustalW (161) and colored with Aline (162). (E) *T. potens* apo-IscR recognizes the upstream *suf* operon region between genes TherJR_0922 and TherJR_0923. Incubation of either apo-IscR Cys-to-Ser mutant (apo-IscR^{Tp}) or its as-purified wild-type version (apo-IscR^{Tp}-wt) with the putative *suf* promoter region (*suf*, Table 3) resulted in a mobility-shift (arrow).

Cluster-less (apo) IscR from *E. coli* was shown to activate *suf* operon expression during stress conditions, such as iron starvation (85). The as-purified apo form of the protein encoded by *T. potens* gene TherJR_1914 (apo-IscR^{Tp}-wt) was found to bind to the upstream region of the putative *suf* operon, between genes TherJR_0922 and TherJR_0923 (Fig. 17E). A similar behavior was observed for a triple mutant (C92/101/107S) of IscR^{Tp} (apo-IscR^{Tp}; Fig. 17D), where all putative cluster-binding cysteine residues (Fig. 17D) were replaced by serine. Given the structural similarity between cysteine and serine and the requirement for homogeneous sample for downstream functional and structural assays, this variant was used in all experiments where the apo form of IscR^{Tp} was required.

The ability of apo-IscR^{Tp}-wt and apo-IscR^{Tp} to bind the promoter region of the *suf* operon suggests that IscR^{Tp} can function as a Fe/S cluster regulator in this organism, with the apo form involved in the regulation of *suf* operon expression, as observed for *E. coli.* Although such regulators have been found and characterized in a number of Gram-negative bacteria (238, 147, 187, 142, 239), the characterization of orthologous proteins from Gram-positive species has not yet been reported. Therefore, *T. potens* has a unique organization and regulation of Fe/S cluster assembly genes among Gram-positive bacteria.
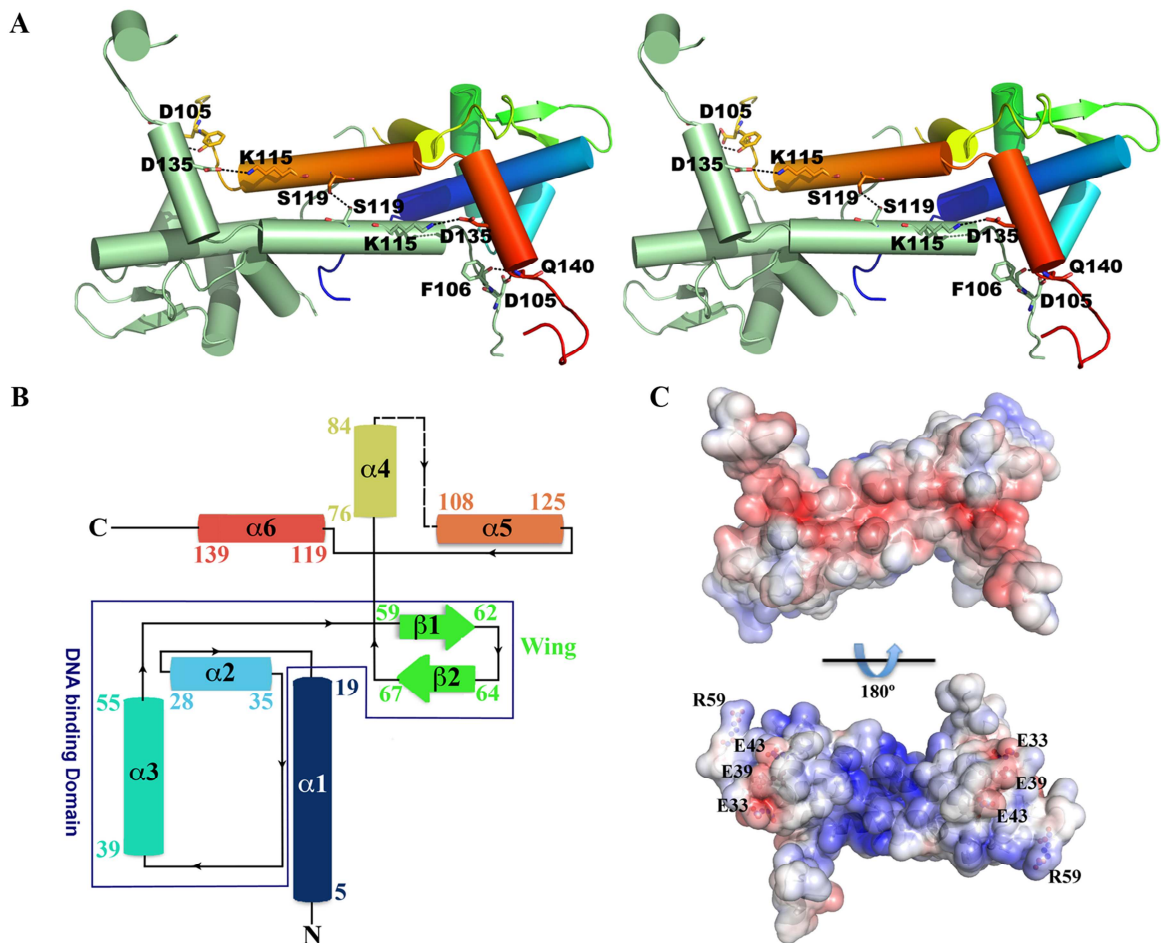
Overall structure of *T. potens* IscR

The three-dimensional structure of free apo *T. potens* IscR, with the putative cluster-binding cysteines mutated to serine (the cluster-less IscR triple-mutants C92/101/107S for *T. potens* are hereby termed apo-IscR^{Tp}) was

determined by X-ray crystallography from tetragonal (P4$_1$) crystals diffracting to 1.6 Å resolution. The crystallographic asymmetric unit contains the functional IscR homodimer (Fig. 18A). Apo-IscR^{Tp} monomers are predominantly α-helical and, while the N-terminal region is formed by three consecutive α-helices preceding the characteristic wing β-hairpin, the C-terminal domain is exclusively α-helical (Fig. 18B). Within each monomer, the N-terminal α-helix (α1) interfaces with the wing-helix subdomain (α2-α3-β1-β2) and with the N-terminal end of the dimerization helix (α5) from the adjacent monomer. The dimerization helix, which comprises two of the putative iron-sulfur cluster binding residues (101 and 107), is further stabilized by close contacts with helix α6 from the adjacent monomer. Residues 86 to 100, encompassing part of the putative iron-sulfur cluster-binding segment (Fig. 17D), are disordered in both monomers and could not be modeled (Fig. 18A, 18B). The structures of the monomers are nearly identical, superposing with an r.m.s.d. of 0.17 Å for 133 aligned Cα atoms.

Apo-IscR^{Tp} dimer formation involves mostly interactions between residues from helix α5 of each monomer, but residues from helices α1 and α4 further stabilize the homodimer. The extensive dimerization interface between the two helices α5 is hydrophobic, except for a single hydrogen bond between the side chains of neighboring Ser119 residues. The association of the adjacent helices α5 is locked on each side by a salt bridge involving Lys115 and Asp135, two residues that are not strictly conserved in closely related IscR molecules (17D, 18A). Further inter-monomer polar interactions are established between the side chain of Gln140 at the C-terminus of helix α6 and Asp105 OD1 and Phe106 O (Fig. 18A).

In agreement with its DNA-binding function (Fig. 17E), the electrostatic surface potential of apo-IscR^{Tp} is highly polarized (Fig. 18C), being predominantly negative at the solvent-exposed face of helices α5 and α6, and positively charged at the opposite, putative DNA-binding side. This asymmetric surface charge distribution promotes initial DNA positioning by non-specific electrostatic contacts, prior to fine-tuning through the establishment of base- and shape-specific interactions. Negatively charged residues (Glu33, Glu39 and Glu43) protrude from the positively charged surface (Fig. 18C), resembling *E. coli* IscR (216). Among these residues, Glu39 is unique in *T. potens* IscR (replaced by a leucine residue in closely related molecules; Fig. 17D).

Fig. 18 - The 3D structure of _T. potens_ IscR. (A) Stereoscopic view of the biologically active apo-IscR[Tp] dimer, highlighting important residues (represented as sticks) at the dimerization interface. One of the monomers is colored from N- (blue) to C-terminal (red), with highlighted residues color-coded (nitrogen blue, oxygen red). Hydrogen bonds are represented as dashed lines. (B) Topology diagram of the apo-IscR[Tp] monomer. Secondary structure element colors match those of A. (C) Solid-surface representation of the apo-IscR[Tp] dimer, with mapped electrostatic surface potential contoured from **+**5 (blue) to **–**5 (red) kbTe−1 [kb, Boltzmann's constant; T, temperature (K); e, charge of an electron].

T. potens IscR belongs to the Rrf2-like family of transcriptional regulators and displays highest structural similarity with the global cysteine regulator CymR from _B. subtilis_ (PDB entry 2Y75; (163)) and _S. aureus_ (PDB entry 3T8T; (169)) as well as with the recently determined structure of _E. coli_ IscR (PDB entry 4HF0; (216)), superposing with these models with an r.m.s.d of 1.5-2.3 Å. The conserved DNA-binding helix-turn-helix motif can also be superposed to the corresponding domain of more distantly related proteins, albeit with somewhat higher r.m.s.d. values (Table 6). The DNA-binding winged-helix motif is structurally similar in the selected structures (Fig. 19A, 19B) and most structural differences occur in the

dimerization helix α5 and in the length and orientation of helix α4, which precedes the iron-sulfur cluster-binding region.

Table 6- Structural similarity between *T. potens* IscR and other winged-helix transcription regulators

Protein	PDB entry	r.m.s.d. (Å)	No. of aligned Cα atoms	Amino acid sequence identity (%)[*]	Z-score
B. subtilis CymR	2Y75	1.5	119	55	17.2
E. coli IscR (unliganded)	4HF0	2.0	116	41	16.8
E. coli IscR (DNA complex)	4HF1	2.3	120	40	16.3
S. aureus CymR	3T8T	2.3	119	46	15.9
Putative transcriptional regulator from *L. inocua*	3LWF	3.8	124	48	14.9
B. cereus protein BC1842	1YLF	2.7	118	20	13.9

*- Structure-based sequence alignment, as calculated by Dali server (http://ekhidna.biocenter.helsinki.fi/dali_server/start; (65))

Fig. 19 - IscR from *T. potens* is structurally similar to other winged-helix transcriptional regulators. Superposition of apo-IscRTp monomer (green) with (A) free *E. coli* apo-IscR C92/98/104A (blue; PDB entry 4HF0) and (B) free *B. subtilis* CymR (magenta; PDB entry 2Y75) highlighting the overall structural conservation.

Subtle structural differences modulate DNA sequence recognition specificity

As observed for apo-IscR^{Tp}, the apo-IscR^{Ec} biological dimer is highly polarized with a clustering of basic residues on the DNA-interacting surface (Fig. 13). Apo-IscR^{Ec} residues contributing to the partial negative charge within the

DNA-binding surface (Glu33, Asp30 and Glu43; Fig. 13) are structurally equivalent to the acidic residues identified on the equivalent side of apo-IscR^{Tp}. However, only Glu43 contacts directly the bound oligonucleotide. Together with Gln44 (conserved) and Ser40 (variable), Glu43 is involved in base-specific recognition within the major groove (Fig. 20A) and was shown to specifically discriminate against type-1 promoter sequences in *E. coli* (see Chapter 3, (216))*.* Overall, there is a stricking conservation of the DNA-binding interface (Fig. 17D; Fig. 20A). Apo-IscR^{Tp} differs from the *E. coli* homologue only at four positions within the interaction surface, which could result in altered DNA binding affinity and specificity: Ser27 (Pro27 in apo-IscR^{Ec}), Pro40 (Ser40 in apo-IscR^{Ec}) and Ala61-Gln62 (Pro61-Gly62 in apo-IscR^{Ec}). The replacement of Pro27 by a serine is likely to increase the flexibility of the linker between the first two α-helices, although a large change in DNA affinity is not predictable. In contrast, the substitution of Pro61-Gly62 by an Ala-Gln dipeptide can impact the conformation of the wing β-hairpin and interfere with the tight packing of this structural element within the minor groove. In particular, the residue at position 40 is likely to play a key role in sequence-specific recognition of DNA (Fig. 20B).

In the IscR^{Ec}-DNA complex the protein packs very tightly within the major groove, leaving limited space for bulkier residues (Fig. 20A, 20B). Although a proline could be accommodated at the N-terminus of helix α3 without helical disruption (Fig. 20B), the resulting steric hindrance might prevent the placement and base readout of the conserved Glu43-Gln44 and/or contacts of the residues interacting with the phosphate backbone (Tyr9, Ser38, Tyr41). Substitution of the purines interacting with Ser40 (G20' and A19) prevents binding of *E. coli* apo-IscR to the *hya* promoter sequence, highlighting the importance of this residue for base-specific recognition (144). Further, mutation of Ser40 to alanine in *E. coli* IscR decreases binding to the *hya* promoter by 90% when compared to the wild type protein, a decrease that is sequence-dependent and more pronounced for type-2 sites (216).
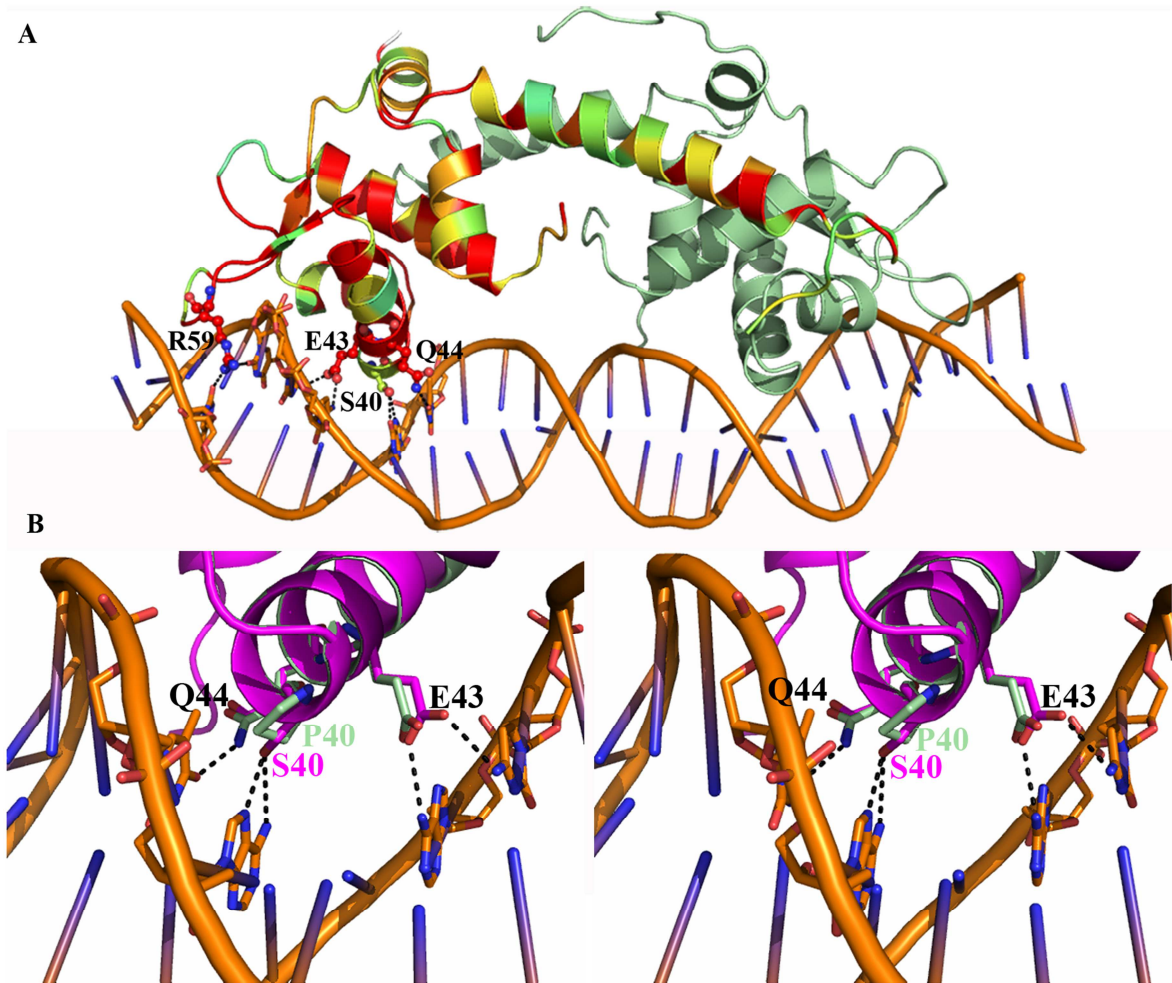
Fig. 20 – Sequence conservation at the IscR-DNA interface (A) Bidentate binding of apo-IscR^{Ec} (C92/98/104S) to the *hya* promoter DNA sequence. In one of the monomers, residues are colored according to conservation, where red corresponds to positions strictly conserved between E. coli and *T. potens* IscR. Residues at the DNA-interacting interface are represented as balls and sticks. Hydrogen bonds between apo-IscR^{Ec} and DNA are represented as dotted lines. (B) Apo-IscR^{Ec} S40 interacts specifically with the *hya* promoter and is substituted by a proline in apo-IscR^{Tp}. Stereoscopic view of key residues involved in DNA recognition by apo-IscR^{Ec} (magenta) and corresponding residues in apo-IscR^{Tp} (green) are represented as sticks and color-coded (nitrogen blue, oxygen red).

The influence of Pro40 in apo-IscR^{Tp} interaction with DNA is evidenced by its inability to bind the *E. coli hya* promoter sequence (Fig. 21A). Replacement of Pro40 in IscR^{Tp} by the structurally equivalent amino acid in *E. coli* IscR (apo-IscR^{Tp}-P40S) is sufficient to allow binding to the heterologous promoter (Fig. 21A). The presence of a serine residue at position 40 is likely to alleviate the tight packing of IscR within the major groove of DNA, reducing steric hindrance and allowing binding. Accordingly, the IscR^{Tp}-E43A mutant, where the shorter alanine side chain can provide room for positional adjustments of this region, also recognized the *hya* sequence (Table 3, Fig. 21A) with an affinity comparable to

that of the *E. coli* protein, as assessed by microscale thermophoresis (Table 7). Taken together, these results suggest that substitution of Ser40 by a proline in apo-IscR^{Tp} prevents base recognition through steric hindrance, an impairment lifted by introducing less bulky residues at either position 40 or 43.
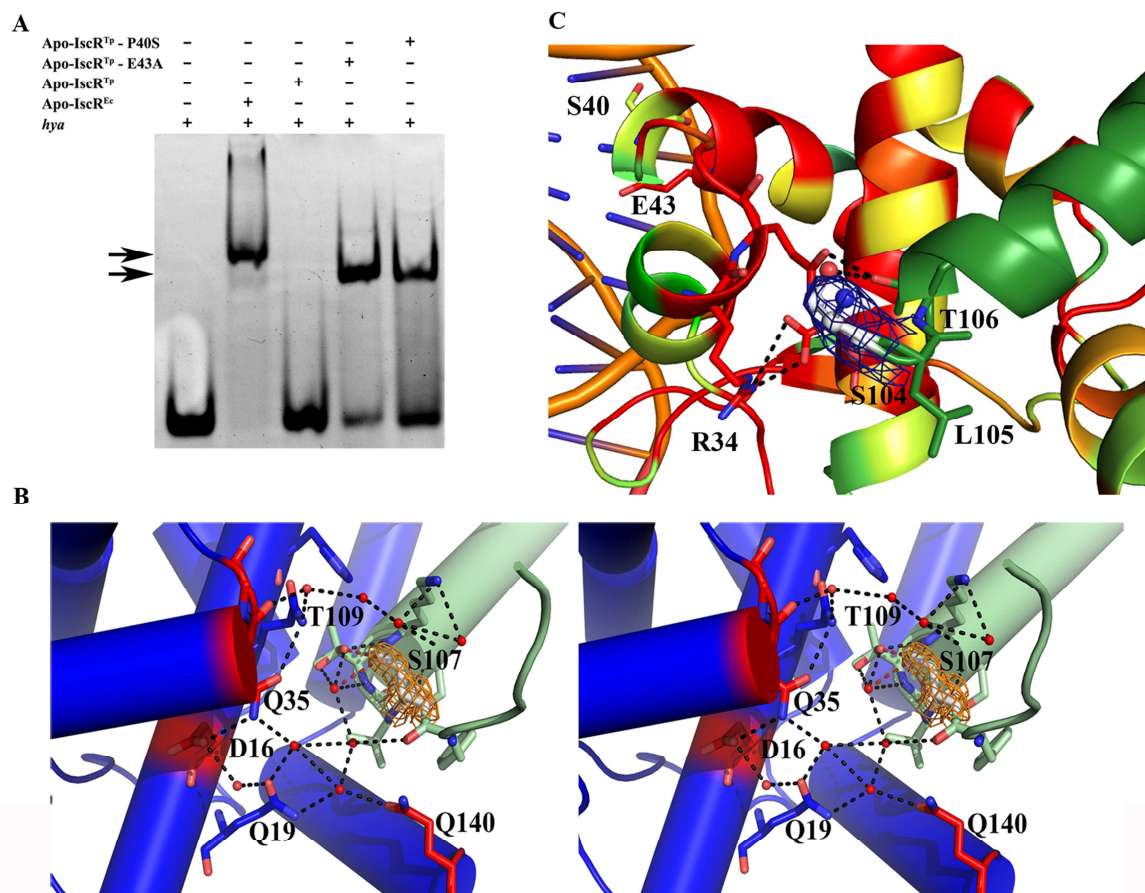
Fig. 21 - Binding of IscR to type-2 promoter sequences. (A) Electrophoretic mobility-shift assay analysis of apo-IscR binding to the *E. coli hya* promoter. Arrows denote observed band-shifts. (B) Stereoscopic view of the intricate network of hydrogen bonds in apo-IscR^{Tp} (one monomer of the functional dimer is colored green and the other one blue) centered on the cluster-binding residue 107 (light gray). The 2Fo – Fc electron density map around residue 107 is represented as an orange mesh. Water molecules and strictly conserved residues in closely related IscR molecules are colored red. (C) In apo-IscR^{Ec} (C92/98/104S), serine 104 (ball and stick) participates in a network of polar interactions with neighboring residues (sticks), cross-linking helices α1, α2, and α5. The corresponding cysteine residue in the wild-type protein could be part of a sensing mechanism for the presence of the Fe/S cluster.

Position of the cluster-binding residues

In contrast to previous studies with *E. coli* IscR, where all putative cluster-binding cysteine residues were mutated to alanine in order to obtain homogeneous cluster-less protein (144, 216, 145), in *T. potens* IscR the corresponding residues

were mutated to serine, which is a closer structural match. In both *E. coli* IscR and apo-IscR[Tp] structures, the region involved in iron-sulfur cluster association is partially disordered, but the serine residues replacing Cys107 in apo-IscR[Tp] and Cys104 in apo-IscR[Ec] are clearly visible in the electron density maps (Fig. 21B, 21C). In contrast to what is observed for the Cys-to-Ala mutant structure of *E. coli* free apo-IscR where the two visible cluster ligands (Ala104 and His107) are on the outer face of the longer dimerization helix α5 (216), in apo-IscR[Tp] the equivalent Ser107 is part of the coil region preceding helix α5 and the crystal structure shows it participates in a water-mediated network of hydrogen bonds connecting this structural segment to helices α1 and α2 (Fig. 21B). In particular, the Ser107 side-chain is hydrogen-bonded to Thr109 OG1 within each monomer. Both residues also establish polar interactions with ordered solvent molecules that participate in a hydrogen bond network interfacing the two monomers of the functional dimer and involving the side chains of Gln19, Asp16, and Gln35 from the adjacent monomer (the last two residues strictly conserved across IscR molecules, Fig. 17D). Of particular relevance is the involvement of Asp16 side chain in a salt bridge with Arg34 within the DNA-binding helix-turn-helix motif. The cluster-binding segment is further stabilized by a polar contact with Gln140 of the adjacent monomer, which also connects the corresponding helices α1 and α6. Altogether, this polar interaction network tightly connects the cluster-binding segment at the N-terminal portion of helix α5 from one monomer with the N-terminal helix α1, helix α6 and helix α2 from the adjacent monomer. Particularly, this network suggests an interconnection between structural changes in the cluster-binding segment and functional effects at the DNA-binding interface.

The geometry of the hydrogen bonds established by the mutated Ser107 in apo-IscR[Tp], and the rotational freedom of Thr109, evidenced by the two discrete conformations of its side-chain in the current crystal structure, are compatible with the existence of similar hydrogen bonds involving Cys107 in the cluster-free wild-type IscR. Indeed, the cysteine side chain thiol group is a moderately good hydrogen bond donor, sometimes crucial for protein activity and function (240-243).

In the crystal structure of the apo-IscR[Ec]-DNA complex, Ser104 (structurally equivalent to Ser107 in *T. potens* IscR) is also well defined in the electron density

maps. In one of the monomers, Ser104 is part of helix α5, as previously observed (216). However, in the other monomer of the apo-IscR^{Ec} dimer this residue hydrogen bonds to the conserved Thr106 (Thr109 in *T. potens* IscR), which in turn engages in a network of direct polar contacts crosslinking the dimerization helix α5 to the C-terminus of the adjacent helix α2 (Arg34, Gln35) and to helix α1 (Asp16) (Fig. 21C). This hydrogen bond network involves direct interactions between the amino acid side chains, in contrast to what is observed in apo-IscR^{Tp}, where solvent molecules mediate some of the contacts. In the Cys-to-Ala triple mutant of *E. coli* IscR this arrangement of polar contacts is preserved, with the expected exception of residue 104, which is there an alanine (216).

The predicted function of residue 107/104 (in *T. potens* and *E. coli*, respectively) in iron-sulfur cluster binding, as well as its location between the dimerization helix of one monomer and the first helix of the helix-turn-helix DNA-binding motif of the neighboring subunit, suggest a possible role as a central nanoswitch, whereby cluster binding-induced movement could trigger a global motion involving both the dimer interface and the DNA-binding region from the opposite monomer. The resultingstructural changes could explain the observed alteration in DNA binding specificity upon cluster association (216).

A single mutation allows apo-IscR^{Tp} to recognize type-1 promoter sequences from *T. potens* and *E. coli*

In *E. coli*, holo-IscR was shown to interact with both type-1 and type-2 DNA motifs in a similar manner, while apo-IscR bound solely to type-2 promoter sequences (144). Recently, it was also demonstrated that replacement of Glu43 by alanine in *E. coli* IscR C92/98/104A removed unfavorable interactions with type-1 motifs, allowing recognition of these promoters (216). The *T. potens isc* promoter region displays *cis*-regulatory elements similar to those identified in the type-1 *E. coli iscRSUA-hscBA-fdx*, including the -35 hexamer and the -10 element sequences (142). In fact, it is possible to delimit a segment (*iscTp_1*; Fig. 22A, Table 3) displaying 48% identity to the *E. coli isc* promoter sequence and containing a -10 element and a consensus **-35** hexamer of the Eσ^{70}-binding site with a 20-bp spacer region (216).
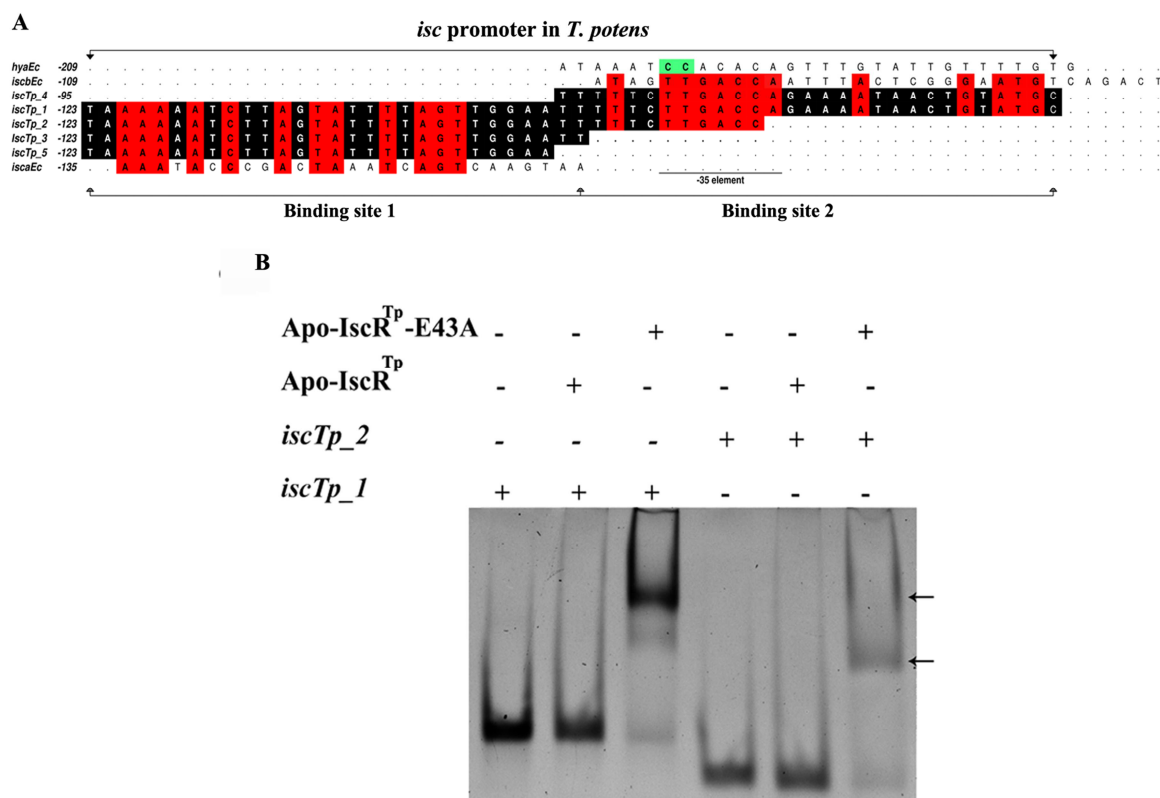
Fig. 22 - The *T. potens isc* promoter region contains two binding sites for IscR^{Tp}. (A) IscR binding sites in type-1 [*T. potens* isc (*iscTp*) and *E. coli isca* (*iscaEc*) and *iscb* (*iscbEc*)] and type-2 [*E. coli hya* (*hyaEc*)] promoters. Numbers refer to the most upstream base of each IscR site relative to the corresponding start codon. Conserved bases between the *isc* promoters are highlighted in red whereas bases conserved between the five *T. potens isc* promoter sequences are shaded black. The highly conserved CC motif in type-2 promoters is colored green (12). (B) DNA recognition was assessed by electrophoretic mobility shift assay of the complexes formed between apo-IscR^{Tp} or apo-IscR^{Tp} E43A and either the full (*iscTp_1*) or trimmed (*iscTp_2*) *isc* promoter sequence. DNA band-shifts are denoted by arrows.

Similar to what is observed for *E. coli* apo-IscR and *isc*, apo-IscR^{Tp} does not bind *iscTp_1* (Fig. 22B). Using an enzymatic system under oxygen-depleted atmosphere (195), a Fe/S cluster could be reversibly reconstituted in wild-type apo-IscR^{Tp} yielding the holo form of the protein, as judged by the appearance of an absorption maximum at 420 nm (Fig. 23A). A dose-dependent structural change of *iscTp_1* DNA could be identified by circular dichroism spectroscopy, upon holo-IscR^{Tp}-wt binding (Fig. 23B). These results demonstrate that, as expected for a *bona fide* IscR, the enzymatically reconstituted Fe/S cluster-bound form of IscR^{Tp}-wt binds to the *T. potens isc* promoter region (Fig. 23B). As seen for *E. coli* IscR (216), the single point mutant apo-IscR^{Tp} E43A binds specifically to the *iscTp_1* sequence, seemingly forming two distinct complexes – with either one or two IscR dimers binding to the target sequence – as suggested by the two observed DNA band shifts (Fig. 22B). This is further supported by the observation

of a single complex with the 3'-trimmed *iscTp_1* sequence, termed *iscTp_2* (Fig. 22A, 22B; Table 3). In *E. coli*, DNase footprinting led to the identification of two IscR binding sites within the *isc* promoter region, *iscra* and *iscrb* (147). Two highly homologous regions could be identified in the *T. potens isc* promoter, *iscTp_3* and *iscTp_4* (Fig. 22A, Table 7), to which apo-IscR^{Tp} E43A displays specific binding (Fig. 24A, Table 7). Further, removal of the two 3'-end nucleotides of *iscTp_3*, yielding the shorter *iscTp_5* (Fig. 22A, Table 7), effectively prevents binding of apo-IscR^{Tp} E43A (Fig. 24A, Table 7), in good agreement with the observed bidentate binding of IscR to the minor groove of AT-rich segments at the termini of its recognition sequence (Fig. 20A).

Table 7 - Binding affinities between IscR and type-1 and type-2 promoter sequences determined by microscale thermophoresis

DNA sequence	IscR variant	Dissociation constant K_d (nM)
hyaEc	Apo-IscR^{Tp} E43A	340 ± 52
	Apo-IscR^{Tp}	n. d.
	Apo-IscR^{Tp} P40S	11900 ± 3340
iscbEc	Apo-IscR^{Tp} E43A	97 ± 6
	Apo-IscR^{Tp}	n. d.
iscTp_3	Apo-IscR^{Tp} E43A	320 ± 19
	Apo-IscR^{Tp}	n. d.
iscTp_4	Apo-IscR^{Tp} E43A	905 ± 87 [a]
	Apo-IscR^{Tp}	n. d.
iscTp_5	Apo-IscR^{Tp} E43A	n. d.

n. d. – binding not detected
[a] The K_d value might be overestimated, since saturation was not reached.
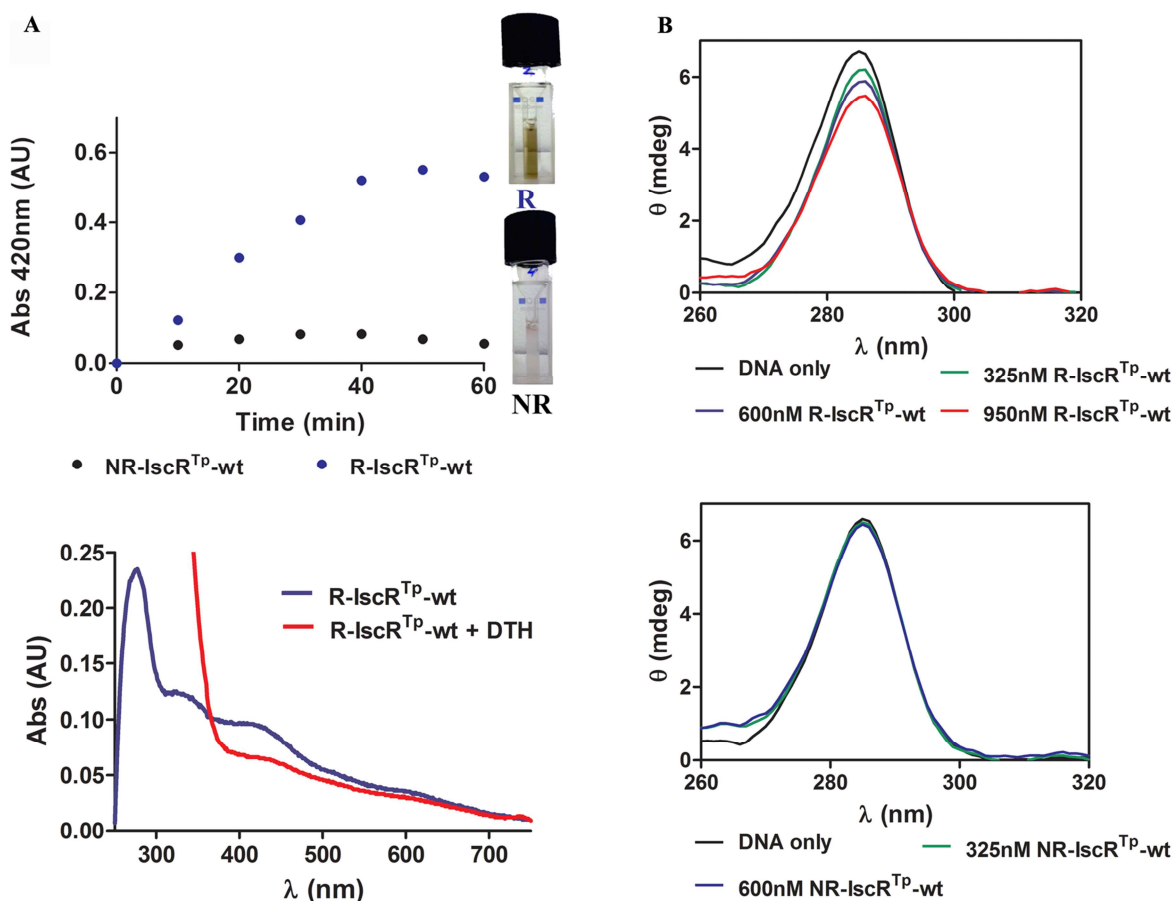
Fig. 23 - *T. potens* IscR is a Fe/S-containing protein that binds the *isc* promoter sequence (A) Upper panel: Time course of Fe/S cluster assembly on apo-IscR^{Tp}-wt. There is a time-dependent increase of the characteristic Fe/S cluster absorption peak at 420nm for reconstituted apo-IscR^{Tp}-wt (R-IscR^{Tp}-wt; blue circles), while no noticeable variation could be observed for the assay performed in the absence of cysteine (NR-IscR^{Tp}-wt, black circles). At the end of the assay, the reaction containing R-IscR^{Tp}-wt displayed a characteristic brown colour (top cuvette; R), which was essentially absent in the control reaction (bottom cuvette; NR). Lower panel: UV/Visible absorption spectra of R-IscR^{Tp}-wt. The spectrum of purified R-IscR^{Tp}-wt (blue curve) displays local maxima at 420 nm and 320 nm that are characteristic of Fe/S clusters, which disappeared upon reduction with 2 mM dithionite (red curve). (B) Fe/S cluster binding modulates recognition of type-1 promoter DNA sequences by IscR. Circular dichroism spectra of *iscTp_1* DNA sequence (Table 3) with increasing concentrations of R-IscR^{Tp}-wt (top panel) or NR-IscR^{Tp}- wt (bottom panel). The spectra were recorded upon successive additions of each purified protein to an *iscTp_1* solution (2 µM). A significant change in ellipticity at the characteristic B-DNA peak at 285 nm (4) can only be observed upon R-IscR^{Tp}-wt addition, indicating that only the Fe/S cluster-containing form of IscR^{Tp}-wt is able to recognize the *Thermincola potens isc* promoter sequence and induce local DNA structural changes. Experiments were carried out at 20°C in 40 mM Tris pH 8, 150 mM KCl, 5% (v/v) glycerol, 1mM DTT.

In line with the considerable conservation between *E. coli* and *T. potens* IscR proteins and *isc* promoter sequences, there is cross-recognition between the transcriptional regulator of *T. potens* and the *E. coli* promoter. While apo-IscR^{Tp} does not bind *E. coli iscrb* (*iscbEc*, Table 7), this sequence is specifically recognized by the E43A mutant (Fig. 24B; Table 7), as observed for *E. coli* apo-IscR (216). Therefore, the unique mechanism of promoter sequence discrimination by IscR seems to be conserved between these organisms.
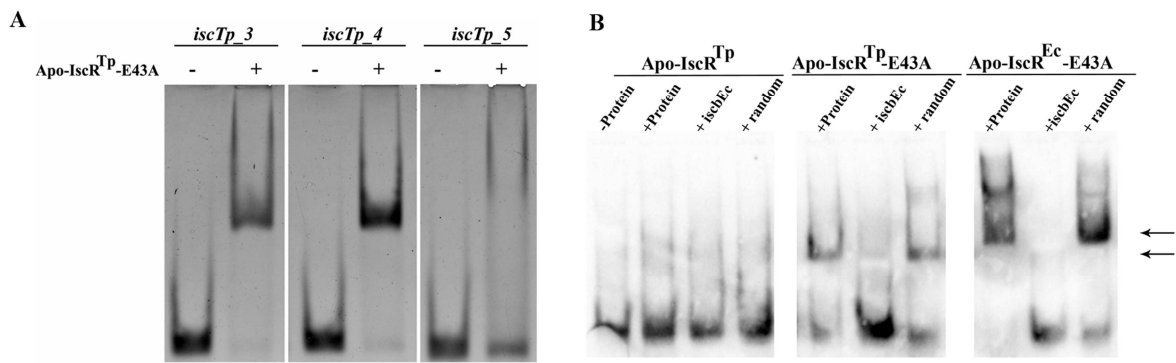
Fig. 24 - **Modulation of apo-IscR^{Tp} specificity by a single point mutation.** (A) There are two independent binding sites for apo-IscR^{Tp} E43A in the *T. potens isc* promoter. Purified apo-IscR^{Tp} E43A (7.5 µM) was incubated with *iscTp_3*, *iscTp_4* and *iscTp_5* sequences, analyzed by nondenaturing PAGE, and visualized by ethidium bromide staining. An arrow denotes the DNA band-shift upon complex formation. (B) Cross-recognition of the *E. coli isc* promoter by *T. potens* IscR. Purified proteins (apo-IscR^{Tp}, apo-IscR^{Tp} E43A, or apo-IscR^{Ec} E43A) were incubated with DIG-labeled *iscrb* promoter sequence (*iscbEc*) (Table 3) and analyzed by nondenaturing PAGE. An arrow denotes bands indicative of DNA– IscR complex formation. Where indicated, cold *iscrb* or a similarly sized random sequence (*random*) was added in 100-fold molar excess as competitor

4.4. Discussion

We performed a detailed analysis of the product of gene TherJR_1914 from *T. potens*, undoubtedly establishing its functional relationship with the Fe/S cluster-binding transcription regulator, IscR, known to control Fe/S cluster biogenesis in several Gram-negative bacteria. The identification of an IscR homologue in *T. potens* was unprecedented: most other Gram-positive bacteria studied so far do not code for any IscR-like proteins nor have an *isc* operon, and the rare cases where an *isc* operon is present (e.g. the DMRB *Desulfobacterium hafniense* or the bacterium *Clostridium perfringens* (233)) lack the SUF machinery.

The combination of biochemical and structural studies, on *T. potens* IscR and its homologue from *E. coli*, revealed also an unforeseen conservation of the unique mode of IscR promoter sequence recognition and discrimination. Despite extensive conservation of the DNA-binding surface, apo-IscR^{Tp} was unable to recognize the heterologous *hya* promoter from *E. coli*. Residue at position 40 played a pivotal role in this process, since relief of steric hindrance (P40S mutant) was sufficient to promote binding. These subtle differences in specificity highlight the precise tailoring of each IscR molecule to its cognate partners, despite overall conservation of the recognition mechanism.

Similar to the *E. coli* molecule (see Chapter 3, (144)), the cluster-less form of the protein binds to the here-identified *T. potens suf* (type-2) promoter, while the novel type-1 promoter (*isc*) is recognized by holo-IscR. In the absence of the Fe/S cluster, the strictly conserved Glu43 residue is pivotal for discriminating between type-1 and type-2 promoters by establishing specific interactions with an invariant CC dinucleotide in type-2 sequences. In fact, mutation of this residue to an uncharged alanine seems to mimic the cluster-induced specificity switch of IscR, allowing the cluster-less regulator to recognize and to bind to type-1 promoter sequences (216). In apo-IscR^{Tp}, the E43A mutation promotes binding to two sequences upstream of the *T. potens iscRSU* operon. These regions are highly homologous to the *E. coli isc* sequences recognized by both holo- and mutant apo-IscR E43A. Given that one of these sequences (*iscTp_4*) contains a -35-element sequence, we propose that *T. potens* holo-IscR may act as a repressor of Fe/S biogenesis by hindering RNA polymerase binding. As a whole, our results

suggest a conserved regulation mechanism by IscR, where Fe/S cluster binding to this transcription regulator enables recognition of type-1 promoters, a process that is mimicked by the E43A mutation.

By using structurally relevant mutants, where serine replaces all putative cluster-coordinating cysteine residues, a network of polar interactions could be identified, connecting the cluster-binding region of one subunit to the DNA-contacting interface of its neighbour in the functional IscR dimer. Any perturbation resulting from cluster ligation could therefore be allosterically transmitted to the nucleic acid-binding region that comprises the conserved Glu43. Regulation through Fe/S cluster ligation allows *T. potens* IscR to act as a sensor and to be a central player of an auto-regulatory loop responsible for keeping the appropriate levels of cellular Fe/S cluster formation and delivery.

Chapter 5

General discussion

General discussion

Iron-sulfur proteins are ubiquitous cellular components participating in various fundamental biological processes in virtually all organisms. Fe/S cluster homeostasis and maturation of apotargets is thereby essential for bacterial survival and adaptation to environmental changes. Therefore, this process is tightly regulated in a wide range of microorganisms. Although IscR was first discovered as the negative autoregulator of the *E. coli* housekeeping Fe/S cluster biogenesis system, it was later implicated in the regulation of ~40 genes. Regulation of the *isc* operon relies on a feedback mechanism where the Fe/S cluster of IscR functions as a reporter of cellular Fe/S cluster homeostasis. Promoters under IscR control were divided in type-1 and type-2 motifs according to their DNA sequences and while both apo- and [2Fe-2S]-IscR bind with similar affinity to type-2 sites, only [2Fe-2S]-IscR recognizes type-1 promoters. Despite the similar affinity *in vitro*, binding of *E. coli* [2Fe-2S]-IscR to type-2 sequences is prevented by competitive binding of other transcription factors known to regulate the expression of these promoters under anaerobic conditions. Thus, apo-IscR function *in vivo* is restricted to aerobic conditions.

SoxR is a well-characterized [2Fe-2S]-containing regulator that activates the transcription of the soxS gene, whose product is known to control the superoxide response regulon (244). Although both SoxR and IscR contain a single helix-turn-helix DNA-binding domain and harbor a [2Fe-2S] cluster, their function is regulated by distinct mechanisms (57, 146). Transcription activity of SoxR is restricted to its oxidized form ([2Fe-2S]$^{2+}$-SoxR), while both apo and [2Fe-2S]-IscR regulate transcription and exhibit different DNA binding specificities (62, 146, 144). Moreover, contrary to SoxR, cluster oxidation has no functional role in IscR activity (143). Rather, O_2 availability *in vivo* directly modulates cluster ligation and subsequent DNA recognition, which is translated in differential expression of IscR-controlled promoters (146, 144). Under anaerobic conditions, Fe/S clusters are stably bound to proteins and the demand for their biosynthesis is low, leading [2Fe-2S]-IscR to bind to the *isc* promoter and repress the expression of the ISC machinery (146, 147). During aerobic growth, Fe/S clusters are subjected to oxidative damage and the demand for their production increases, which leads to

derepression of the *isc* operon, accumulation of apo-IscR, and the concomitant binding to type-2 promoters to repress the expression of Fe/S cluster–containing anaerobic respiratory proteins and induce the expression of the SUF system for prompt replacement of damaged Fe/S clusters (146, 147, 18, 159, 145).

This study correlates the *in vivo* regulation of Fe/S cluster ligation with Fe/S-dependent changes in DNA sequence specificity by pinpointing structural determinants that enable IscR to discriminate between two types of binding motifs and thereby regulate target promoters according to cluster occupancy. Structural analysis of apo-IscR^{Ec} in complex with a type-2 site, allowed the identification of critical interactions dictating specificity and led to the discovery of a key residue, Glu43, acting as a discriminatory filter between the two types of promoters recognized by IscR due to unfavorable interactions with a conserved TT dinucleotide in type-1 motifs. These findings suggest that recognition of type-1 promoters by IscR is highly dependent on the remodeling of the protein-DNA interface triggered by Fe/S cluster ligation that most probably relocates the negatively charged Glu43 residue and eliminates inhibitory interactions (Fig. 25).

Fe/S cluster biosynthesis is a well studied biological process in Gram-negative bacteria, which encode both the SUF and the ISC systems (72). IscR orthologs were thought to be restricted to Gram-negative microoganisms and it was generally accepted that Gram-positive bacteria express a single Fe/S cluster biogenesis pathway encompassing the sufCDSUB genes (136). However, this view was challenged by the previous identification of a gene coding for a putative IscR homolog in *C. perfringens* (233) and the herein reported characterization of a functional IscR in *T. potens* that binds to the upstream regions of the *suf* and *isc* operons. Although characterization of the apo-form of IscR^{Tp} highlighted common mechanistic features, DNA sequence specificity is modulated by structural differences between the *E. coli* and *T. potens* IscR proteins, with emphasis on the topologically equivalent Glu43 and the variable S40 residues. Substitution of S40 by a proline in *T. potens* IscR greatly affects recognition of the *E. coli* type-2 *hya* sequence possibly due to steric hindrance. However, the functional role of Glu43 is conserved in *T. potens* and elimination of its acidic side chain broadens IscR^{Tp} DNA specificity to include type-1 promoters. These findings are consistent with the notion that each transcription factor is perfectly adapted to recognize its cognate

promoter sequence and highlight the relevance of amino acid sequence and protein structure for productive binding and DNA sequence discrimination.

Although the region encompassing the Fe/S cluster was partially disordered in the two structures reported here, a serine residue replacing one of the cluster-coordinating cysteines in *T. potens* and *E. coli* IscR was clearly visible in both electron density maps and analysis of their interactions with neighbor residues provided insights into the mechanism of signal communication induced by cluster ligation. Residue 107/104 (in *T. potens* and *E. coli*, respectively) is a central feature of a network of polar interactions that bridges the cluster-binding region of one monomer and the HTH DNA-binding domain of the opposing subunit. Hence, any perturbation resulting from Fe/S cluster ligation is expected to be propagated through a network of interactions that favors recognition of type-1 sites.

The identification of *T. potens isc* and *suf* operons and the assignment of the *TherJR_1914* gene product as the functional *T. potens* IscR regulator raise interesting biological questions. *T. potens* is a current-producing bacterium that was isolated from a thermophilic anaerobic MFC and whose respiratory metal reduction is associated with an increased number of cell wall-associated multiheme c-type cytochromes (MHCs) (228, 229, 245). Besides MHCs, *T. potens* respiration was proposed to involve the Fe/S-containing respiratory chain enzymes, NADH dehydrogenase (complex I) and cytochrome bc(1) (complex III), which are probably matured *via* the ISC biosynthetic machinery (246, 229, 247). Hence, accurate synthesis and delivery of Fe/S clusters to respiratory complexes is expected to be of utmost importance for *T. potens* survival and should be tightly regulated (229). It can be hypothesized that, in environments that are mainly anoxic, the [2Fe-2S]-form of IscR predominates and regulates ISC machinery expression, whereas *suf* operon expression is activated to counteract oxidative stress conditions known to be highly detrimental to the functioning of Fe/S-containing proteins (18). Consistent with the metabolic relevance of Fe/S-containing proteins, *T. potens* codes for rubredoxin, rubrerythrin and superoxide reductase desulfoferrofoxin proteins (genes TherJR_1986, TherJR_0440, TherJR_0441, respectively) that constitute a well-known oxidative stress protection mechanism in several anaerobic bacteria, namely *Desulfovibrio vulgaris* (248). Thus, harboring two tightly regulated Fe/S cluster biogenesis pathways provides a robust mechanism to control intracellular Fe/S cluster homeostasis and

enables *T. potens* to thrive in environments with fluctuating oxygen concentrations and might be one of the reasons why this bacterium produces more electrical current that any other known microorganism (249). However, the substantial lack of information about *T. potens* coupled with its uniqueness among Gram-positive bacteria hampers further understanding of how tight regulation of Fe/S cluster biogenesis is physiologically relevant for this microorganism.
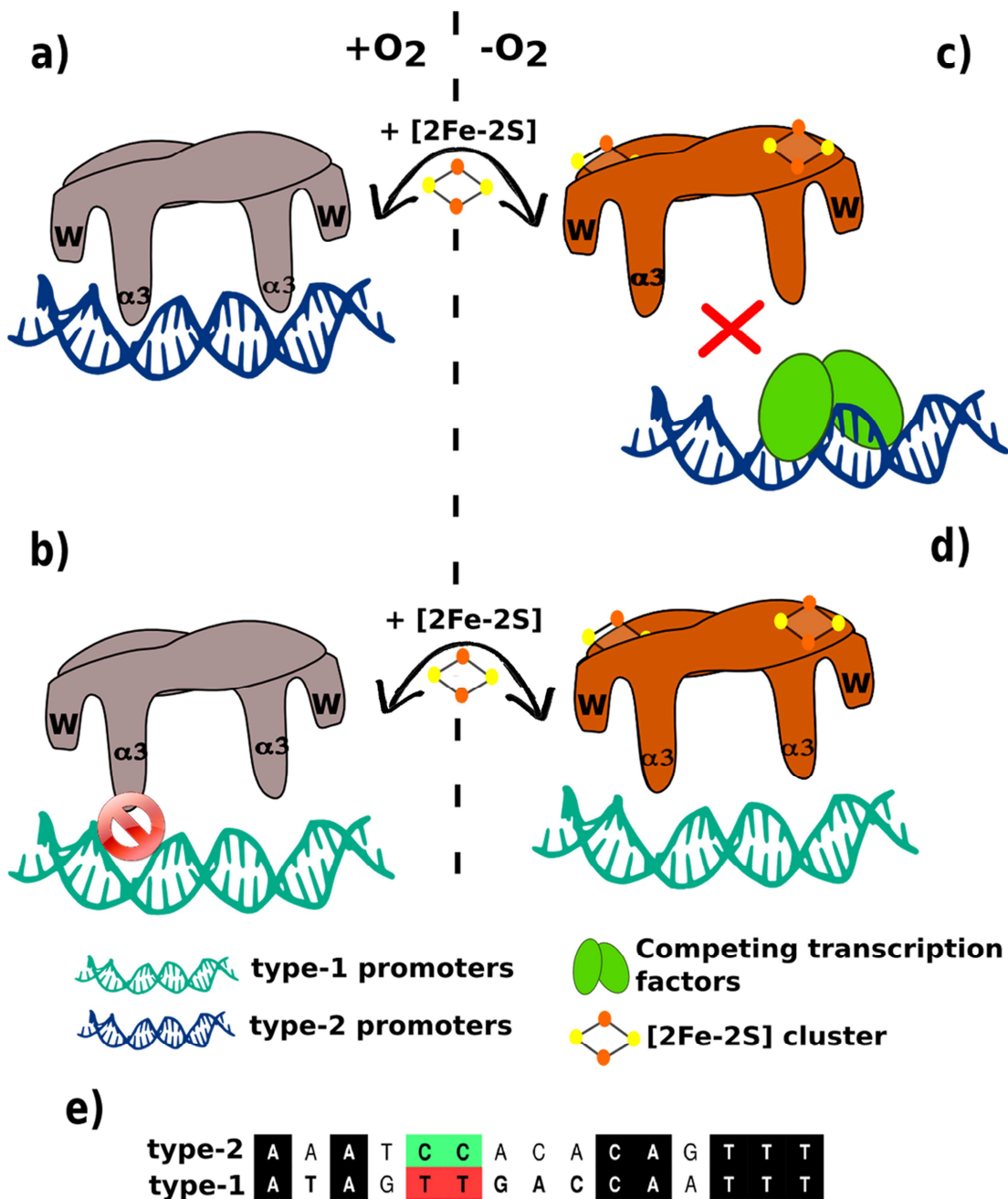
Fig. 25 - **Model for IscR discrimination between type-1 and type-2 promoter sequences.** Interaction of apo-IscR (a,b) and [2Fe-2S]-IscR (c,d) with type-1 and type-2 sites (e). The acidic Glu43 side chain interacts with the CC dinucleotide in type-2 promoters (a, c, e), but the

unfavorable interaction with the TT dinucleotide has an inhibitory effect on type-1 sites recognition (b,e). Although binding of [2Fe-2S]-IscR to type-2 sequences is possible *in vitro*, it is prevented *in vivo* by additional transcription factors bound at target promoters (c). Upon cluster binding, a conformational change lifts the unfavorable interactions with the type-1 TT dinucleotide through displacement of the Glu43 side chain, which is denoted by a curved arrow (d).

In summary, our findings unveil an unforeseen conservation of cofactor-based transcription regulation mechanism. Under anaerobiosis, structural changes induced by cluster ligation allow the specific recognition of type-1 promoters by IscR. Although there is a wide range of transcription factors whose function requires a cofactor, to our knowledge, IscR is the only active regulator in both apo and holo-forms whose DNA-binding specificity was found to be modulated by cofactor binding.

Chapter 6

Future Perspectives

Future perspectives

The emergence and spread of antibiotic resistance in pathogenic bacteria is now a serious threat to global public health (250). The discovery of drugs with novel modes of action will be vital for the replacement of current drugs for which resistance is widespread. Identifying a suitable target is the first step in a structure-based drug design approach. When choosing a potential antimicrobial drug target, three requirements must be convened: the target is i) essential for pathogen survival; ii) its function is restricted to the pathogen; and iii) small molecules can be used to modify its activity (251). During the past decade, IscR was identified as a potential target for novel antimicrobial agents due to its role as a global regulator contributing to the overall virulence of several human and plant pathogens (185, 191, 186). However, additional experiments are required to assess if non-toxic antimicrobial agents can modulate IscR transcriptional activity. Nevertheless, structure-based drug design provides an excellent platform for the identification of novel antibacterial agents and the structural and biochemical characterization of IscR described herein is of utmost importance to pursue such line of research.

Our studies unveil a novel paradigm on Fe/S cluster biogenesis with the identification of the *isc* and *suf* operons in a Gram-positive bacterium, *T. potens*, as well as the discovery of its functional IscR regulator. To gain further insights into *T. potens* Fe/S cluster biogenesis, multiple questions need to be addressed. First, it is necessary to characterize *T. potens* IscR *in vivo* and its function under different environmental conditions, namely oxidative stress. The outcome of this characterization could provide experimental evidence of the link between tight regulation of Fe/S cluster biogenesis and the physiology of this bacterium. Second, given the controversy on SufU function in Gram-positive bacteria, where it was shown to act as an enhancer of the cysteine desulfurase activity rather than as a scaffold, it would be of interest to assign the functional role of the TherJR_1912 gene product, whose amino acid sequence is closely related to its Gram-negative bacteria scaffold counterparts (139, 227, 140). Third, given the lack of a SufS encoding gene, one would expect this function to be compensated by additional *T. potens* cysteine desulfurases homologous to CsdA/SufS proteins, but

the interaction between these proteins and the predicted *T. potens* SufBCD scaffold protein needs to be tested *in vitro*.

Ultimately, the work described in this thesis contributes for a deeper understanding of Fe/S cluster biogenesis regulation by IscR and demonstrates the conservation of its unique mechanism of sequence discrimination. Description of features governing DNA recognition links the structure of IscR with *in vivo* sequence discrimination, which is essential for accurate control of target promoters according to environmental conditions. Given the relevance of IscR for pathogen virulence and the prospective use of *T. potens* in bioremediation and renewable energy production, our findings create exciting novel avenues of research with potential therapeutic and industrial applications.

Appendix

Table A. 1 – Forward and reverse primers used for construct generation

Protein	Vector	Gene Acession Number	Restriction sites	Forward primer (5′→3′)	Reverse primer (5′→3′)
IscR^{Ec}-wt	pETZ2_1a	P0AGK8	*Nco*I and *Hind*III	ccatgggaaga ctgacatctaaa ggg	attcaagctttta agcgcgtaact t
IscR^{Tp}-wt	pET30a	D5X843	*Nde*I and *Xho*I	cagggccatatg ggccttaaagtc agtacgaaaggt	ctcgaattcgg atccggtctcg aggatgtagta catgtaccc

Table A. 2 Forward and reverse primers used for site-directed mutagenesis. The mutated nucleotides are underlined

Protein	Substitution	Forward primer (5′→3′)	Reverse primer (5′→3′)
Apo-IscR^{Tp} (C92/101/107S)	C92S	cattgctcctgtcgag**ag** tgtgtctcaggatga	tcatcctgagacacactct cgacaggagcaatg
	C101S	tctcaggatgatccgga acat**a**gcctgaaattcg	cgaatttcaggctatgttcc ggatcatcctgaga
	C107S	ggaacattgcctgaaatt cgactt**a**gcgtgacga aatc	gatttcgtcacgctaaagt cgaatttcaggcaatgttc c
Apo-IscR^{Ec} (C92/98/104S)	C92S	gtagatgccacccgt**ag** tcagggtaaaggcg	cgcctttaccctgactacg ggtggcatctac
	C98S	cagggtaaaggcggc**ag** ccagggcggcg	cgccgccctggctgccgcctt taccctg
	C104S	gccagggcggcgataa a**ag**cctgaccc	gggtcaggcttttatcgcc gccctggc
Apo-IscR^{Tp} E43A (C92/101/107S/ E43A)	E43A	gtcagaaccgtatttgg**c** acagctgattgccgtac	gtacggcaatcagctgtg ccaaatacggttctgac
Apo-IscR^{Ec} E43A (C92/98/104S/E43A)	E43A	atttccctttcttatctgg**c** acaactgttttcccgtctg	cagacgggaaaacagtt gtgccagataagaaagg gaaat
Apo-IscR^{Tp} P40S (C92/101/107S/P42S)	P40S	cggcaaggcttgtcaga at**c**gtatctggaacag	ctgttccagatacgcttctg acaagccttgccg

Bibliography

1. Bagg A & Neilands JB (1987) Ferric uptake regulation protein acts as a repressor, employing iron (II) as a cofactor to bind the operator of an iron transport operon in Escherichia coli. *Biochemistry* 26(17):5471-5477.
2. Huynh BH, Patil DS, Moura I, Teixeira M, Moura JJ, DerVartanian DV, Czechowski MH, Prickril BC, Peck HD, Jr., & LeGall J (1987) On the active sites of the [NiFe] hydrogenase from Desulfovibrio gigas. Mossbauer and redox-titration studies. *J Biol Chem* 262(2):795-800.
3. Nordlund P & Eklund H (1995) Di-iron-carboxylate proteins. *Curr Opin Struct Biol* 5(6):758-766.
4. Beinert H & Kiley PJ (1999) Fe-S proteins in sensing and regulatory functions. *Curr Opin Chem Biol* 3(2):152-157.
5. Johnson DC, Dean DR, Smith AD, & Johnson MK (2005) Structure, function, and formation of biological iron-sulfur clusters. *Annu Rev Biochem* 74:247-281.
6. Kiley PJ & Beinert H (2003) The role of Fe-S proteins in sensing and regulation in bacteria. *Curr Opin Microbiol* 6(2):181-185.
7. Beinert H, Holm RH, & Munck E (1997) Iron-sulfur clusters: nature's modular, multipurpose structures. *Science* 277(5326):653-659.
8. Py B & Barras F (2010) Building Fe-S proteins: bacterial strategies. *Nat Rev Microbiol* 8(6):436-446.
9. Moulis JM, Davasse V, Golinelli M-P, Meyer J, & Quinkal I (1996) The coordination sphere of iron-sulfur clusters: lessons from site-directed mutagenesis experiments. *J Biol Inorg Chem* 1(1):2-14.
10. Meyer J (2008) Iron-sulfur protein folds, iron-sulfur chemistry, and evolution. *J Biol Inorg Chem* 13(2):157-170.
11. Cammack R (2013) Iron–Sulfur Proteins. *Encyclopedia of Biological Chemistry*, eds Lennarz WJ & Lane MD (Academic Press, Waltham), pp 657-664.
12. Noodleman L, Lovell T, Liu T, Himo F, & Torres RA (2002) Insights into properties and energetics of iron-sulfur proteins from simple clusters to nitrogenase. *Curr Opin Chem Biol* 6(2):259-273.
13. Moore GR, Pettigrew GW, & Rogers NK (1986) Factors influencing redox potentials of electron transfer proteins. *Proc Natl Acad Sci U S A* 83(14):4998-4999.
14. Banci L, Bertini I, Ferretti S, Luchinat C, & Piccioli M (1993) The structure of iron-sulfur clusters in proteins as monitored by NMR, mössbauer, EPR and molecular dynamics. *J Mol Struct* 292(0):207-219.
15. Solomon EI, Pavel EG, Loeb KE, & Campochiaro C (1995) Magnetic circular dichroism spectroscopy as a probe of the geometric and electronic structure of non-heme ferrous enzymes. *Coord Chem Rev* 144(0):369-460.
16. Johnson CE, Cammack R, Rao KK, & Hall DO (1971) The interpretation of the EPR and Mossbauer spectra of two-iron, one-electron, iron-sulphur proteins. *Biochem Biophys Res Commun* 43(3):564-571.
17. Cheng H & Markley JL (1995) NMR spectroscopic studies of paramagnetic proteins: iron-sulfur proteins. *Annu Rev Biophys Biomol Struct* 24:209-237.
18. Imlay JA (2006) Iron-sulphur clusters and the problem with oxygen. *Mol Microbiol* 59(4):1073-1082.
19. Imlay JA (2008) Cellular defenses against superoxide and hydrogen peroxide. *Annu Rev Biochem* 77:755-776.
20. Schieber M & Chandel NS (2014) ROS Function in Redox Signaling and Oxidative Stress. *Curr Biol* 24(10):R453-R462.

21. Tripathi P (2007) Nitric oxide and immune response. *Indian J Biochem Biophys* 44(5):310-319.

22. Derbyshire ER & Marletta MA (2012) Structure and regulation of soluble guanylate cyclase. *Annu Rev Biochem* 81:533-559.

23. Poole RK & Hughes MN (2000) New functions for the ancient globin family: bacterial responses to nitric oxide and nitrosative stress. *Mol Microbiol* 36(4):775-783.

24. Spiro S (2006) Nitric oxide-sensing mechanisms in Escherichia coli. *Biochem Soc Trans* 34(Pt 1):200-202.

25. Green J & Paget MS (2004) Bacterial redox sensors. *Nat Rev Microbiol* 2(12):954-966.

26. Cross CE, Halliwell B, Borish ET, Pryor WA, Ames BN, Saul RL, McCord JM, & Harman D (1987) Oxygen radicals and human disease. *Ann Intern Med* 107(4):526-545.

27. Messner KR & Imlay JA (1999) The identification of primary sites of superoxide and hydrogen peroxide formation in the aerobic respiratory chain and sulfite reductase complex of Escherichia coli. *J Biol Chem* 274(15):10119-10128.

28. Crack JC, Smith LJ, Stapleton MR, Peck J, Watmough NJ, Buttner MJ, Buxton RS, Green J, Oganesyan VS, Thomson AJ, & Le Brun NE (2011) Mechanistic insight into the nitrosylation of the [4Fe-4S] cluster of WhiB-like proteins. *J Am Chem Soc* 133(4):1112-1121.

29. Crack JC, Stapleton MR, Green J, Thomson AJ, & Le Brun NE (2013) Mechanism of [4Fe-4S](Cys)4 cluster nitrosylation is conserved among NO-responsive regulators. *J Biol Chem* 288(16):11492-11502.

30. Cruz-Ramos H, Crack J, Wu G, Hughes MN, Scott C, Thomson AJ, Green J, & Poole RK (2002) NO sensing by FNR: regulation of the Escherichia coli NO-detoxifying flavohaemoglobin, Hmp. *EMBO J* 21(13):3235-3244.

31. Ding H & Demple B (2000) Direct nitric oxide signal transduction via nitrosylation of iron-sulfur centers in the SoxR transcription activator. *Proc Natl Acad Sci U S A* 97(10):5146-5150.

32. Lewandowska H, Kalinowska M, Brzoska K, Wojciuk K, Wojciuk G, & Kruszewski M (2011) Nitrosyl iron complexes--synthesis, structure and biology. *Dalton Trans* 40(33):8273-8289.

33. Yang W, Rogers PA, & Ding H (2002) Repair of nitric oxide-modified ferredoxin [2Fe-2S] cluster by cysteine desulfurase (IscS). *J Biol Chem* 277(15):12868-12873.

34. Crack JC, Green J, Hutchings MI, Thomson AJ, & Le Brun NE (2012) Bacterial iron-sulfur regulatory proteins as biological sensor-switches. *Antioxid Redox Signal* 17(9):1215-1231.

35. Green J, Crack JC, Thomson AJ, & LeBrun NE (2009) Bacterial sensors of oxygen. *Curr Opin Microbiol* 12(2):145-151.

36. Crack JC, Green J, Thomson AJ, & Le Brun NE (2012) Iron-sulfur cluster sensor-regulators. *Curr Opin Chem Biol* 16(1-2):35-44.

37. Unden G & Bongaerts J (1997) Alternative respiratory pathways of Escherichia coli: energetics and transcriptional regulation in response to electron acceptors. *Biochim Biophys Acta* 1320(3):217-234.

38. Gonzalez R, Tao H, Purvis JE, York SW, Shanmugam KT, & Ingram LO (2003) Gene array-based identification of changes that contribute to ethanol tolerance in ethanologenic Escherichia coli: comparison of KO11 (parent) to LY01 (resistant mutant). *Biotechnol Prog* 19(2):612-623.

39. Salmon K, Hung SP, Mekjian K, Baldi P, Hatfield GW, & Gunsalus RP (2003) Global gene expression profiling in Escherichia coli K12. The effects of oxygen availability and FNR. *J Biol Chem* 278(32):29837-29855.

40. Green J, Bennett B, Jordan P, Ralph ET, Thomson AJ, & Guest JR (1996) Reconstitution of the [4Fe-4S] cluster in FNR and demonstration of the aerobic-anaerobic transcription switch in vitro. *Biochem J* 316 (Pt 3):887-892.

41. Korner H, Sofia HJ, & Zumft WG (2003) Phylogeny of the bacterial superfamily of Crp-Fnr transcription regulators: exploiting the metabolic spectrum by controlling alternative gene programs. *FEMS Microbiol Rev* 27(5):559-592.

42. Shaw DJ, Rice DW, & Guest JR (1983) Homology between CAP and Fnr, a regulator of anaerobic respiration in Escherichia coli. *J Mol Biol* 166(2):241-247.

43. Mettert EL, Outten FW, Wanta B, & Kiley PJ (2008) The impact of O(2) on the Fe-S cluster biogenesis requirements of Escherichia coli FNR. *J Mol Biol* 384(4):798-811.

44. Lazazzera BA, Beinert H, Khoroshilova N, Kennedy MC, & Kiley PJ (1996) DNA binding and dimerization of the Fe-S-containing FNR protein from Escherichia coli are regulated by oxygen. *J Biol Chem* 271(5):2762-2768.

45. Crack JC, Green J, Cheesman MR, Le Brun NE, & Thomson AJ (2007) Superoxide-mediated amplification of the oxygen-induced switch from [4Fe-4S] to [2Fe-2S] clusters in the transcriptional regulator FNR. *Proc Natl Acad Sci U S A* 104(7):2092-2097.

46. Reinhart F, Achebach S, Koch T, & Unden G (2008) Reduced apo-fumarate nitrate reductase regulator (apoFNR) as the major form of FNR in aerobically growing Escherichia coli. *J Bacteriol* 190(3):879-886.

47. Sutton VR, Stubna A, Patschkowski T, Munck E, Beinert H, & Kiley PJ (2004) Superoxide destroys the [2Fe-2S]2+ cluster of FNR from Escherichia coli. *Biochemistry* 43(3):791-798.

48. Khoroshilova N, Popescu C, Munck E, Beinert H, & Kiley PJ (1997) Iron-sulfur cluster disassembly in the FNR protein of Escherichia coli by O2: [4Fe-4S] to [2Fe-2S] conversion with loss of biological activity. *Proc Natl Acad Sci U S A* 94(12):6087-6092.

49. Dibden DP & Green J (2005) In vivo cycling of the Escherichia coli transcription factor FNR between active and inactive states. *Microbiology* 151(Pt 12):4063-4070.

50. Stevanin TM, Ioannidis N, Mills CE, Kim SO, Hughes MN, & Poole RK (2000) Flavohemoglobin Hmp affords inducible protection for Escherichia coli respiration, catalyzed by cytochromes bo' or bd, from nitric oxide. *J Biol Chem* 275(46):35868-35875.

51. Greenberg JT, Monach P, Chou JH, Josephy PD, & Demple B (1990) Positive control of a global antioxidant defense regulon activated by superoxide-generating agents in Escherichia coli. *Proc Natl Acad Sci U S A* 87(16):6181-6185.

52. Nunoshiba T, deRojas-Walker T, Wishnok JS, Tannenbaum SR, & Demple B (1993) Activation by nitric oxide of an oxidative-stress response that defends Escherichia coli against activated macrophages. *Proc Natl Acad Sci U S A* 90(21):9993-9997.

53. Storz G & Imlay JA (1999) Oxidative stress. *Curr Opin Microbiol* 2(2):188-194.

54. Amabile-Cuevas CF & Demple B (1991) Molecular characterization of the soxRS genes of Escherichia coli: two genes control a superoxide stress regulon. *Nucleic Acids Res* 19(16):4479-4484.

55. Hidalgo E, Bollinger JM, Jr., Bradley TM, Walsh CT, & Demple B (1995) Binuclear [2Fe-2S] clusters in the Escherichia coli SoxR protein and role of the metal centers in transcription. *J Biol Chem* 270(36):20908-20914.

56. Wu J, Dunham WR, & Weiss B (1995) Overproduction and physical characterization of SoxR, a [2Fe-2S] protein that governs an oxidative response regulon in Escherichia coli. *J Biol Chem* 270(17):10323-10327.

57. Ding H, Hidalgo E, & Demple B (1996) The redox state of the [2Fe-2S] clusters in SoxR protein regulates its activity as a transcription factor. *J Biol Chem* 271(52):33173-33175.

58. Nunoshiba T, Hidalgo E, Amabile Cuevas CF, & Demple B (1992) Two-stage control of an oxidative stress regulon: the Escherichia coli SoxR protein triggers redox-inducible expression of the soxS regulatory gene. *J Bacteriol* 174(19):6054-6060.

59. Pomposiello PJ, Bennik MH, & Demple B (2001) Genome-wide transcriptional profiling of the Escherichia coli responses to superoxide stress and sodium salicylate. *J Bacteriol* 183(13):3890-3902.

60. Griffith KL, Shah IM, & Wolf RE, Jr. (2004) Proteolytic degradation of Escherichia coli transcription activators SoxS and MarA as the mechanism for reversing the induction of the superoxide (SoxRS) and multiple antibiotic resistance (Mar) regulons. *Mol Microbiol* 51(6):1801-1816.

61. Dietrich LE, Teal TK, Price-Whelan A, & Newman DK (2008) Redox-active antibiotics control gene expression and community behavior in divergent bacteria. *Science* 321(5893):1203-1206.

62. Gaudu P & Weiss B (1996) SoxR, a [2Fe-2S] transcription factor, is active only in its oxidized form. *Proc Natl Acad Sci U S A* 93(19):10094-10098.

63. Gorodetsky AA, Dietrich LE, Lee PE, Demple B, Newman DK, & Barton JK (2008) DNA binding shifts the redox potential of the transcription factor SoxR. *Proc Natl Acad Sci U S A* 105(10):3684-3689.

64. Watanabe S, Kita A, Kobayashi K, & Miki K (2008) Crystal structure of the [2Fe-2S] oxidative-stress sensor SoxR bound to DNA. *Proc Natl Acad Sci U S A* 105(11):4121-4126.

65. Holm L & Rosenstrom P (2010) Dali server: conservation mapping in 3D. *Nucleic Acids Res* 38(Web Server issue):W545-549.

66. Kobayashi K, Mizuno M, Fujikawa M, & Mizutani Y (2011) Protein conformational changes of the oxidative stress sensor, SoxR, upon redox changes of the [2Fe-2S] cluster probed with ultraviolet resonance Raman spectroscopy. *Biochemistry* 50(44):9468-9474.

67. Hidalgo E, Ding H, & Demple B (1997) Redox signal transduction via iron-sulfur clusters in the SoxR transcription activator. *Trends Biochem Sci* 22(6):207-210.

68. Gu M & Imlay JA (2011) The SoxRS response of Escherichia coli is directly activated by redox-cycling drugs rather than by superoxide. *Mol Microbiol* 79(5):1136-1150.

69. Sheplock R, Recinos DA, Mackow N, Dietrich LE, & Chander M (2013) Species-specific residues calibrate SoxR sensitivity to redox-active molecules. *Mol Microbiol* 87(2):368-381.

70. Singh AK, Shin JH, Lee KL, Imlay JA, & Roe JH (2013) Comparative study of SoxR activation by redox-active compounds. *Mol Microbiol* 90(5):983-996.

71. Poole RK (2005) Nitric oxide and nitrosative stress tolerance in bacteria. *Biochem Soc Trans* 33(Pt 1):176-180.

72. Roche B, Aussel L, Ezraty B, Mandin P, Py B, & Barras F (2013) Iron/sulfur proteins biogenesis in prokaryotes: formation, regulation and diversity. *Biochim Biophys Acta* 1827(3):455-469.

73. Ayala-Castro C, Saini A, & Outten FW (2008) Fe-S cluster assembly pathways in bacteria. *Microbiol Mol Biol Rev* 72(1):110-125.

74. Xu XM & Moller SG (2011) Iron-sulfur clusters: biogenesis, molecular mechanisms, and their functional significance. *Antioxid Redox Signal* 15(1):271-307.

75. Jacobson MR, Cash VL, Weiss MC, Laird NF, Newton WE, & Dean DR (1989) Biochemical and genetic analysis of the nifUSVWZM cluster from Azotobacter vinelandii. *Mol Gen Genet* 219(1-2):49-57.

76. Olson JW, Agar JN, Johnson MK, & Maier RJ (2000) Characterization of the NifU and NifS Fe-S cluster formation proteins essential for viability in Helicobacter pylori. *Biochemistry* 39(51):16213-16219.

77. Lill R, Dutkiewicz R, Elsasser HP, Hausmann A, Netz DJ, Pierik AJ, Stehling O, Urzica E, & Muhlenhoff U (2006) Mechanisms of iron-sulfur protein maturation in mitochondria, cytosol and nucleus of eukaryotes. *Biochim Biophys Acta* 1763(7):652-667.

78. Balk J & Pilon M (2011) Ancient and essential: the assembly of iron-sulfur clusters in plants. *Trends Plant Sci* 16(4):218-226.

79. Schwartz CJ, Djaman O, Imlay JA, & Kiley PJ (2000) The cysteine desulfurase, IscS, has a major role in in vivo Fe-S cluster formation in Escherichia coli. *Proc Natl Acad Sci U S A* 97(16):9009-9014.

80. Smith AD, Agar JN, Johnson KA, Frazzon J, Amster IJ, Dean DR, & Johnson MK (2001) Sulfur transfer from IscS to IscU: the first step in iron-sulfur cluster biosynthesis. *J Am Chem Soc* 123(44):11103-11104.

81. Wollers S, Layer G, Garcia-Serres R, Signor L, Clemancey M, Latour JM, Fontecave M, & Ollagnier de Choudens S (2010) Iron-sulfur (Fe-S) cluster assembly: the SufBCD complex is a new type of Fe-S scaffold with a flavin redox cofactor. *J Biol Chem* 285(30):23331-23341.

82. Bonomi F, Iametti S, Morleo A, Ta D, & Vickery LE (2008) Studies on the mechanism of catalysis of iron-sulfur cluster transfer from IscU[2Fe2S] by HscA/HscB chaperones. *Biochemistry* 47(48):12795-12801.

83. Chahal HK, Dai Y, Saini A, Ayala-Castro C, & Outten FW (2009) The SufBCD Fe-S scaffold complex interacts with SufA for Fe-S cluster transfer. *Biochemistry* 48(44):10644-10653.

84. Unciuleac MC, Chandramouli K, Naik S, Mayer S, Huynh BH, Johnson MK, & Dean DR (2007) In vitro activation of apo-aconitase using a [4Fe-4S] cluster-loaded form of the IscU [Fe-S] cluster scaffolding protein. *Biochemistry* 46(23):6812-6821.

85. Outten FW, Djaman O, & Storz G (2004) A suf operon requirement for Fe-S cluster assembly during iron starvation in Escherichia coli. *Mol Microbiol* 52(3):861-872.

86. Flint DH (1996) Escherichia coli contains a protein that is homologous in function and N-terminal sequence to the protein encoded by the nifS gene of Azotobacter vinelandii and that can participate in the synthesis of the Fe-S cluster of dihydroxy-acid dehydratase. *J Biol Chem* 271(27):16068-16074.

87. Kato S, Mihara H, Kurihara T, Takahashi Y, Tokumoto U, Yoshimura T, & Esaki N (2002) Cys-328 of IscS and Cys-63 of IscU are the sites of disulfide bridge formation in a covalently bound IscS/IscU complex: implications for the

mechanism of iron-sulfur cluster assembly. *Proc Natl Acad Sci U S A* 99(9):5948-5952.

88. Zheng L, Cash VL, Flint DH, & Dean DR (1998) Assembly of iron-sulfur clusters. Identification of an iscSUA-hscBA-fdx gene cluster from Azotobacter vinelandii. *J Biol Chem* 273(21):13264-13272.

89. Agar JN, Krebs C, Frazzon J, Huynh BH, Dean DR, & Johnson MK (2000) IscU as a scaffold for iron-sulfur cluster biosynthesis: sequential assembly of [2Fe-2S] and [4Fe-4S] clusters in IscU. *Biochemistry* 39(27):7856-7862.

90. Bonomi F, Iametti S, Ta D, & Vickery LE (2005) Multiple turnover transfer of [2Fe2S] clusters by the iron-sulfur cluster assembly scaffold proteins IscU and IscA. *J Biol Chem* 280(33):29513-29518.

91. Urbina HD, Silberg JJ, Hoff KG, & Vickery LE (2001) Transfer of sulfur from IscS to IscU during Fe/S cluster assembly. *J Biol Chem* 276(48):44521-44526.

92. Wu SP, Wu G, Surerus KK, & Cowan JA (2002) Iron-sulfur cluster biosynthesis. Kinetic analysis of [2Fe-2S] cluster transfer from holo ISU to apo Fd: role of redox chemistry and a conserved aspartate. *Biochemistry* 41(28):8876-8885.

93. Vinella D, Loiseau L, Ollagnier de Choudens S, Fontecave M, & Barras F (2013) In vivo [Fe-S] cluster acquisition by IscR and NsrR, two stress regulators in Escherichia coli. *Mol Microbiol* 87(3):493-508.

94. Shi R, Proteau A, Villarroya M, Moukadiri I, Zhang L, Trempe JF, Matte A, Armengod ME, & Cygler M (2010) Structural basis for Fe-S cluster assembly and tRNA thiolation mediated by IscS protein-protein interactions. *PLoS Biol* 8(4):e1000354.

95. Hoff KG, Silberg JJ, & Vickery LE (2000) Interaction of the iron-sulfur cluster assembly protein IscU with the Hsc66/Hsc20 molecular chaperone system of Escherichia coli. *Proc Natl Acad Sci U S A* 97(14):7790-7795.

96. Silberg JJ, Tapley TL, Hoff KG, & Vickery LE (2004) Regulation of the HscA ATPase reaction cycle by the co-chaperone HscB and the iron-sulfur cluster assembly protein IscU. *J Biol Chem* 279(52):53924-53931.

97. Fuzery AK, Oh JJ, Ta DT, Vickery LE, & Markley JL (2011) Three hydrophobic amino acids in Escherichia coli HscB make the greatest contribution to the stability of the HscB-IscU complex. *BMC Biochem* 12:3.

98. Fuzery AK, Tonelli M, Ta DT, Cornilescu G, Vickery LE, & Markley JL (2008) Solution structure of the iron-sulfur cluster cochaperone HscB and its binding surface for the iron-sulfur assembly scaffold protein IscU. *Biochemistry* 47(36):9394-9404.

99. Chandramouli K & Johnson MK (2006) HscA and HscB stimulate [2Fe-2S] cluster transfer from IscU to apoferredoxin in an ATP-dependent reaction. *Biochemistry* 45(37):11087-11095.

100. Tokumoto U & Takahashi Y (2001) Genetic analysis of the isc operon in Escherichia coli involved in the biogenesis of cellular iron-sulfur proteins. *J Biochem* 130(1):63-71.

101. Takahashi Y & Tokumoto U (2002) A third bacterial system for the assembly of iron-sulfur clusters with homologs in archaea and plastids. *J Biol Chem* 277(32):28380-28383.

102. Jang S & Imlay JA (2010) Hydrogen peroxide inactivates the Escherichia coli Isc iron-sulphur assembly system, and OxyR induces the Suf system to compensate. *Mol Microbiol* 78(6):1448-1467.

103. Tian T, He H, & Liu XQ (2014) The SufBCD protein complex is the scaffold for iron-sulfur cluster assembly in Thermus thermophiles HB8. *Biochem Biophys Res Commun* 443(2):376-381.

104. Rangachari K, Davis CT, Eccleston JF, Hirst EM, Saldanha JW, Strath M, & Wilson RJ (2002) SufC hydrolyzes ATP and interacts with SufB from Thermotoga maritima. *FEBS Lett* 514(2-3):225-228.

105. Saini A, Mapolelo DT, Chahal HK, Johnson MK, & Outten FW (2010) SufD and SufC ATPase activity are required for iron acquisition during in vivo Fe-S cluster formation on SufB. *Biochemistry* 49(43):9402-9412.

106. Loiseau L, Ollagnier-de-Choudens S, Nachin L, Fontecave M, & Barras F (2003) Biogenesis of Fe-S cluster by the bacterial Suf system: SufS and SufE form a new type of cysteine desulfurase. *J Biol Chem* 278(40):38352-38359.

107. Outten FW, Wood MJ, Munoz FM, & Storz G (2003) The SufE protein and the SufBCD complex enhance SufS cysteine desulfurase activity as part of a sulfur transfer pathway for Fe-S cluster assembly in Escherichia coli. *J Biol Chem* 278(46):45713-45719.

108. Layer G, Gaddam SA, Ayala-Castro CN, Ollagnier-de Choudens S, Lascoux D, Fontecave M, & Outten FW (2007) SufE transfers sulfur from SufS to SufB for iron-sulfur cluster assembly. *J Biol Chem* 282(18):13342-13350.

109. Chahal HK & Outten FW (2012) Separate FeS scaffold and carrier functions for SufB(2)C(2) and SufA during in vitro maturation of [2Fe2S] Fdx. *J Inorg Biochem* 116:126-134.

110. Py B, Moreau PL, & Barras F (2011) Fe-S clusters, fragile sentinels of the cell. *Curr Opin Microbiol* 14(2):218-223.

111. Vinella D, Brochier-Armanet C, Loiseau L, Talla E, & Barras F (2009) Iron-sulfur (Fe/S) protein biogenesis: phylogenomic and genetic studies of A-type carriers. *PLoS Genet* 5(5):e1000497.

112. Krebs C, Agar JN, Smith AD, Frazzon J, Dean DR, Huynh BH, & Johnson MK (2001) IscA, an alternate scaffold for Fe-S cluster biosynthesis. *Biochemistry* 40(46):14069-14080.

113. Ollagnier-de Choudens S, Nachin L, Sanakis Y, Loiseau L, Barras F, & Fontecave M (2003) SufA from Erwinia chrysanthemi. Characterization of a scaffold protein required for iron-sulfur cluster assembly. *J Biol Chem* 278(20):17993-18001.

114. Ollagnier-de-Choudens S, Sanakis Y, & Fontecave M (2004) SufA/IscA: reactivity studies of a class of scaffold proteins involved in [Fe-S] cluster assembly. *J Biol Inorg Chem* 9(7):828-838.

115. Lu J, Yang J, Tan G, & Ding H (2008) Complementary roles of SufA and IscA in the biogenesis of iron-sulfur clusters in Escherichia coli. *Biochem J* 409(2):535-543.

116. Gupta V, Sendra M, Naik SG, Chahal HK, Huynh BH, Outten FW, Fontecave M, & Ollagnier de Choudens S (2009) Native Escherichia coli SufA, coexpressed with SufBCDSE, purifies as a [2Fe-2S] protein and acts as an Fe-S transporter to Fe-S target enzymes. *J Am Chem Soc* 131(17):6149-6153.

117. Bencze KZ, Kondapalli KC, Cook JD, McMahon S, Millan-Pacheco C, Pastor N, & Stemmler TL (2006) The structure and function of frataxin. *Crit Rev Biochem Mol Biol* 41(5):269-291.

118. Delatycki MB, Williamson R, & Forrest SM (2000) Friedreich ataxia: an overview. *J Med Genet* 37(1):1-8.

119. Pandolfo M & Pastore A (2009) The pathogenesis of Friedreich ataxia and the structure and function of frataxin. *J Neurol* 256 Suppl 1:9-17.

120. Li DS, Ohshima K, Jiralerspong S, Bojanowski MW, & Pandolfo M (1999) Knock-out of the cyaY gene in Escherichia coli does not affect cellular iron content and sensitivity to oxidants. *FEBS Lett* 456(1):13-16.

121. Pohl T, Walter J, Stolpe S, Soufo JH, Grauman PL, & Friedrich T (2007) Effects of the deletion of the Escherichia coli frataxin homologue CyaY on the respiratory NADH:ubiquinone oxidoreductase. *BMC Biochem* 8:13.

122. Vivas E, Skovran E, & Downs DM (2006) Salmonella enterica strains lacking the frataxin homolog CyaY show defects in Fe-S cluster metabolism in vivo. *J Bacteriol* 188(3):1175-1179.

123. Bou-Abdallah F, Adinolfi S, Pastore A, Laue TM, & Dennis Chasteen N (2004) Iron binding and oxidation kinetics in frataxin CyaY of Escherichia coli. *J Mol Biol* 341(2):605-615.

124. Prischi F, Konarev PV, Iannuzzi C, Pastore C, Adinolfi S, Martin SR, Svergun DI, & Pastore A (2010) Structural bases for the interaction of frataxin with the central components of iron-sulphur cluster assembly. *Nat Commun* 1:95.

125. Layer G, Ollagnier-de Choudens S, Sanakis Y, & Fontecave M (2006) Iron-sulfur cluster biosynthesis: characterization of Escherichia coli CYaY as an iron donor for the assembly of [2Fe-2S] clusters in the scaffold IscU. *J Biol Chem* 281(24):16256-16263.

126. Adinolfi S, Iannuzzi C, Prischi F, Pastore C, Iametti S, Martin SR, Bonomi F, & Pastore A (2009) Bacterial frataxin CyaY is the gatekeeper of iron-sulfur cluster formation catalyzed by IscS. *Nat Struct Mol Biol* 16(4):390-396.

127. Kim JH, Frederick RO, Reinen NM, Troupis AT, & Markley JL (2013) [2Fe-2S]-ferredoxin binds directly to cysteine desulfurase and supplies an electron for iron-sulfur cluster assembly but is displaced by the scaffold protein or bacterial frataxin. *J Am Chem Soc* 135(22):8117-8120.

128. Yan R, Konarev PV, Iannuzzi C, Adinolfi S, Roche B, Kelly G, Simon L, Martin SR, Py B, Barras F, Svergun DI, & Pastore A (2013) Ferredoxin competes with bacterial frataxin in binding to the desulfurase IscS. *J Biol Chem* 288(34):24777-24787.

129. Ranquet C, Ollagnier-de-Choudens S, Loiseau L, Barras F, & Fontecave M (2007) Cobalt stress in Escherichia coli. The effect on the iron-sulfur proteins. *J Biol Chem* 282(42):30442-30451.

130. Shimomura Y, Kamikubo H, Nishi Y, Masako T, Kataoka M, Kobayashi Y, Fukuyama K, & Takahashi Y (2007) Characterization and crystallization of an IscU-type scaffold protein with bound [2Fe-2S] cluster from the hyperthermophile, aquifex aeolicus. *J Biochem* 142(5):577-586.

131. Chillappagari S, Seubert A, Trip H, Kuipers OP, Marahiel MA, & Miethke M (2010) Copper stress affects iron homeostasis by destabilizing iron-sulfur cluster formation in Bacillus subtilis. *J Bacteriol* 192(10):2512-2524.

132. Dai Y & Outten FW (2012) The E. coli SufS-SufE sulfur transfer system is more resistant to oxidative stress than IscS-IscU. *FEBS Lett* 586(22):4016-4022.

133. Fantino JR, Py B, Fontecave M, & Barras F (2010) A genetic analysis of the response of Escherichia coli to cobalt stress. *Environ Microbiol* 12(10):2846-2857.

134. Wang T, Shen G, Balasubramanian R, McIntosh L, Bryant DA, & Golbeck JH (2004) The sufR gene (sll0088 in Synechocystis sp. strain PCC 6803) functions as a repressor of the sufBCDS operon in iron-sulfur cluster biogenesis in cyanobacteria. *J Bacteriol* 186(4):956-967.

135. Huet G, Daffe M, & Saves I (2005) Identification of the Mycobacterium tuberculosis SUF machinery as the exclusive mycobacterial system of [Fe-S]

cluster assembly: evidence for its implication in the pathogen's survival. *J Bacteriol* 187(17):6137-6146.

136. Riboldi GP, de Mattos EP, & Frazzon J (2013) Biogenesis of [Fe-S] cluster in Firmicutes: an unexploited field of investigation. *Antonie Van Leeuwenhoek* 104(3):283-300.

137. Roche B, Aussel L, Ezraty B, Mandin P, Py B, & Barras F (2013) Reprint of: Iron/sulfur proteins biogenesis in prokaryotes: formation, regulation and diversity. *Biochim Biophys Acta* 1827(8-9):923-937.

138. Riboldi GP, Verli H, & Frazzon J (2009) Structural studies of the Enterococcus faecalis SufU [Fe-S] cluster protein. *BMC Biochem* 10:3.

139. Albrecht AG, Netz DJ, Miethke M, Pierik AJ, Burghaus O, Peuckert F, Lill R, & Marahiel MA (2010) SufU is an essential iron-sulfur cluster scaffold protein in Bacillus subtilis. *J Bacteriol* 192(6):1643-1651.

140. Selbach BP, Chung AH, Scott AD, George SJ, Cramer SP, & Dos Santos PC (2014) Fe-S cluster biogenesis in Gram-positive bacteria: SufU is a zinc-dependent sulfur transfer protein. *Biochemistry* 53(1):152-160.

141. Patschowski T, Bates DM, & Kiley PJ (2000) Mechanism for sensing and responding to oxygen deprivation in prokaryotic organisms. *Bacterial Stress Responses*, eds Storz G & Hengge-Aronis R (ASM Press).

142. Schwartz CJ, Giel JL, Patschkowski T, Luther C, Ruzicka FJ, Beinert H, & Kiley PJ (2001) IscR, an Fe-S cluster-containing transcription factor, represses expression of Escherichia coli genes encoding Fe-S cluster assembly proteins. *Proc Natl Acad Sci U S A* 98(26):14895-14900.

143. Fleischhacker AS, Stubna A, Hsueh KL, Guo Y, Teter SJ, Rose JC, Brunold TC, Markley JL, Munck E, & Kiley PJ (2012) Characterization of the [2Fe-2S] cluster of Escherichia coli transcription factor IscR. *Biochemistry* 51(22):4453-4462.

144. Nesbit AD, Giel JL, Rose JC, & Kiley PJ (2009) Sequence-specific binding to a subset of IscR-regulated promoters does not require IscR Fe-S cluster ligation. *J Mol Biol* 387(1):28-41.

145. Yeo WS, Lee JH, Lee KC, & Roe JH (2006) IscR acts as an activator in response to oxidative stress for the suf operon encoding Fe-S assembly proteins. *Mol Microbiol* 61(1):206-218.

146. Giel JL, Nesbit AD, Mettert EL, Fleischhacker AS, Wanta BT, & Kiley PJ (2013) Regulation of iron-sulphur cluster homeostasis through transcriptional control of the Isc pathway by [2Fe-2S]-IscR in Escherichia coli. *Mol Microbiol* 87(3):478-492.

147. Giel JL, Rodionov D, Liu M, Blattner FR, & Kiley PJ (2006) IscR-dependent gene expression links iron-sulphur cluster assembly to the control of O2-regulated genes in Escherichia coli. *Mol Microbiol* 60(4):1058-1075.

148. Borukhov S & Severinov K (2002) Role of the RNA polymerase sigma subunit in transcription initiation. *Res Microbiol* 153(9):557-562.

149. Gourse RL, Ross W, & Gaal T (2000) UPs and downs in bacterial transcription initiation: the role of the alpha subunit of RNA polymerase in promoter recognition. *Molecular Microbiology* 37(4):687-695.

150. Frazzon J & Dean DR (2001) Feedback regulation of iron-sulfur cluster biosynthesis. *Proc Natl Acad Sci U S A* 98(26):14751-14753.

151. Lee JH, Yeo WS, & Roe JH (2004) Induction of the sufA operon encoding Fe-S assembly proteins by superoxide generators and hydrogen peroxide: involvement of OxyR, IHF and an unidentified oxidant-responsive factor. *Mol Microbiol* 51(6):1745-1755.

152. Zheng M, Åslund F, & Storz G (1998) Activation of the OxyR Transcription Factor by Reversible Disulfide Bond Formation. *Science* 279(5357):1718-1722.

153. Lee JH, Yeo WS, & Roe JH (2003) Regulation of the sufABCDSE operon by fur. *J Microbiol* 41(2):109-114.

154. Lee KC, Yeo WS, & Roe JH (2008) Oxidant-responsive induction of the suf operon, encoding a Fe-S assembly system, through Fur and IscR in Escherichia coli. *J Bacteriol* 190(24):8244-8247.

155. Varghese S, Wu A, Park S, Imlay KR, & Imlay JA (2007) Submicromolar hydrogen peroxide disrupts the ability of Fur protein to control free-iron levels in Escherichia coli. *Mol Microbiol* 64(3):822-830.

156. Masse E, Vanderpool CK, & Gottesman S (2005) Effect of RyhB small RNA on global iron use in Escherichia coli. *J Bacteriol* 187(20):6962-6971.

157. Desnoyers G, Morissette A, Prevost K, & Masse E (2009) Small RNA-induced differential degradation of the polycistronic mRNA iscRSUA. *EMBO J* 28(11):1551-1561.

158. Richard DJ, Sawers G, Sargent F, McWalter L, & Boxer DH (1999) Transcriptional regulation in response to oxygen and nitrate of the operons encoding the [NiFe] hydrogenases 1 and 2 of Escherichia coli. *Microbiology* 145 (Pt 10):2903-2912.

159. Nesbit AD, Fleischhacker AS, Teter SJ, & Kiley PJ (2012) ArcA and AppY antagonize IscR repression of hydrogenase-1 expression under anaerobic conditions, revealing a novel mode of O2 regulation of gene expression in Escherichia coli. *J Bacteriol* 194(24):6892-6899.

160. Stewart V, Bledsoe PJ, & Williams SB (2003) Dual overlapping promoters control napF (periplasmic nitrate reductase) operon expression in Escherichia coli K-12. *J Bacteriol* 185(19):5862-5870.

161. Thompson JD, Gibson TJ, & Higgins DG (2002) Multiple sequence alignment using ClustalW and ClustalX. *Curr Protoc Bioinformatics* Chapter 2:Unit 2 3.

162. Bond CS & Schuttelkopf AW (2009) ALINE: a WYSIWYG protein-sequence alignment editor for publication-quality alignments. *Acta Crystallogr D Biol Crystallogr* 65(Pt 5):510-512.

163. Shepard W, Soutourina O, Courtois E, England P, Haouz A, & Martin-Verstraete I (2011) Insights into the Rrf2 repressor family--the structure of CymR, the global cysteine regulator of Bacillus subtilis. *FEBS J* 278(15):2689-2701.

164. Tucker NP, Le Brun NE, Dixon R, & Hutchings MI (2010) There's NO stopping NsrR, a global regulator of the bacterial NO stress response. *Trends Microbiol* 18(4):149-156.

165. Todd JD, Wexler M, Sawers G, Yeoman KH, Poole PS, & Johnston AW (2002) RirA, an iron-responsive regulator in the symbiotic bacterium Rhizobium leguminosarum. *Microbiology* 148(Pt 12):4059-4071.

166. Tucker NP, Hicks MG, Clarke TA, Crack JC, Chandra G, Le Brun NE, Dixon R, & Hutchings MI (2008) The transcriptional repressor protein NsrR senses nitric oxide directly via a [2Fe-2S] cluster. *PLoS One* 3(11):e3623.

167. Even S, Burguiere P, Auger S, Soutourina O, Danchin A, & Martin-Verstraete I (2006) Global control of cysteine metabolism by CymR in Bacillus subtilis. *J Bacteriol* 188(6):2184-2197.

168. Tanous C, Soutourina O, Raynal B, Hullo MF, Mervelet P, Gilles AM, Noirot P, Danchin A, England P, & Martin-Verstraete I (2008) The CymR regulator in complex with the enzyme CysK controls cysteine metabolism in Bacillus subtilis. *J Biol Chem* 283(51):35551-35560.

169. Ji Q, Zhang L, Sun F, Deng X, Liang H, Bae T, & He C (2012) Staphylococcus aureus CymR is a new thiol-based oxidation-sensing regulator of stress resistance and oxidative response. *J Biol Chem* 287(25):21102-21109.

170. Soutourina O, Dubrac S, Poupel O, Msadek T, & Martin-Verstraete I (2010) The pleiotropic CymR regulator of Staphylococcus aureus plays an important role in virulence and stress response. *PLoS Pathog* 6(5):e1000894.

171. Soutourina O, Poupel O, Coppee JY, Danchin A, Msadek T, & Martin-Verstraete I (2009) CymR, the master regulator of cysteine metabolism in Staphylococcus aureus, controls host sulphur source utilization and plays a role in biofilm formation. *Mol Microbiol* 73(2):194-211.

172. Kommineni S, Yukl E, Hayashi T, Delepine J, Geng H, Moenne-Loccoz P, & Nakano MM (2010) Nitric oxide-sensitive and -insensitive interaction of Bacillus subtilis NsrR with a ResDE-controlled promoter. *Mol Microbiol* 78(5):1280-1293.

173. Kommineni S, Lama A, Popescu B, & Nakano MM (2012) Global transcriptional control by NsrR in Bacillus subtilis. *J Bacteriol* 194(7):1679-1688.

174. Henares B, Kommineni S, Chumsakul O, Ogasawara N, Ishikawa S, & Nakano MM (2014) The ResD Response Regulator, through Functional Interaction with NsrR and Fur, Plays Three Distinct Roles in Bacillus subtilis Transcriptional Control. *J Bacteriol* 196(2):493-503.

175. Yukl ET, Elbaz MA, Nakano MM, & Moenne-Loccoz P (2008) Transcription Factor NsrR from Bacillus subtilis Senses Nitric Oxide with a 4Fe-4S Cluster (dagger). *Biochemistry* 47(49):13084-13092.

176. Bsat N, Herbig A, Casillas-Martinez L, Setlow P, & Helmann JD (1998) Bacillus subtilis contains multiple Fur homologues: identification of the iron uptake (Fur) and peroxide regulon (PerR) repressors. *Mol Microbiol* 29(1):189-198.

177. Isabella VM, Lapek JD, Jr., Kennedy EM, & Clark VL (2009) Functional analysis of NsrR, a nitric oxide-sensing Rrf2 repressor in Neisseria gonorrhoeae. *Mol Microbiol* 71(1):227-239.

178. Rodionov DA, Dubchak IL, Arkin AP, Alm EJ, & Gelfand MS (2005) Dissimilatory metabolism of nitrogen oxides in bacteria: comparative reconstruction of transcriptional networks. *PLoS Comput Biol* 1(5):e55.

179. Eisenreich W, Heesemann J, Rudel T, & Goebel W (2013) Metabolic host responses to infection by intracellular bacterial pathogens. *Front Cell Infect Microbiol* 3:24.

180. Nairz M, Schroll A, Sonnweber T, & Weiss G (2010) The struggle for iron - a metal at the host-pathogen interface. *Cell Microbiol* 12(12):1691-1702.

181. Dietz I, Jerchel S, Szaszak M, Shima K, & Rupp J (2012) When oxygen runs short: the microenvironment drives host-pathogen interactions. *Microbes Infect* 14(4):311-316.

182. Green J, Rolfe MD, & Smith LJ (2014) Transcriptional regulation of bacterial virulence gene expression by molecular oxygen and nitric oxide. *Virulence* 5(4).

183. Troxell B & Hassan HM (2013) Transcriptional regulation by Ferric Uptake Regulator (Fur) in pathogenic bacteria. *Front Cell Infect Microbiol* 3:59.

184. Kim SH, Lee BY, Lau GW, & Cho YH (2009) IscR modulates catalase A (KatA) activity, peroxide resistance and full virulence of Pseudomonas aeruginosa PA14. *J Microbiol Biotechnol* 19(12):1520-1526.

185. Lim JG & Choi SH (2014) IscR is a global regulator essential for pathogenesis of Vibrio vulnificus and induced by host cells. *Infect Immun* 82(2):569-578.

186. Rincon-Enriquez G, Crete P, Barras F, & Py B (2008) Biogenesis of Fe/S proteins and pathogenicity: IscR plays a key role in allowing Erwinia chrysanthemi to adapt to hostile conditions. *Mol Microbiol* 67(6):1257-1273.

187. Runyen-Janecky L, Daugherty A, Lloyd B, Wellington C, Eskandarian H, & Sagransky M (2008) Role and regulation of iron-sulfur cluster biosynthesis genes in Shigella flexneri virulence. *Infect Immun* 76(3):1083-1092.

188. Young LS (1984) The clinical challenge of infections due to Pseudomonas aeruginosa. *Rev Infect Dis* 6 Suppl 3:S603-607.

189. Wong SM, Bernui M, Shen H, & Akerley BJ (2013) Genome-wide fitness profiling reveals adaptations required by Haemophilus in coinfection with influenza A virus in the murine lung. *Proc Natl Acad Sci U S A* 110(38):15413-15418.

190. Lim JG, Park JH, & Choi SH (2014) Low cell density regulator AphA upregulates the expression of Vibrio vulnificus iscR gene encoding the Fe-S cluster regulator IscR. *J Microbiol*.

191. Miller HK, Kwuan L, Schwiesow L, Bernick DL, Mettert E, Ramirez HA, Ragle JM, Chan PP, Kiley PJ, Lowe TM, & Auerbuch V (2014) IscR Is Essential for Yersinia pseudotuberculosis Type III Secretion and Virulence. *PLoS Pathog* 10(6):e1004194.

192. Bandyopadhyay S, Gama F, Molina-Navarro MM, Gualberto JM, Claxton R, Naik SG, Huynh BH, Herrero E, Jacquot JP, Johnson MK, & Rouhier N (2008) Chloroplast monothiol glutaredoxins as scaffold proteins for the assembly and delivery of [2Fe-2S] clusters. *EMBO J* 27(7):1122-1133.

193. Lill R, Hoffmann B, Molik S, Pierik AJ, Rietzschel N, Stehling O, Uzarska MA, Webert H, Wilbrecht C, & Mühlenhoff U (2012) The role of mitochondria in cellular iron–sulfur protein biogenesis and iron metabolism. *Biochimica et Biophysica Acta (BBA) - Molecular Cell Research* 1823(9):1491-1508.

194. Olichon A & Surrey T (2007) Selection of genetically encoded fluorescent single domain antibodies engineered for efficient expression in Escherichia coli. *J Biol Chem* 282(50):36314-36320.

195. Prischi F, Pastore C, Carroni M, Iannuzzi C, Adinolfi S, Temussi P, & Pastore A (2010) Of the vulnerability of orphan complex proteins: the case study of the E. coli IscU and IscS proteins. *Protein Expr Purif* 73(2):161-166.

196. Ferrari S, Harley VR, Pontiggia A, Goodfellow PN, Lovell-Badge R, & Bianchi ME (1992) SRY, like HMG1, recognizes sharp angles in DNA. *EMBO J* 11(12):4497-4506.

197. Carpenter ML & Kneale GG (1994) Circular dichroism for the analysis of protein-DNA interactions. *Methods Mol Biol* 30:339-345.

198. Jerabek-Willemsen M, Wienken CJ, Braun D, Baaske P, & Duhr S (2011) Molecular interaction studies using microscale thermophoresis. *Assay Drug Dev Technol* 9(4):342-353.

199. Flot D, Mairs T, Giraud T, Guijarro M, Lesourd M, Rey V, van Brussel D, Morawe C, Borel C, Hignette O, Chavanne J, Nurizzo D, McSweeney S, & Mitchell E (2010) The ID23-2 structural biology microfocus beamline at the ESRF. *J Synchrotron Radiat* 17(1):107-118.

200. Kabsch W (2010) XDS. *Acta Crystallogr D Biol Crystallogr* 66(2):125-132.

201. Kabsch W (2010) Integration, scaling, space-group assignment and post-refinement. *Acta Crystallogr D Biol Crystallogr* 66(2):133-144.

202. Collaborative Computational Project N (1994) The CCP4 suite: programs for protein crystallography. *Acta Crystallogr D Biol Crystallogr* 50(Pt 5):760-763.

203. Sheldrick GM (2010) Experimental phasing with SHELXC/D/E: combining chain tracing with density modification. *Acta Crystallogr D Biol Crystallogr* 66(Pt 4):479-485.

204. Pape T & Schneider TR (2004) HKL2MAP: a graphical user interface for macromolecular phasing with SHELX programs. *J Appl Crystallogr* 37(5):843-844.

205. McCoy AJ, Grosse-Kunstleve RW, Adams PD, Winn MD, Storoni LC, & Read RJ (2007) Phaser crystallographic software. *J Appl Crystallogr* 40(Pt 4):658-674.

206. Emsley P & Cowtan K (2004) Coot: model-building tools for molecular graphics. *Acta Crystallogr D Biol Crystallogr* 60(Pt 12 Pt 1):2126-2132.

207. Adams PD, Afonine PV, Bunkoczi G, Chen VB, Davis IW, Echols N, Headd JJ, Hung LW, Kapral GJ, Grosse-Kunstleve RW, McCoy AJ, Moriarty NW, Oeffner R, Read RJ, Richardson DC, Richardson JS, Terwilliger TC, & Zwart PH (2010) PHENIX: a comprehensive Python-based system for macromolecular structure solution. *Acta Crystallogr D Biol Crystallogr* 66(Pt 2):213-221.

208. Lill R (2009) Function and biogenesis of iron-sulphur proteins. *Nature* 460(7257):831-838.

209. Fleischhacker AS & Kiley PJ (2011) Iron-containing transcription factors and their roles as sensors. *Curr Opin Chem Biol* 15(2):335-341.

210. Cary PD & Kneale GG (2009) Circular dichroism for the analysis of protein-DNA interactions. *Methods Mol Biol* 543:613-624.

211. Blout ER, Schmier I, & Simmons NS (1962) New Cotton Effects in Polypeptides and Proteins. *J Am Chem Soc* 84(16):3193-3194.

212. Kerppola TK & Curran T (1991) DNA bending by Fos and Jun: the flexible hinge model. *Science* 254(5035):1210-1214.

213. Dickerson RE (1998) DNA bending: the prevalence of kinkiness and the virtues of normality. *Nucleic Acids Res* 26(8):1906-1926.

214. Kim J, Zwieb C, Wu C, & Adhya S (1989) Bending of DNA by gene-regulatory proteins: construction and use of a DNA bending vector. *Gene* 85(1):15-23.

215. Wu HM & Crothers DM (1984) The locus of sequence-directed and protein-induced DNA bending. *Nature* 308(5959):509-513.

216. Rajagopalan S, Teter SJ, Zwart PH, Brennan RG, Phillips KJ, & Kiley PJ (2013) Studies of IscR reveal a unique mechanism for metal-dependent regulation of DNA binding specificity. *Nat Struct Mol Biol* 20(6):740-747.

217. Zheng G, Lu XJ, & Olson WK (2009) Web 3DNA--a web server for the analysis, reconstruction, and visualization of three-dimensional nucleic-acid structures. *Nucleic Acids Res* 37(Web Server issue):W240-246.

218. van Dijk M & Bonvin AM (2009) 3D-DART: a DNA structure modelling server. *Nucleic Acids Res* 37(Web Server issue):W235-239.

219. Rohs R, West SM, Sosinsky A, Liu P, Mann RS, & Honig B (2009) The role of DNA shape in protein-DNA recognition. *Nature* 461(7268):1248-1253.

220. West SM, Rohs R, Mann RS, & Honig B (2010) Electrostatic interactions between arginines and the minor groove in the nucleosome. *J Biomol Struct Dyn* 27(6):861-866.

221. Haran TE & Mohanty U (2009) The unique structure of A-tracts and intrinsic DNA bending. *Q Rev Biophys* 42(1):41-81.

222. Zeng J, Zhang X, Wang Y, Ai C, Liu Q, & Qiu G (2008) Glu43 is an essential residue for coordinating the [Fe2S2] cluster of IscR from Acidithiobacillus ferrooxidans. *FEBS Lett* 582(28):3889-3892.

223. Luscombe NM, Laskowski RA, & Thornton JM (2001) Amino acid-base interactions: a three-dimensional analysis of protein-DNA interactions at an atomic level. *Nucleic Acids Res* 29(13):2860-2874.

224. Kondo J & Westhof E (2011) Classification of pseudo pairs between nucleotide bases and amino acids by analysis of nucleotide-protein complexes. *Nucleic Acids Res* 39(19):8628-8637.

225. Fontecave M, Choudens SO, Py B, & Barras F (2005) Mechanisms of iron-sulfur cluster assembly: the SUF machinery. *J Biol Inorg Chem* 10(7):713-721.

226. Takahashi Y & Nakamura M (1999) Functional assignment of the ORF2-iscS-iscU-iscA-hscB-hscA-fdx-ORF3 gene cluster involved in the assembly of Fe-S clusters in Escherichia coli. *J Biochem* 126(5):917-926.

227. Riboldi GP, de Oliveira JS, & Frazzon J (2011) Enterococcus faecalis SufU scaffold protein enhances SufS desulfurase activity by acquiring sulfur from its cysteine-153. *Biochim Biophys Acta* 1814(12):1910-1918.

228. Byrne-Bailey KG, Wrighton KC, Melnyk RA, Agbo P, Hazen TC, & Coates JD (2010) Complete genome sequence of the electricity-producing "Thermincola potens" strain JR. *J Bacteriol* 192(15):4078-4079.

229. Carlson HK, Iavarone AT, Gorur A, Yeo BS, Tran R, Melnyk RA, Mathies RA, Auer M, & Coates JD (2012) Surface multiheme c-type cytochromes from Thermincola potens and implications for respiratory metal reduction by Gram-positive bacteria. *Proc Natl Acad Sci U S A* 109(5):1702-1707.

230. Yuvaniyama P, Agar JN, Cash VL, Johnson MK, & Dean DR (2000) NifS-directed assembly of a transient [2Fe-2S] cluster within the NifU protein. *Proc Natl Acad Sci U S A* 97(2):599-604.

231. Trotter V, Vinella D, Loiseau L, Ollagnier de Choudens S, Fontecave M, & Barras F (2009) The CsdA cysteine desulphurase promotes Fe/S biogenesis by recruiting Suf components and participates to a new sulphur transfer pathway by recruiting CsdL (ex-YgdL), a ubiquitin-modifying-like protein. *Mol Microbiol* 74(6):1527-1542.

232. Hoff KG, Ta DT, Tapley TL, Silberg JJ, & Vickery LE (2002) Hsc66 substrate specificity is directed toward a discrete region of the iron-sulfur cluster template protein IscU. *J Biol Chem* 277(30):27353-27359.

233. Andre G, Haudecoeur E, Monot M, Ohtani K, Shimizu T, Dupuy B, & Martin-Verstraete I (2010) Global regulation of gene expression in response to cysteine availability in Clostridium perfringens. *BMC Microbiol* 10:234.

234. Shen G, Balasubramanian R, Wang T, Wu Y, Hoffart LM, Krebs C, Bryant DA, & Golbeck JH (2007) SufR coordinates two [4Fe-4S]2+, 1+ clusters and functions as a transcriptional repressor of the sufBCDS operon and an autoregulator of sufR in cyanobacteria. *J Biol Chem* 282(44):31909-31919.

235. Mansy SS, Wu G, Surerus KK, & Cowan JA (2002) Iron-sulfur cluster biosynthesis. Thermatoga maritima IscU is a structured iron-sulfur cluster assembly protein. *J Biol Chem* 277(24):21397-21404.

236. Larkin MA, Blackshields G, Brown NP, Chenna R, McGettigan PA, McWilliam H, Valentin F, Wallace IM, Wilm A, Lopez R, Thompson JD, Gibson TJ, & Higgins DG (2007) Clustal W and Clustal X version 2.0. *Bioinformatics* 23(21):2947-2948.

237. Reboiro-Jato D, Reboiro-Jato M, Fdez-Riverola F, Vieira CP, Fonseca NA, & Vieira J (2012) ADOPS--Automatic Detection Of Positively Selected Sites. *J Integr Bioinform* 9(3):200.

238. Choi YS, Shin DH, Chung IY, Kim SH, Heo YJ, & Cho YH (2007) Identification of Pseudomonas aeruginosa genes crucial for hydrogen peroxide resistance. *J Microbiol Biotechnol* 17(8):1344-1352.

239. Zeng J, Zhang K, Liu J, & Qiu G (2008) Expression, purification, and characterization of iron-sulfur cluster assembly regulator IscR from Acidithiobacillus ferrooxidans. *J Microbiol Biotechnol* 18(10):1672-1677.

240. Fuentes-Prior P & Salvesen GS (2004) The protein structures that shape caspase activity, specificity, activation and inhibition. *Biochem J* 384(Pt 2):201-232.

241. Gregoret LM, Rader SD, Fletterick RJ, & Cohen FE (1991) Hydrogen bonds involving sulfur atoms in proteins. *Proteins* 9(2):99-107.

242. Turk V, Stoka V, Vasiljeva O, Renko M, Sun T, Turk B, & Turk D (2012) Cysteine cathepsins: from structure, function and regulation to new frontiers. *Biochim Biophys Acta* 1824(1):68-88.

243. Zhou P, Tian F, Lv F, & Shang Z (2009) Geometric characteristics of hydrogen bonds involving sulfur atoms in proteins. *Proteins* 76(1):151-163.

244. Tsaneva IR & Weiss B (1990) soxR, a locus governing a superoxide response regulon in Escherichia coli K-12. *J Bacteriol* 172(8):4197-4205.

245. Wrighton KC, Thrash JC, Melnyk RA, Bigi JP, Byrne-Bailey KG, Remis JP, Schichnes D, Auer M, Chang CJ, & Coates JD (2011) Evidence for direct electron transfer by a gram-positive bacterium isolated from a microbial fuel cell. *Appl Environ Microbiol* 77(21):7633-7639.

246. Albracht SP & Subramanian J (1977) The number of Fe atoms in the iron-sulphur centers of the respiratory chain. *Biochim Biophys Acta* 462(1):36-48.

247. Lanciano P, Vergnes A, Grimaldi S, Guigliarelli B, & Magalon A (2007) Biogenesis of a respiratory complex is orchestrated by a single accessory protein. *J Biol Chem* 282(24):17468-17474.

248. Lumppio HL, Shenvi NV, Summers AO, Voordouw G, & Kurtz DM, Jr. (2001) Rubrerythrin and rubredoxin oxidoreductase in Desulfovibrio vulgaris: a novel oxidative stress protection system. *J Bacteriol* 183(1):101-108.

249. Wrighton KC, Agbo P, Warnecke F, Weber KA, Brodie EL, DeSantis TZ, Hugenholtz P, Andersen GL, & Coates JD (2008) A novel ecological role of the Firmicutes identified in thermophilic microbial fuel cells. *ISME J* 2(11):1146-1156.

250. Balsalobre LC, Dropa M, & Matte MH (2014) An overview of antimicrobial resistance and its public health significance. *Braz J Microbiol* 45(1):1-5.

251. Drinkwater N & McGowan S (2014) From crystal to compound: structure-based antimalarial drug discovery. *Biochem J* 461(3):349-369.

The unique regulation of iron-sulfur cluster biogenesis in a Gram-positive bacterium

Joana A. Santos[a,b], Noelia Alonso-García[a], Sandra Macedo-Ribeiro[a,1], and Pedro José Barbosa Pereira[a,1]

[a]Instituto de Biologia Molecular e Celular (IBMC), Universidade do Porto, 4150-180 Porto, Portugal; and [b]Instituto de Ciências Biomédicas de Abel Salazar (ICBAS), Universidade do Porto, 4050-313 Porto, Portugal

Iron-sulfur clusters function as cofactors of a wide range of proteins, with diverse molecular roles in both prokaryotic and eukaryotic cells. Dedicated machineries assemble the clusters and deliver them to the final acceptor molecules in a tightly regulated process. In the prototypical Gram-negative bacterium *Escherichia coli*, the two existing iron-sulfur cluster assembly systems, iron-sulfur cluster (ISC) and sulfur assimilation (SUF) pathways, are closely interconnected. The ISC pathway regulator, IscR, is a transcription factor of the helix-turn-helix type that can coordinate a [2Fe-2S] cluster. Redox conditions and iron or sulfur availability modulate the ligation status of the labile IscR cluster, which in turn determines a switch in DNA sequence specificity of the regulator: cluster-containing IscR can bind to a family of gene promoters (type-1) whereas the clusterless form recognizes only a second group of sequences (type-2). However, iron-sulfur cluster biogenesis in Gram-positive bacteria is not so well characterized, and most organisms of this group display only one of the iron-sulfur cluster assembly systems. A notable exception is the unique Gram-positive dissimilatory metal reducing bacterium *Thermincola potens*, where genes from both systems could be identified, albeit with a diverging organization from that of Gram-negative bacteria. We demonstrated that one of these genes encodes a functional IscR homolog and is likely involved in the regulation of iron-sulfur cluster biogenesis in *T. potens*. Structural and biochemical characterization of *T. potens* and *E. coli* IscR revealed a strikingly similar architecture and unveiled an unforeseen conservation of the unique mechanism of sequence discrimination characteristic of this distinctive group of transcription regulators.

Rrf2-like regulator | transcription regulation | helix-turn-helix motif | DNA recognition | specificity modulation

Iron-sulfur (Fe/S) proteins play crucial roles for the functioning of both prokaryotic and eukaryotic cells, being required for biological functions ranging from electron transport to redox and nonredox catalysis, and from DNA synthesis and repair to sensing in regulatory processes (1). The main role of the Fe/S cluster assembly machineries is to mobilize iron and sulfur atoms from their storage sources, assemble the two components into an Fe/S cluster, and then transfer the newly formed cluster to the final protein acceptors (2). In *Escherichia coli*, there are two of these Fe/S cluster "factories," the ISC (iron-sulfur cluster) and SUF (sulfur assimilation) systems, whose corresponding genes are organized in two operons, *iscSUA-hscBA-fdx* and *sufABCDSE*, respectively (2, 3). Deletion mutants of the ISC system display a variety of growth defects due to loss of Fe/S cluster-containing enzyme activity and disruption of sulfur metabolism whereas failure of both the ISC and SUF systems leads to synthetic lethality (4, 5).

In *E. coli*, the ISC machinery is considered the housekeeping system responsible for the maturation of a large variety of Fe/S proteins whereas the SUF system is triggered under stress conditions, such as oxidative stress or iron starvation (6). ISC pathway regulator (IscR) is a [2Fe-2S] cluster-containing transcription factor with a single predicted helix-turn-helix motif, first identified for its role in regulating expression of the ISC

biogenesis pathway (7) and subsequently found to control the expression of more than 40 genes in *E. coli* (7, 8). According to the currently accepted model for Fe/S cluster biogenesis, under conditions unfavorable for Fe/S cluster formation, the labile IscR cluster is lost, and IscR-mediated repression of the *isc* (iron-sulfur cluster) operon is alleviated. At the same time, apo-IscR activates the *suf* (sulfur assimilation) operon to further compensate for damage or loss of Fe/S clusters (9, 10). Once the demand for Fe/S biogenesis is met, higher levels of cluster-containing holo-IscR exist, causing an increased repression of the ISC pathway. Moreover, under iron limitation, the ISC and SUF machineries are unable to maintain the levels of holo-IscR, and therefore this feedback mechanism allows IscR to sense Fe/S demand and enables *E. coli* to respond appropriately to stress conditions (11).

There are two classes of IscR binding sites in the *E. coli* genome: a type-1 site deduced from *iscR*, *yadR*, and *yhgI* promoter regions and a type-2 site compiled from the IscR sites upstream of the *hyaA*, *ydiU*, and *sufA* promoters (8). Interestingly, IscR binds type-1 promoters solely in its holo-form whereas binding to type-2 promoters was shown to be independent of the presence of the Fe/S cluster (12). In *E. coli*, IscR mutation E43A enabled specific recognition of type-1 promoters by apo-IscR, likely mimicking the interaction mode of the cluster-bound form of the protein (13).

Significance

Iron-sulfur clusters are ubiquitous cofactors of proteins intervening in disparate biological processes. Iron-sulfur cluster biosynthesis pathways are tightly regulated in Gram-negative bacteria. One of the participating transcription factors, iron-sulfur cluster pathway (ISC) regulator (IscR), can itself bind an iron-sulfur cluster. Depending on its ligation status, IscR recognizes and binds to distinct promoters, therefore modulating cluster biosynthesis. This unique protein at the crossroad between the ISC and sulfur assimilation (SUF) iron-sulfur cluster biosynthetic pathways was thought to be restricted to Gram-negative bacteria. We demonstrated the existence of a functional IscR in the unique Gram-positive bacterium *Thermincola potens*. Structural and functional analysis of *T. potens* and *Escherichia coli* IscR unveiled a conserved mechanism of promoter discrimination, along with subtle structural differences that explain their distinct DNA sequence recognition specificity.

Although a molecular-level understanding of the complex processes of Fe/S cluster biosynthesis in several organisms is now emerging from the combination of in vivo and in vitro approaches, these machineries are still poorly understood in Gram-positive bacteria. Although homologs of the *E. coli* ISC or SUF systems are present in several organisms, some species exhibit unusual Fe/S cluster biosynthetic machineries. Most Gram-positive bacteria carry only a *suf* operon, containing genes coding for SufU and the SufBCD complex (14, 15), but no *sufE* or *sufA*-related genes, even if in some cases *sufA* can be found elsewhere in the genome (14, 16).

Thermincola potens (strain JR) is an anaerobic, thermophilic, Gram-positive dissimilatory metal-reducing bacterium (DMRB), isolated from a thermophilic microbial fuel cell (17). It is of the first Gram-positive DMRB for which there is a complete genome sequence, which revealed an unusual abundance of multiheme c-type cytochromes (17, 18). Using homology searches, we identified a series of genes with sequence similarity to both *E. coli* SUF and ISC machineries in the *T. potens* genome, including a gene locus coding for a putative IscR protein. Taken together, our results both identify and characterize a unique Fe/S biogenesis regulator in Gram-positive bacteria. Through structural and biochemical analysis of both *T. potens* and *E. coli* apo-IscR proteins and their E43A mutants, we were able to unveil subtle structural features important for DNA recognition and binding specificity.

Results

Unique Fe/S Cluster Biogenesis in *T. potens*. In Gram-positive bacteria, there is conservation of the *suf* operon, often present as *suf*CDSUB, which is the only machinery for Fe/S cluster biosynthesis in the majority of these organisms (14, 19). Surprisingly, homology searches on the Gram-positive DMRB *T. potens* JR genome (17) allowed identifying two gene loci with sequence similarity to *E. coli* SUF and ISC machineries (Fig. 1A). In *T. potens*, there are ORFs coding for homologs of the transcription factor IscR (TherJR_1914, 37% identical to the *E. coli* protein) (7), the cysteine desulfurase IscS (TherJR_1913) (4, 20), and the scaffold IscU (TherJR_1912) (21) from the ISC pathway. An additional *suf*-like operon in *T. potens* comprises homologs of sufC (TherJR_0923), sufB, and sufD (TherJR_0924) from the *E. coli* SUF pathway, and the chaperones hcsA (TherJR_0925) and hcsB (TherJR_0926) from the *E. coli* isc operon (22–24).

Compared with other Gram-positive bacteria, namely from the *Firmicutes* phylum, some unique features of the *T. potens* suf operon become evident. In *T. potens*, the suf operon does not code for cysteine desulfurase (SufS) homologs although there are elsewhere in the *T. potens* genome two additional genes coding for putative cysteine desulfurases (TherJR_0460 and TherJR_3003) homologous to CsdA/SufS, which can function as complementary sulfur sources for Fe/S cluster biogenesis, possibly through the recruitment of the SUF machinery (25). The *T. potens* suf operon is also devoid of homologs of SufU, recently reported to be a zinc-dependent sulfurtransferase in *Bacillus subtilis* (26), but encodes a sufBD protein, which together with sufC was shown to act as scaffold in Gram-negative bacteria (27, 28). Furthermore, the suf operon in *T. potens* includes the hscA and hscB genes coding for the chaperones responsible for transferring preformed clusters from the scaffold IscU to final acceptors and that, in *E. coli*, are cotranscribed with the isc and not with the suf operon (4). Additionally, genes coding for A-type carriers are absent from the *T. potens* genome.

IscU is a highly conserved protein that functions as scaffold for cluster assembly and subsequent transfer. Preserved features include the cluster ligands (three cysteines and one histidine), an aspartate residue that plays a critical role in cluster transfer to apo-proteins and the LPPVK motif recognized by the chaperone

HscA (29) (Fig. S1). Some Gram-positive bacteria (e.g., *Enterococcus faecalis*) were shown to possess an IscU homolog, SufU, which does not contain the HscA recognition site and has a 19-residue insertion between the first two conserved cysteines (14). The *T. potens* scaffold protein displays conservation of the characteristic IscU LPPVK motif and does not contain the insertion signature specific of SufU-type proteins. Accordingly, phylogenetic analysis of IscU and SufU protein sequences places the protein encoded by the TherJR_1912 gene between the Gram-negative IscU-type and the SufU-like proteins from Gram-positive bacteria (Fig. 1B).

As previously reported for *Clostridium perfringens* (30), searches for Fe/S cluster biogenesis operons in Gram-positive bacteria with completely sequenced genomes, namely the DMRBs *Desulfitobacterium hafniense* and *Desulfotomaculum reducens*, revealed that they possess a single ISC gene locus (iscRSU) but no SUF apparatus. In contrast, in other Gram-positive bacteria (e.g., *E. faecalis*), only the SUF pathway can be found. Therefore, contrary to other Gram-positive bacteria described so far, *T. potens* not only has two gene loci coding for the two Fe/S cluster biosynthesis machineries present in *E. coli* (ISC and SUF), but these systems display a unique organization.

The *T. potens* TherJR_1914 Gene Codes for IscR. IscR is a [2Fe-2S] cluster-containing transcriptional regulator encoded by the first gene of the iscRSUA-hscBA-fdx operon that regulates both ISC and SUF systems in *E. coli* and other Gram-negative bacteria (10, 11). Apart from the sequence-unrelated SufR found in cyanobacteria (31, 32), no IscR homolog was described in Gram-positive bacteria, with the possible exception of some species of the *Clostridium* genus for which functional data are still lacking (30). In *T. potens*, the TherJR_1914 gene encodes a protein of the Rrf2 family of transcriptional regulators, sharing only 37% identity with *E. coli* IscR but with full conservation of the cysteine residues known to coordinate the [2Fe-2S] cluster (Cys$^{92, 98, 104}$, *E. coli* numbering) (Fig. 1C) (10).

Clusterless (apo) IscR from *E. coli* was shown to activate suf operon expression during stress conditions, such as iron starvation (6). The as-purified apo form of the protein encoded by *T. potens* gene TherJR_1914 (apo-IscR^{Tp}-wt) was found to bind to the upstream region of the putative suf operon, between genes TherJR_0922 and TherJR_0923 (Fig. 1D). A similar behavior was observed for a triple mutant (C92/101/107S) of IscR^{Tp} (apo-IscR^{Tp}) (Fig. 1D) where all putative cluster-binding cysteine residues (Fig. 1C) were replaced by serine. Given the structural similarity between cysteine and serine and the requirement for homogeneous sample for downstream functional and structural assays, this variant was used in all experiments where the apo form of IscR^{Tp} was required. The ability of apo-IscR^{Tp}-wt and apo-IscR^{Tp} to bind the promoter region of the suf operon suggests that IscR^{Tp} can function as an Fe/S cluster regulator in this organism, with the apo form involved in the regulation of the suf operon expression, as observed for *E. coli*. Although such regulators have been found and characterized in a number of Gram-negative bacteria (7, 8, 33–35), the characterization of orthologous proteins from Gram-positive species has not yet been reported. Therefore, *T. potens* has a unique organization and regulation of Fe/S cluster assembly genes, among Gram-positive bacteria.

Overall Structure of *T. potens* IscR. The 3D structure of free apo *T. potens* IscR, with the putative cluster-binding cysteines mutated to serine (the clusterless IscR triple-mutants C92/101/107S for *T. potens* or C92/98/104S for *E. coli* are hereby termed apo-IscR^{Tp} and apo-IscR^{Ec}, respectively) was determined by X-ray crystallography from tetragonal (P4$_1$) crystals diffracting to 1.6-Å resolution. The crystallographic asymmetric unit contains the functional IscR homodimer (Fig. 2A). Apo-IscR^{Tp} monomers
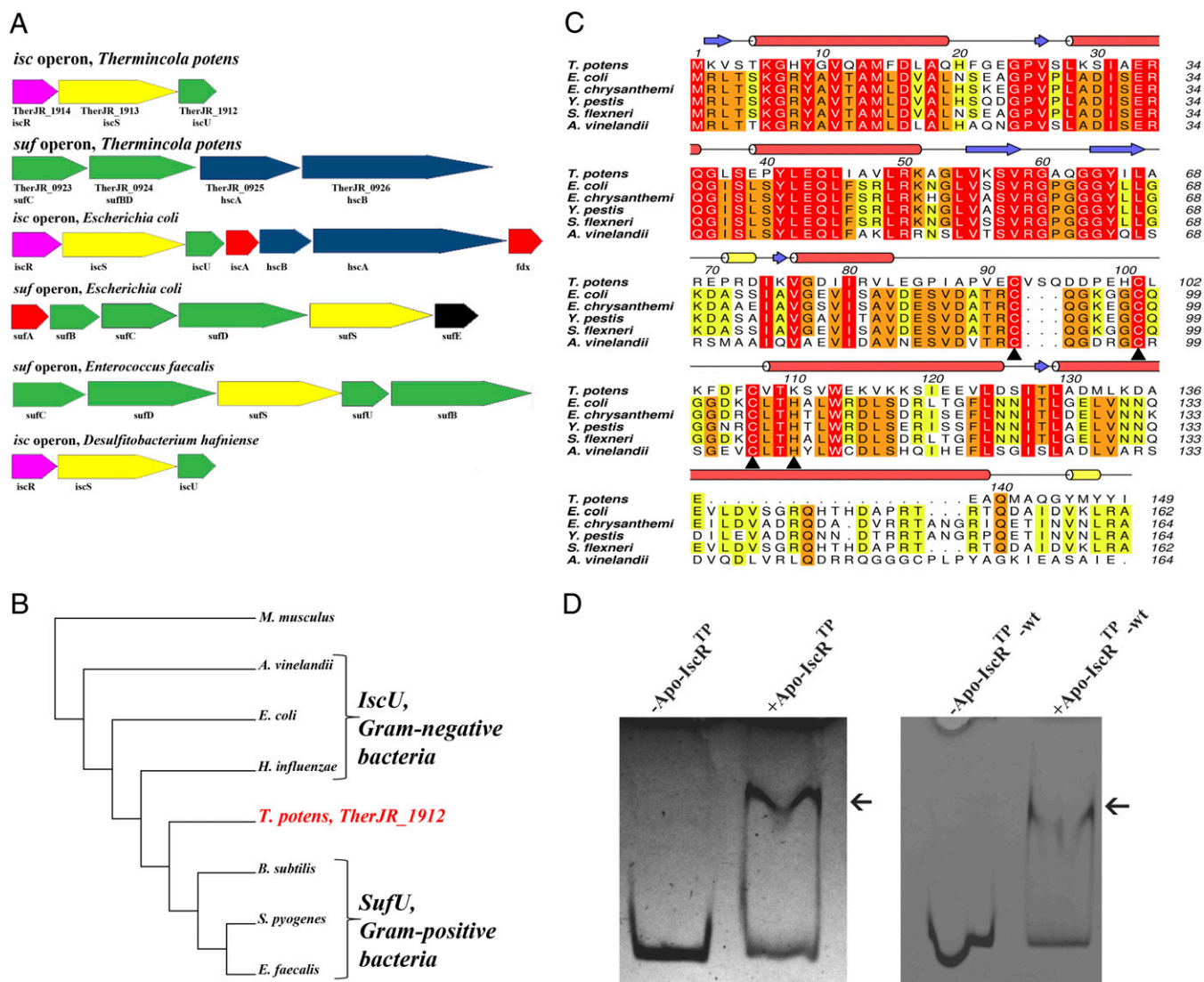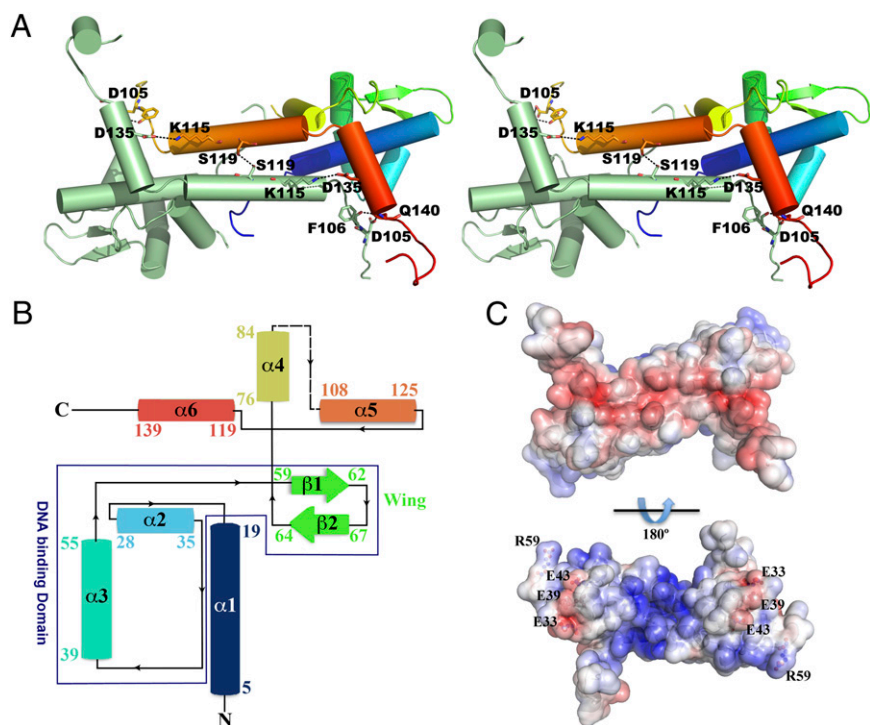
Fig. 1. Identification of an Fe/S cluster biosynthesis regulator in *T. potens*. (*A*) *T. potens* possesses a unique organization of genes involved in Fe/S cluster biosynthesis, with both *isc* and *suf* operons. Colors denote gene function conservation between Gram-negative (*E. coli*), Gram-positive (*E. faecalis*), and DMRB Gram-positive bacteria (*T. potens* and *D. hafniense*). (*B*) The amino acid sequence of *T. potens* scaffold protein reveals features characteristic of the IscU-proteins from Gram-negative bacteria. Neighbor-joining phylogenetic analysis of conserved protein sequences of putative IscU-type or SufU-type proteins in both Gram-positive (*T. potens*, *Streptococcus pyogenes*, *E. faecalis*, *B. subtilis*) and Gram-negative bacteria (*E. coli*, *Azotobacter vinelandii*, *Haemophilus influenza*), using *Mus musculus* as outgroup. The sequences were aligned with three distinct alignment algorithms as implemented in ADOPS (57). The resulting cladogram places the *T. potens* scaffold protein between IscU proteins from Gram-negative bacteria and SufU proteins from other Gram-positive bacteria. (*C*) The *T. potens* TherJR_1914 gene codes for a protein that is highly homologous to IscR from Gram-negative bacteria. Strictly conserved amino acids are highlighted in red, and increasing residue conservation is represented by a color gradient from green to red. Alignment prepared with ClustalW (58) and colored with Aline (59). (*D*) *T. potens* apo-IscR recognizes the upstream *suf* operon region between genes TherJR_0922 and TherJR_0923. Incubation of either apo-IscR Cys-to-Ser mutant (apo-IscR^{TP}) or its as-purified wild-type version (apo-IscR^{TP}-wt) with the putative *suf* promoter region (*suf* sequence) (Table S1) resulted in a mobility-shift (arrow).

are predominantly α-helical and, whereas the N-terminal region is formed by three consecutive α-helices preceding the characteristic wing β-hairpin, the C-terminal domain is exclusively α-helical (Fig. 2*B*). Within each monomer, the N-terminal α-helix (α1) interfaces with the wing-helix subdomain (α2-α3-β1-β2) and with the N-terminal end of the dimerization helix (α5) from the adjacent monomer. The dimerization helix, which comprises two of the putative iron-sulfur cluster binding residues (101 and 107), is further stabilized by close contacts with helix α6 from the adjacent monomer. Residues 86–100, encompassing part of the putative iron-sulfur cluster-binding segment (Fig. 2*B*), are disordered in both monomers and could not be modeled (Fig. 2 *A* and *B*). The structures of the monomers are

nearly identical, superposing with an rmsd of 0.17 Å for 133 aligned Cα atoms.

Apo-IscR^{TP} dimer formation involves mostly interactions between residues from helix α5 of each monomer, but residues from helices α1 and α4 further stabilize the homodimer. The extensive dimerization interface between the two helices α5 is hydrophobic, except for a single hydrogen bond between the side chains of neighboring Ser119 residues. Further intermonomer polar interactions are established between the side chain of Gln140 at the C terminus of helix α6 and Asp105 OD1 and Phe106 O (Fig. 2*A*).

In agreement with its DNA-binding function (Fig. 1*D*), the electrostatic surface potential of apo-IscR^{TP} is highly polarized

Fig. 2. The 3D structure of *T. potens* IscR. (*A*) Stereoscopic view of the biologically active apo-IscR^{Tp} dimer, highlighting important residues (represented as sticks) at the dimerization interface. One of the monomers is colored from N- (blue) to C-terminal (red), with highlighted residues color-coded (nitrogen blue, oxygen red). Hydrogen bonds are represented as dashed lines. (*B*) Topology diagram of the apo-IscR^{Tp} monomer. Secondary structure element colors match those of *A*. (*C*) Solid-surface representation of the apo-IscR^{Tp} dimer, with mapped electrostatic surface potential contoured from +5 (blue) to −5 (red) kbTe^{-1} [kb, Boltzmann's constant; T, temperature (K); e, charge of an electron].

(Fig. 2*C*), being predominantly negative at the solvent-exposed face of helices α5 and α6, and positively charged at the opposite, putative DNA-binding side. This asymmetric surface-charge distribution promotes initial DNA positioning by nonspecific electrostatic contacts, before fine-tuning through the establishment of base- and shape-specific interactions. Negatively charged residues (Glu33, Glu39, and Glu43) protrude from this positively charged surface (Fig. 2*C*), resembling *E. coli* IscR (13). Among these residues, Glu39 is unique in *T. potens* IscR (replaced by a leucine residue in closely related molecules) (Fig. 1*C*).

T. potens IscR belongs to the Rrf2-like family of transcriptional regulators and displays highest structural similarity with the global cysteine regulator CymR from *B. subtilis* (PDB ID code 2Y75) (36) and *S. aureus* (PDB ID code 3T8T) (37) as well as with the recently determined structure of *E. coli* IscR (PDB ID code 4HF0) (13), superposing with these models with an rmsd of 1.5–2.3 Å. The conserved DNA-binding helix-turn-helix motif can also be superposed to the corresponding domain of more distantly related proteins, albeit with somewhat higher rmsd values (Table 1). The DNA-binding winged-helix motif is structurally similar in the selected structures (Fig. 3 *A* and *B*), and most structural differences occur in the dimerization helix α5

and in the length and orientation of helix α4, which precedes the iron-sulfur cluster-binding region.

Molecular Details of IscR-DNA Interaction. To better grasp the fine molecular details of specific promoter sequence recognition by IscR, we determined the structure of apo-IscR from *E. coli* (C92/98/104S triple mutant with the putative cluster-binding cysteine residues mutated to serine; apo-IscR^{Ec}) in complex with the *E. coli hya* (hydrogenase-1) promoter sequence (8, 12, 31). The asymmetric unit contains the apo-IscR^{Ec} biological dimer bound to a 26-bp double-stranded oligonucleotide with a single nucleotide overhang at the 5′ end of each strand (Fig. 4*A* and Table S1). This structure is very similar to the recently reported model of *E. coli* apo-IscR (C92/98/104A triple mutant) in complex with DNA (PDB ID code 4HF1) (13). Overall, the protein main chains of the two models superpose with an rmsd of 0.5 Å for 124 aligned Cα atoms. DNA binding induces a small concerted movement of the wing-helix motif within each apo-IscR^{Ec} monomer and of the dimerization helix α5 of the adjacent monomer (Fig. S2 *A* and *B*) (13). In the complex, helix α3 of the winged-helix motif from each apo-IscR^{Ec} monomer is presented to the major groove of the corresponding DNA half-site whereas the β-hairpin inserts into the minor groove (Fig. 4*A*).

Table 1. Structural similarity between *T. potens* IscR and other winged-helix transcription regulators

Protein	PDB ID code	rmsd, Å	No. of aligned Cα atoms	Amino acid sequence identity, %*	Z-score
B. subtilis CymR	2y75	1.5	119	55	17.2
E. coli IscR (unliganded)	4hf0	2.0	116	41	16.8
E. coli IscR (DNA complex)	4hf1	2.3	120	40	16.3
S. aureus CymR	3t8t	2.3	119	46	15.9
Putative transcriptional regulator from *L. innocua*	3lwf	3.8	124	48	14.9
B. cereus protein BC1842	1ylf	2.7	118	20	13.9

S. aureus, *Staphylococcus aureus*; *L. innocua*, *Listeria innocua*; *B. cereus*, *Bacillus cereus*.
*Structure-based sequence alignment, as calculated by Dali server (http://ekhidna.biocenter.helsinki.fi/dali_server/start) (60).
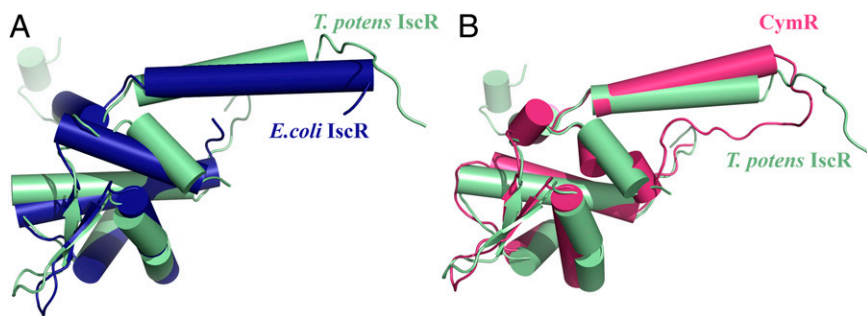
Fig. 3. IscR from *T. potens* is structurally similar to other winged-helix transcriptional regulators. Superposition of apo-IscR^{Tp} monomer (green) with (*A*) free *E. coli* apo-IscR C92/98/104A (blue; PDB ID code 4HF0) and (*B*) free *B. subtilis* CymR (magenta; PDB ID code 2Y75) highlighting the overall structural conservation.

As observed for apo-IscR^{Tp}, the apo-IscR^{Ec} biological dimer is highly polarized with a clustering of basic residues on the DNA-interacting surface (Fig. S2C). Although the positive electrostatic surface might be required to orient the protein toward productive binding with the DNA duplex, in the apo-IscR^{Ec}-DNA complex very few protein-DNA interactions involve basic side chains. A notable exception is Arg59 that protrudes from the β-hairpin wing and wedges into the symmetrically related AT-rich regions of the narrow groove (Fig. 4*A*). Accordingly, the *E. coli* apo-IscR R59A mutant is unable to bind to either type-1

or type-2 promoter sequences, demonstrating the relevance of this residue for DNA recognition (13). Further interactions with the minor grove are established by residues at the tip of the wing (Gly60-Pro61) that slot between deoxyribose moieties and by Pro27 that packs against phosphodiester linkages.

Apo-IscR^{Ec} residues contributing to the partial negative charge within the DNA-binding surface (Glu33, Asp30, and Glu43) (Fig. S2C) are structurally equivalent to the acidic residues identified on the equivalent side of apo-IscR^{Tp}. However, only Glu43 contacts directly the bound oligonucleotide. Together
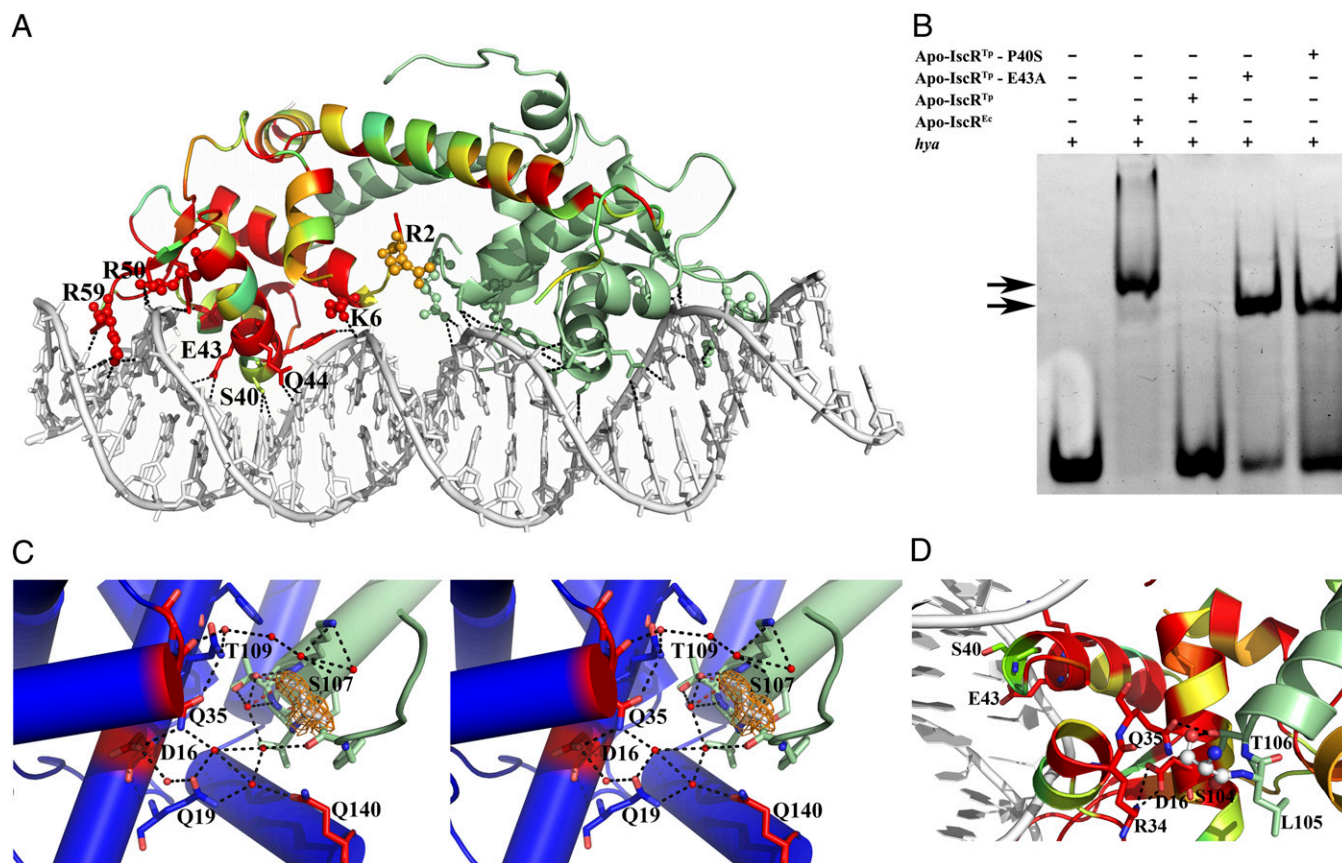
Fig. 4. Binding of IscR to type-2 promoter sequences. (*A*) Bidentate binding of apo-IscR^{Ec} (C92/98/104S) to the *hya* promoter DNA sequence. In one of the monomers, residues are colored according to conservation, where red corresponds to positions strictly conserved between *E. coli* and *T. potens* IscR. Residues at the DNA-interacting interface are highlighted as sticks and basic residues as spheres. Hydrogen bonds between apo-IscR^{Ec} and DNA are represented as dotted lines. (*B*) Electrophoretic mobility-shift assay analysis of apo-IscR binding to the *E. coli* *hya* promoter. Arrows denote observed band-shifts. (*C*) Stereoscopic view of the intricate network of hydrogen bonds in apo-IscR^{Tp} (one monomer of the functional dimer is colored green and the other one blue) centered on the cluster-binding residue 107 (light gray). The $2F_o - F_c$ electron density map around residue 107 is represented as an orange mesh. Water molecules and strictly conserved residues in closely related IscR molecules are colored red. (*D*) In apo-IscR^{Ec} (C92/98/104S), serine 104 (ball and stick) participates in a network of polar interactions with neighboring residues (sticks), cross-linking helices α1, α2, and α5. The corresponding cysteine residue in the wild-type protein could be part of a sensing mechanism for the presence of the Fe/S cluster.

with Gln44 (conserved) and Ser40 (variable), Glu43 is involved in base-specific recognition within the major groove (Fig. 4A). It has been demonstrated that Glu43 is a crucial selectivity filter that negatively affects binding of *E. coli* apo-IscR to type-1 promoter sequences, containing thymine at positions 6 and 7, due to lack of suitable hydrogen-bond donors (13).

Subtle Structural Differences Modulate DNA Sequence Recognition Specificity. Overall, there is a striking conservation of the DNA-binding interface (Figs. 1C and 4A). Apo-IscR^{Tp} differs from the *E. coli* homolog only at four positions within the interaction surface, which could result in altered DNA binding affinity and specificity: Ser27 (Pro27 in apo-IscR^{Ec}), Pro40 (Ser40 in apo-IscR^{Ec}), and Ala61-Gln62 (Pro61-Gly62 in apo-IscR^{Ec}). The replacement of Pro27 by a serine is likely to increase the flexibility of the linker between the first two α-helices although a large change in DNA affinity is not predictable. In contrast, the substitution of Pro61-Gly62 by an Ala-Gln dipeptide can impact the conformation of the wing β-hairpin and interfere with the tight packing of this structural element within the minor groove. In particular, the residue at position 40 is likely to play a key role in sequence-specific recognition of DNA. In the apo-IscR^{Ec}-DNA complex, the protein packs very tightly within the major groove, leaving limited space for bulkier residues (Fig. 4A). Although a proline could be accommodated at the N terminus of helix α3 without helical disruption, the resulting steric hindrance might prevent the placement and base readout of the conserved Glu43-Gln44 and/or contacts of the residues interacting with the phosphate backbone (Tyr9, Ser38, Tyr41). Substitution of the purines interacting with Ser40 (G20′ and A19) prevents binding of *E. coli* apo-IscR to the *hya* promoter sequence, highlighting the importance of this residue for base-specific recognition (12). Further, mutation of Ser40 to alanine in *E. coli* IscR decreases binding to the *hya* promoter by 90% compared with the wild-type protein, a decrease that is sequence-dependent and more pronounced for type-2 sites (13).

The influence of Pro40 in apo-IscR^{Tp} interaction with DNA is evidenced by its inability to bind the *E. coli hya* promoter sequence (Fig. 4B and Table S2). Replacement of Pro40 in apo-IscR^{Tp} by the structurally equivalent amino acid in *E. coli* IscR (apo-IscR^{Tp} P40S) is sufficient to allow binding to the heterologous promoter (Fig. 4B and Table S2). The presence of a serine residue at position 40 is likely to alleviate the tight packing of IscR within the major groove of DNA, reducing steric hindrance and allowing binding. Accordingly, the IscR^{Tp} E43A mutant, where the shorter alanine side chain can provide room for positional adjustments of this region, also recognized the *hya* sequence (Fig. 4B) with an affinity comparable with that of the *E. coli* protein, as assessed by microscale thermophoresis (Table S2). Taken together, these results suggest that substitution of Ser40 by a proline in apo-IscR^{Tp} prevents base recognition through steric hindrance, an impairment lifted by introducing less bulky residues at either position 40 or 43.

Position of the Cluster-Binding Residues. In contrast to previous studies with *E. coli* IscR, where all putative cluster-binding cysteine residues were mutated to alanine to obtain homogeneous clusterless protein (10, 12, 13), in *T. potens* IscR, the corresponding residues were mutated to serine, which is a closer structural match. In all *E. coli* and *T. potens* IscR structures, the region involved in iron-sulfur cluster association is partially disordered, but the serine residues replacing Cys107 in apo-IscR^{Tp} and Cys104 in apo-IscR^{Ec} are clearly visible in the electron density maps (Fig. 4 C and D). In contrast to what is observed for the Cys-to-Ala mutant structure of *E. coli* free apo-IscR where the two visible cluster ligands (Ala104 and His107) are on the outer face of the longer dimerization helix α5 (13), in apo-IscR^{Tp}, the equivalent Ser107 is part of the coil region preceding

helix α5, and the crystal structure shows that it participates in a water-mediated network of hydrogen bonds connecting this structural segment to helices α1 and α2 (Fig. 4C). In particular, the Ser107 side-chain is hydrogen-bonded to Thr109 OG1 within each monomer. Both residues also establish polar interactions with ordered solvent molecules that participate in a hydrogen-bond network interfacing the two monomers of the functional dimer and involving the side chains of Gln19, Asp16, and Gln35 from the adjacent monomer (the last two residues strictly conserved across IscR molecules) (Fig. 1C). Of particular relevance is the involvement of Asp16 side chain in a salt bridge with Arg34 within the DNA-binding helix-turn-helix motif. The cluster-binding segment is further stabilized by a polar contact with Gln140 of the adjacent monomer, which also connects the corresponding helices α1 and α6. Altogether, this polar interaction network tightly connects the cluster-binding segment at the N-terminal portion of helix α5 from one monomer with the N-terminal helix α1, helix α6, and helix α2 from the adjacent monomer. Particularly, this network suggests an interconnection between structural changes in the cluster-binding segment and functional effects at the DNA-binding interface.

The geometry of the hydrogen bonds established by the mutated Ser107 in apo-IscR^{Tp}, and the rotational freedom of Thr109, evidenced by the two discrete conformations of its side-chain in the current crystal structure, are compatible with the existence of similar hydrogen bonds involving Cys107 in the cluster-free wild-type IscR. Indeed, the cysteine side chain thiol group is a moderately good hydrogen bond donor, sometimes crucial for protein activity and function (38–41).

In the crystal structure of the apo-IscR^{Ec}-DNA complex, Ser104 (structurally equivalent to Ser107 in apo-IscR^{Tp}) is also well defined in the electron density maps. In one of the monomers, Ser104 is part of helix α5, as previously reported for the triple Cys-to-Ala mutant structure (13). However, in the other monomer of the apo-IscR^{Ec} dimer, this residue hydrogen bonds to the conserved Thr106 (Thr109 in *T. potens* IscR), which in turn engages in a network of direct polar contacts cross-linking the dimerization helix α5 to the C terminus of the adjacent helix α2 (Arg34, Gln35) and to helix α1 (Asp16) (Fig. 4D). This hydrogen bond network involves direct interactions between the amino acid side chains, in contrast to what is observed in apo-IscR^{Tp}, where solvent molecules mediate some of the contacts. In the Cys-to-Ala triple mutant of *E. coli* IscR, this arrangement of polar contacts is preserved, with the expected exception of residue 104, which is there an alanine (13).

The predicted function of residue 107/104 (in *T. potens* and *E. coli*, respectively) in iron-sulfur cluster binding, as well as its location between the dimerization helix of one monomer and the first helix of the helix-turn-helix DNA-binding motif of the neighboring subunit, suggest a possible role as a central nanoswitch, whereby cluster binding-induced movement could trigger a global motion involving both the dimer interface and the DNA-binding region from the opposite monomer. The resulting structural changes could explain the observed alteration in DNA binding specificity upon cluster association (13).

A Single Mutation Allows apo-IscR^{Tp} to Recognize Type-1 Promoter Sequences from *T. potens* and *E. coli*. In *E. coli*, holo-IscR was shown to interact with both type-1 and type-2 DNA motifs in a similar manner whereas apo-IscR bound solely to type-2 promoter sequences (12). Recently, it was also demonstrated that replacement of Glu43 by alanine in *E. coli* IscR C92/98/104A removed unfavorable interactions with type-1 motifs, allowing recognition of these promoters (13). The *T. potens isc* promoter region displays *cis*-regulatory elements similar to those identified in the type-1 *E. coli* iscRSUA-HscBA-fdx, including the −35 hexamer and the −10 element sequences (7). In fact, it is possible to delimit a segment (*iscTp_1*) (Fig. 5A and Table S1) displaying
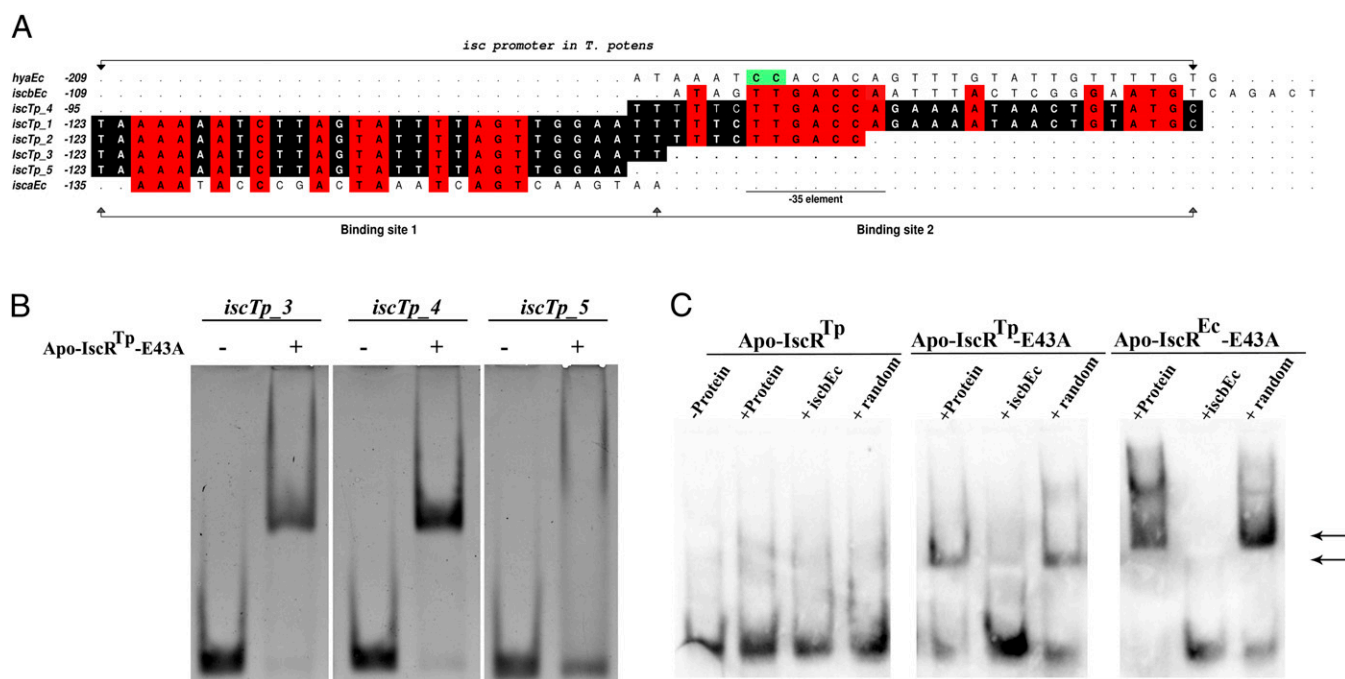
Fig. 5. Modulation of apo-IscR^{Tp} specificity by a single point mutation. (A) IscR binding sites in type-1 [*T. potens isc (iscTp)* and *E. coli isca (iscaEc)* and *iscb (iscbEc)*] and type-2 [*E. coli hya (hyaEc)*] promoters. Numbers refer to the most upstream base of each IscR site relative to the corresponding start codon. Conserved bases between the *isc* promoters are highlighted in red whereas bases conserved between the five *T. potens isc* promoter sequences are shaded black. The highly conserved CC motif in type-2 promoters is colored green (12). (B) There are two independent binding sites for apo-IscR^{Tp} E43A in the *T. potens isc* promoter. Purified apo-IscR^{Tp} E43A (7.5 μM) was incubated with *iscTp_3*, *iscTp_4* and *iscTp_5* sequences, analyzed by nondenaturing PAGE, and visualized by ethidium bromide staining. An arrow denotes the DNA band-shift upon complex formation. (C) Cross-recognition of the *E. coli isc* promoter by *T. potens* IscR. Purified proteins (apo-IscR^{Tp}, apo-IscR^{Tp} E43A, or apo-IscR^{Ec} E43A) were incubated with DIG-labeled *iscrb* promoter sequence (*iscbEc*) (Table S1) and analyzed by nondenaturing PAGE. An arrow denotes bands indicative of DNA–IscR complex formation. Where indicated, cold *iscrb* or a similarly sized random sequence (random) was added in 100-fold molar excess as competitor.

48% identity to the *E. coli isc* promoter sequence and containing a −10 element and a consensus −35 hexamer of the Eσ^{70}-binding site with a 20-bp spacer region (13).

Similar to what is observed for *E. coli* apo-IscR and *isc*, apo-IscR^{Tp} does not bind *iscTp_1* (Fig. S3*A*). Using an enzymatic system under oxygen-depleted atmosphere (42), an Fe/S cluster could be reversibly reconstituted in wild-type apo-IscR^{Tp}, yielding the holo form of the protein (reconstituted IscR^{Tp}-wt; R-IscR^{Tp}-wt), as judged by the appearance of absorption maxima at 320 and 420 nm (Fig. S3*B*). A dose-dependent structural change of *iscTp_1* DNA could be identified by circular dichroism spectroscopy, upon R-IscR^{Tp}-wt binding (Fig. S3*C*). These results demonstrate that, as expected for a bona fide IscR, the enzymatically reconstituted Fe/S cluster-bound form of IscR^{Tp}-wt binds to the *T. potens isc* promoter region (Fig. S3*C*). As seen for *E. coli* IscR (13), the single point mutant apo-IscR^{Tp} E43A binds specifically to the *iscTp_1* sequence, seemingly forming two distinct complexes—with either one or two IscR dimers binding to the target sequence—as suggested by the two observed DNA band shifts (Fig. S3*A*). This finding is further supported by the observation of a single complex with the 3′-trimmed *iscTp_1* sequence, termed *iscTp_2* (Fig. 5*A*, Table S1, and Fig. S3*A*). In *E. coli*, DNase footprinting led to the identification of two IscR binding sites within the *isc* promoter region, *iscra* and *iscrb* (8). Two highly homologous regions could be identified in the *T. potens isc* promoter, *iscTp_3* and *iscTp_4* (Fig. 5*A* and Table S1), to which apo-IscR^{Tp} E43A displays specific binding (Fig. 5*B* and Table S2). Further, removal of the two 3′-end nucleotides of *iscTp_3*, yielding the shorter *iscTp_5* (Fig. 5*A* and Table S1), effectively prevents binding of apo-IscR^{Tp} E43A (Fig. 5*B* and Table S2), in good agreement with the observed bidentate

binding of IscR to the minor groove of AT-rich segments at the termini of its recognition sequence (Fig. 4*A*).

In line with the structural similarity of *E. coli* and *T. potens* IscR proteins and the considerable conservation of *isc* promoter sequences, there is cross-recognition between the transcriptional regulator of *T. potens* and the *E. coli* promoter. Although apo-IscR^{Tp} does not bind *E. coli iscrb* (*iscbEc*, Table S1), this sequence is specifically recognized by the E43A mutant (Fig. 5*C* and Table S2), as observed for *E. coli* apo-IscR (13). Therefore, the unique mechanism of promoter-sequence discrimination by IscR seems to be conserved between these organisms.

Discussion

We performed a detailed analysis of the product of gene TherJR_1914 from *T. potens*, undoubtedly establishing its functional relationship with the Fe/S cluster-binding transcription regulator IscR, known to control Fe/S cluster biogenesis in several Gram-negative bacteria. The identification of an IscR homolog in *T. potens* was unprecedented: most other Gram-positive bacteria studied so far do not code for any IscR-like proteins or have an *isc* operon, and the rare cases where an *isc* operon is present (e.g., the DMRB *D. hafniense* or the bacterium *C. perfringens*) (30) lack the SUF machinery.

The combination of biochemical and structural studies, on *T. potens* IscR and its homolog from *E. coli*, revealed also an unforeseen conservation of the unique mode of IscR promoter sequence recognition and discrimination. Despite extensive conservation of the DNA-binding surface, apo-IscR^{Tp} was unable to recognize the heterologous *hya* promoter from *E. coli*. Residue at position 40 played a pivotal role in this process because relief of steric hindrance (P40S mutant) was sufficient to

promote binding. These subtle differences in specificity highlight the precise tailoring of each IscR molecule to its cognate partners, despite overall conservation of the recognition mechanism.

Similar to the *E. coli* molecule (12), the clusterless form of the protein binds to the here-identified *T. potens suf* (type-2) promoter whereas the previously unidentified type-1 promoter (*isc*) is recognized by holo-IscR. In the absence of the Fe/S cluster, the strictly conserved E43 residue is pivotal for discriminating between type-1 and type-2 promoters by establishing specific interactions with an invariant CC dinucleotide in type-2 sequences. In fact, mutation of this residue to an uncharged alanine seems to mimic the cluster-induced specificity switch of IscR, allowing the clusterless regulator to recognize and to bind to type-1 promoter sequences (13). In apo-IscR^{Tp}, the E43A mutation promotes binding to two sequences upstream of the *T. potens iscRSU* operon. These regions are highly homologous to the *E. coli isc* sequences recognized by both holo- and mutant apo-IscR E43A. Given that one of these sequences (*iscTp_4*) contains a −35-element sequence, we propose that *T. potens* holo-IscR may act as a repressor of Fe/S biogenesis by hindering RNA polymerase binding. As a whole, our results suggest a conserved regulation mechanism by IscR, where Fe/S cluster binding to this transcription regulator enables recognition of type-1 promoters, a process that is mimicked by the E43A mutation.

By using structurally relevant mutants, where serine replaces all putative cluster-coordinating cysteine residues, a network of polar interactions could be identified, connecting the cluster-binding region of one subunit to the DNA-contacting interface of its neighbor in the functional IscR dimer. Any perturbation resulting from cluster ligation could therefore be allosterically transmitted to the nucleic acid-binding region that comprises the conserved E43. Regulation through Fe/S cluster ligation allows *T. potens* IscR to act as a sensor and to be a central player of an auto-regulatory loop responsible for keeping the appropriate levels of cellular Fe/S cluster formation and delivery.

Methods

Protein Expression and Purification. A synthetic *iscr* gene, encoding the same amino acid sequence as TherJR_1914 from the *T. potens* genome, except for a Gly-Leu insertion immediately downstream from the N-terminal methionine, was ordered from Eurofins MWG Operon. The *E. coli iscr* gene (b2531) fragment spanning nucleotides +4 to +489 of the IscR ORF was amplified from an *E. coli* K12 colony using specific primers. Both ORFs were cloned into the NdeI and XhoI sites of the expression vector pET30a (IscR^{Tp}-wt) or into the Acc65I and NcoI sites of the expression vector pETZ2_1a (43). The latter constructs were used to obtain the triple mutants (C92/101/107S for *T. potens* or C92/98/104S for *E. coli*) corresponding to the clusterless forms of the proteins (apo-IscR^{Tp} and apo-IscR^{Ec}) by site-directed mutagenesis.

The N-terminal His$_6$-tagged apo-IscR^{Tp} was overexpressed in *E. coli* BL21 (DE3) cells and the *E. coli* protein in *E. coli* BL21 Star (DE3) (Life Technologies). Briefly, cells were grown in LB medium at 37 °C until OD$_{600}$ = 0.7. At this point, the temperature was decreased to either 25 °C (apo-IscR^{Ec}) or 30 °C (apo-IscR^{Tp}), and the expression was induced with the addition of 0.5 mM isopropyl β-D-1-thiogalactopyranoside (IPTG). Cells were harvested by centrifugation after 4 h and lysed by incubation (60 min on ice with shaking) with 25 μg/mL chicken egg white lysozyme (Sigma). Clarified protein extracts in 20 mM sodium phosphate (pH 7.5), 0.5 M NaCl, 10 mM imidazole, 5% (vol/vol) glycerol, 150 mM arginine, and 2.5 mM β-mercaptoethanol (buffer A) were loaded onto a HisTrap HP column (GE Healthcare) preequilibrated in the same buffer, and bound proteins were eluted with buffer A containing 125 mM imidazole. The IscR-containing fractions were pooled, and the His$_6$ and the solubility tags were removed by incubation with tobacco etch virus (TEV) protease at 4 °C concomitantly to an overnight dialysis against 20 mM sodium phosphate (pH 7.5), 0.2 M NaCl, 10 mM imidazole, 5% (vol/vol) glycerol, 150 mM arginine, and 2.5 mM β-mercaptoethanol. Pure recombinant IscR was separated from the expression tag and noncleaved material by a second immobilized-metal affinity chromatography (IMAC) step, in the same conditions as described above. The buffer was further exchanged for 10 mM Hepes (pH 7.5), 800 mM KCl, and 5% (vol/vol) glycerol using a HiPrep 26/10 (GE Healthcare) desalting column. The protein was either used immediately or flash-frozen in liquid nitrogen and

stored at −80 °C until needed. Final protein concentrations were estimated by measuring the absorbance of the samples at 280 nm.

Point mutants apo-IscR^{Tp} E43A, apo-IscR^{Ec} E43A, and apo-IscR^{Tp} P40S were generated by site-directed mutagenesis of the pETZ2_1a constructs. All IscR protein variants used for biochemical and crystallization experiments were expressed and purified as described for apo-IscR^{Tp}, except for apo-IscR^{Tp}-wt, which was purified by a single IMAC step followed by desalting on a HiPrep 26/10 column (GE Healthcare). The *E. coli* cysteine desulfurase IscS used in reconstitution assays was expressed and purified as described previously (42).

Fe/S Cluster Reconstitution. Reconstitution of the Fe/S cluster of apo-IscR^{Tp}-wt was performed under oxygen-depleted atmosphere (<3 ppm O$_2$) in an anaerobic chamber (Belle Technology). All buffers used were sparged with nitrogen gas for 20 min and kept in the anaerobic chamber for at least 12 h before use. Small volumes of aerobically purified proteins (apo-IscR^{Tp}-wt and *E. coli* IscS), as well as sodium dithionite, cysteine, and iron (II) sources were equilibrated in the same low-oxygen conditions for 1 h.

An apo-IscR^{Tp}-wt solution (25 μM) was mixed with ammonium iron (II) sulfate (Sigma) and L-cysteine (Sigma) in 20-fold and eightfold molar excess, respectively. The reaction [in 50 mM Tris (pH 8), 150 mM NaCl, 5 mM DTT] was started after 10 min by addition of 2 μM *E. coli* IscS, and Fe/S cluster formation was followed by monitoring absorbance at 420 nm. Upon reaction completion, R-IscR^{Tp}-wt was purified by IMAC (His-Buster Nickel spin columns; Amocol). Absorption spectra (250–750 nm) were recorded immediately after purification and upon sample reduction with 2 mM sodium dithionite. Control reactions were performed omitting L-cysteine (nonreconstituted IscR^{Tp}-wt; NR-IscR^{Tp}-wt).

Electrophoretic Mobility-Shift Assay. Complementary oligonucleotides (Sigma) containing the sequence of the *E. coli hya* or of the *T. potens isc* promoter (Table S1) were annealed into double-stranded DNA by heating a 50-μM solution to 95 °C for 5 min in a water bath, followed by slowly (overnight) cooling to room temperature. For electrophoretic mobility-shift assay (EMSA) analysis using the complete sequence of the *T. potens suf* promoter region (Table S1), the sequence upstream of the *sufC* gene (TherJR_0923) was amplified by PCR using a synthetic template (Eurofins). DNA solutions (1 μM) were incubated with 7.5–10 μM purified protein at room temperature for 20 min in binding buffer [40 mM Tris·HCl (pH 8.0), 100–150 mM KCl, 5% (vol/vol) glycerol, and 1 mM DTT], and the resulting complexes were resolved on 8% (wt/vol) nondenaturing polyacrylamide gels using 1× TAE (40 mM Tris·HCl, 20 mM acetic acid, and 1 mM EDTA) as running buffer. DNA was detected by either ethidium bromide staining or chemiluminescent detection. For chemiluminescent detection, annealed DNA probes were end-labeled with digoxigenin using recombinant terminal transferase (Roche). The labeled probes (1.5 μmol) were mixed with 11.25 μmol purified IscR in 15 μL of binding buffer [40 mM Tris·HCl (pH 8.0), 10% (vol/vol) glycerol, 1 mM DTT, and 50 mM KCl]. For competition reactions, labeled probe was added after incubating the protein for 10 min with 100-fold molar excess competitor DNA. The samples were separated in 8% (wt/vol) nondenaturing polyacrylamide gels and electroblotted onto positively charged nylon membrane (GE Healthcare), and the digoxigenin-labeled probes were detected with anti-digoxigenin-AP antibody and the chemiluminescent substrate disodium 2-chloro-5-(4-methoxyspiro [1,2-dioxetane-3,2'-(5'-chloro)tricyclo[3.3.1.1(3,7)]decan]-4-yl)-1-phenyl phosphate (CDP-Star; Roche).

Circular Dichroism Measurements. Binding of wild-type IscR^{Tp} to DNA was monitored by circular dichroism (CD) spectroscopy (44). CD spectra were recorded at 20 °C in 1-nm steps on a temperature-controlled Jasco J-815 spectropolarimeter, continuously purged with nitrogen gas. For each sample, the smoothed average of four spectra was considered. Briefly, either anaerobically reconstituted (R-IscR^{Tp}-wt) or nonreconstituted (NR-IscR^{Tp}-wt) and purified apo-IscR^{Tp}-wt was added incrementally to a sealed 10-mm-path quartz cuvette containing the *iscTp_1* sequence (Table S1) in binding buffer, and CD spectra (260–320 nm) were recorded.

Microscale Thermophoresis Assays. Interactions between IscR variants (apo-IscR^{Tp}, apo-IscR^{Tp} E43A, apo-IscR^{Tp} P40S, and apo-IscR^{Ec} E43A) and the different DNA sequences (*iscTp_3*, *iscTp_4*, *iscTp_5*, *hyaEc*, and *iscbEc*) (Fig. 5A and Table S1) were assessed using microscale thermophoresis (45) with a Monolith NT.115 instrument (NanoTemper Technologies). Purifed proteins (20 μM) were labeled using the Monolith NT.115 Protein Labeling Kit RED-NHS (NanoTemper Technologies) according to the manufacturer's instructions. Labeled proteins were diluted to 50 nM in assay buffer [40 mM Tris·HCl (pH 7.9), 150 mM KCl, 5% (vol/vol) glycerol, 1 mM DTT, 0.1% (vol/vol) Tween

Table 2. Statistics of data collection, processing, and refinement

Dataset	*T. potens* IscR* (native)	*T. potens* IscR* (Se-Met)	*E. coli* IscR-DNA complex*
Crystallographic analysis			
Wavelength, Å	0.9763	0.9792	0.8726
Space group	$P4_1$	$P4_1$	$P2_12_12_1$
Unit cell dimensions, Å	a = b = 53.6; c = 118.4	a = b = 53.4; c = 118.7	a = 49.0; b = 75.8; c = 173.4
Resolution range, Å	53.6–1.60 (1.69–1.60)	48.7–2.47 (2.61–2.47)	46.0–2.49 (2.62–2.49)
Reflections (measured/unique)	196,159–43,750 (28,394/6,325)	111,297/11,861 (13,614/1,647)	87,182/23,387 (12,463/3,244)
Completeness, %	99.7 (98.7)	99.1 (94.1)	99.3 (96.3)
Multiplicity	4.5 (4.5)	9.4 (8.3)	3.7 (3.8)
R_{merge}[†]	0.046 (1.299)	0.190 (1.573)	0.103 (0.911)
R_{pim}[‡]	0.024 (0.688)	0.064 (0.555)	0.061 (0.531)
$\langle I/\sigma(I) \rangle$	14.3 (1.6)	7.3 (1.4)	8.6 (1.5)
Monomers per asymmetric unit	2	2	2
Mathews coefficient, $Å^3 \cdot Da^{-1}$	2.53	2.52	3.13
Solvent content, %	51.4	51.2	60.7
Structure refinement			
Resolution range, Å	48.8–1.60	—	46.0–2.49
R_{factor}[§]/Free R_{factor}[¶]	0.202/0.220	—	0.207/0.251
Unique reflections (work/test set)	41,642/1,973	—	22,057/1,193
Water molecules	156	—	15
Total no. of atoms	2,363	—	2,999
No. of macromolecule atoms	2,205	—	2,984
rmsd bond lengths, Å	0.011	—	0.008
rmsd bond angles, °	1.09	—	1.38
Average overall B factor, $Å^2$	38.1	—	77.7
Ramachandran favored, %	97.5	—	96.0
Ramachandran outliers, %	0.0	—	0.4
PDB entry	4cic	—	4chu

*Values in parentheses correspond to the outermost resolution shell. Each dataset was recorded from a single crystal.

[†]$R_{merge} = \sum_{hkl}\sum_i |I_i(hkl) - \langle I(hkl)\rangle|/\sum_{hkl}\sum_i I_i(hkl)$, where $I_i(hkl)$ is the observed intensity and $\langle I(hkl)\rangle$ is the average intensity of multiple observations of symmetry-related reflections.

[‡]$R_{pim} = \sum_{hkl}[1/(N-1)]^{1/2} \sum_i |I_i(hkl) - \langle I(hkl)\rangle|/\sum_{hkl}\sum_i I_i(hkl)$, where $I_i(hkl)$ is the observed intensity and $\langle I(hkl)\rangle$ is the average intensity of multiple observations of symmetry-related reflections.

[§]$R_{factor} = \sum ||F_o| - |F_c||/\sum|F_o|$, where $|F_o|$ and $|F_c|$ are observed and calculated structure factor amplitudes, respectively.

[¶]Free R_{factor} is the cross-validation R_{factor} computed for a randomly chosen subset of 5% of the total number of reflections, which were not used during refinement.

20]. Ligand dilutions were prepared in assay buffer without Tween 20 and mixed with each protein sample at a volume ratio of 1:1. Measurements with apo-IscR^{Tp}, apo-IscR^{Tp} P40S, and apo-IscR^{Tp} E43A were performed in standard capillaries whereas hydrophilic capillaries were used for measurements with apo-IscR^{Ec} E43A. For each interaction, data from at least two independent runs were averaged, and the average curve was fitted with NTAnalysis software (NanoTemper Technologies).

Crystallization of apo-IscR^{Tp} and apo-IscR^{Ec}:*hya* Complex. Initial crystallization conditions for apo-IscR^{Tp} were screened at 20 °C using the sitting-drop method with commercial sparse-matrix crystallization screens. Drops consisting of equal volumes (1 μL) of protein (at 20 mg/mL) and precipitant solution were equilibrated against a 300-μL reservoir. Crystals were obtained after 2 d using 0.1 M Bis-Tris (pH 6.5) and 3 M NaCl as precipitant. Before data collection, crystals were cryoprotected by immersing them briefly in a 1:1 mixture of precipitant solution and 40% (vol/vol) of 2 mg/mL NDSB-201 (3-(1-pyridino)-1-propane sulfonate) solution in ethylene glycol and flash-cooled in liquid nitrogen (46). Selenomethionyl apo-IscR^{Tp} crystallized in the same conditions and was cryoprotected following the procedure described above.

A 3.8-fold molar excess of apo-IscR^{Ec} was mixed with double-stranded oligonucleotide (prepared as described in *Electrophoretic Mobility-Shift Assay*) comprising region −30 to −55 of the *E. coli hya* promoter sequence with a single-base 5′ overhang (hya_26_OH) (Table S1) and incubated at room temperature for 30 min. The complex was either used immediately or flash frozen in liquid nitrogen and stored at −80 °C. Initial crystallization conditions were established at the High Throughput Crystallization Laboratory of the European Molecular Biology Laboratory, using the sitting-drop method. Crystals were obtained at 20 °C, from 0.2-μL drops composed of identical volumes of complex solution [350 μM protein and 92 μM oligonucleotide in 40 mM Tris·HCl (pH 8.0), 150 mM KCl, 10% (vol/vol) glycerol,

1 mM DTT] and of precipitant [0.1 M citric acid (pH 4.0 or 6.0), 1 M lithium chloride, 20% (wt/vol) PEG 6000]. Better and larger crystals could be obtained from the condition at pH 4.0 using the hanging-drop vapor diffusion method. The optimized crystals were cryoprotected in the same conditions as the apo-IscR^{Tp} crystals.

Data Collection and Processing. X-ray diffraction data were collected from cooled (100 K) single crystals at synchrotron beam lines ID29 (apo-IscR^{Tp} and Se-Met apo-IscR^{Tp}) (47) and ID23-EH2 (apo-IscR^{Ec}:*hya* complex) (48) of the European Synchrotron Radiation Facility. The apo-IscR^{Tp} data were recorded on a Pilatus 6M detector (Dectris) using a wavelength of 0.9763 Å (native dataset) or 0.9792 Å (Se-Met dataset). For the native data, 1,200 images were collected in 0.1° oscillation steps with 0.1-s exposure per frame whereas, for the Se-met data, 3,600 images were recorded in 0.1° oscillation steps with 0.037-s exposure per frame. The apo-IscR^{Ec}:*hya* complex data were recorded on a MX-225 detector (Marresearch) using a wavelength of 0.8726 Å. One hundred images were collected in 0.95° oscillation steps with 5.43-s exposure per frame. Diffraction data were integrated with XDS (49), scaled with XSCALE (50), and reduced with utilities from the CCP4 program suite (51). Data collection statistics are summarized in Table 2.

Structure Solution and Refinement. The structure of apo-IscR^{Tp} was solved by single-wavelength anomalous diffraction using the anomalous signal of selenium-substituted crystals with the SHELXC/SHELXD/SHELXE pipeline (52) and the HKL2MAP GUI (53). The resulting electron density maps were readily interpretable. The structure of the apo-IscR^{Ec}:*hya* complex was solved by molecular replacement with PHASER (54) using a truncated version of the refined apo-IscR^{Tp} structure as search model. For both structures, alternating cycles of model building with COOT (55) and of refinement with PHENIX (56) were performed until model completion. For the apo-IscR^{Tp} structure, the final model comprises residues Gly-3 to Gly85 and Ser101 to Ile149 for subunit

A and Gly-3 to Gly85 and Ser101 to Tyr148 for subunit B whereas the apo-IscR^{Ec}:*hya* complex comprises residues Met0 to Asp88 and Lys103 to Ser139 for subunit A, and Gly1 to Asp84 and Gln93 to Val135 for subunit B. Model refinement statistics are summarized in Table 2.

1. Beinert H, Holm RH, Münck E (1997) Iron-sulfur clusters: Nature's modular, multipurpose structures. *Science* 277(5326):653–659.
2. Ayala-Castro C, Saini A, Outten FW (2008) Fe-S cluster assembly pathways in bacteria. *Microbiol Mol Biol Rev* 72(1):110–125.
3. Fontecave M, Choudens SO, Py B, Barras F (2005) Mechanisms of iron-sulfur cluster assembly: The SUF machinery. *J Biol Inorg Chem* 10(7):713–721.
4. Takahashi Y, Nakamura M (1999) Functional assignment of the ORF2-iscS-iscU-iscA-hscB-hscA-fdx-ORF3 gene cluster involved in the assembly of Fe-S clusters in *Escherichia coli*. *J Biochem* 126(5):917–926.
5. Takahashi Y, Tokumoto U (2002) A third bacterial system for the assembly of iron-sulfur clusters with homologs in archaea and plastids. *J Biol Chem* 277(32):28380–28383.
6. Outten FW, Djaman O, Storz G (2004) A suf operon requirement for Fe-S cluster assembly during iron starvation in *Escherichia coli*. *Mol Microbiol* 52(3):861–872.
7. Schwartz CJ, et al. (2001) IscR, an Fe-S cluster-containing transcription factor, represses expression of *Escherichia coli* genes encoding Fe-S cluster assembly proteins. *Proc Natl Acad Sci USA* 98(26):14895–14900.
8. Giel JL, Rodionov D, Liu M, Blattner FR, Kiley PJ (2006) IscR-dependent gene expression links iron-sulphur cluster assembly to the control of O2-regulated genes in *Escherichia coli*. *Mol Microbiol* 60(4):1058–1075.
9. Lee KC, Yeo WS, Roe JH (2008) Oxidant-responsive induction of the suf operon, encoding a Fe-S assembly system, through Fur and IscR in *Escherichia coli*. *J Bacteriol* 190(24):8244–8247.
10. Yeo WS, Lee JH, Lee KC, Roe JH (2006) IscR acts as an activator in response to oxidative stress for the suf operon encoding Fe-S assembly proteins. *Mol Microbiol* 61(1):206–218.
11. Giel JL, et al. (2013) Regulation of iron-sulphur cluster homeostasis through transcriptional control of the Isc pathway by [2Fe-2S]-IscR in *Escherichia coli*. *Mol Microbiol* 87(3):478–492.
12. Nesbit AD, Giel JL, Rose JC, Kiley PJ (2009) Sequence-specific binding to a subset of IscR-regulated promoters does not require IscR Fe-S cluster ligation. *J Mol Biol* 387(1):28–41.
13. Rajagopalan S, et al. (2013) Studies of IscR reveal a unique mechanism for metal-dependent regulation of DNA binding specificity. *Nat Struct Mol Biol* 20(6):740–747.
14. Riboldi GP, Verli H, Frazzon J (2009) Structural studies of the *Enterococcus faecalis* SufU [Fe-S] cluster protein. *BMC Biochem* 10:3.
15. Riboldi GP, de Oliveira JS, Frazzon J (2011) *Enterococcus faecalis* SufU scaffold protein enhances SufS desulfurase activity by acquiring sulfur from its cysteine-153. *Biochim Biophys Acta* 1814(12):1910–1918.
16. Albrecht AG, et al. (2010) SufU is an essential iron-sulfur cluster scaffold protein in *Bacillus subtilis*. *J Bacteriol* 192(6):1643–1651.
17. Byrne-Bailey KG, et al. (2010) Complete genome sequence of the electricity-producing "*Thermincola potens*" strain JR. *J Bacteriol* 192(15):4078–4079.
18. Carlson HK, et al. (2012) Surface multiheme c-type cytochromes from *Thermincola potens* and implications for respiratory metal reduction by Gram-positive bacteria. *Proc Natl Acad Sci USA* 109(5):1702–1707.
19. Riboldi GP, de Mattos EP, Frazzon J (2013) Biogenesis of [Fe-S] cluster in *Firmicutes*: An unexplored field of investigation. *Antonie van Leeuwenhoek* 104(3):283–300.
20. Zheng L, Cash VL, Flint DH, Dean DR (1998) Assembly of iron-sulfur clusters. Identification of an iscSUA-hscBA-fdx gene cluster from *Azotobacter vinelandii*. *J Biol Chem* 273(21):13264–13272.
21. Yuvaniyama P, Agar JN, Cash VL, Johnson MK, Dean DR (2000) NifS-directed assembly of a transient [2Fe-2S] cluster within the NifU protein. *Proc Natl Acad Sci USA* 97(2):599–604.
22. Rangachari K, et al. (2002) SufC hydrolyzes ATP and interacts with SufB from *Thermotoga maritima*. *FEBS Lett* 514(2-3):225–228.
23. Saini A, Mapolelo DT, Chahal HK, Johnson MK, Outten FW (2010) SufD and SufC ATPase activity are required for iron acquisition during in vivo Fe-S cluster formation on SufB. *Biochemistry* 49(43):9402–9412.
24. Silberg JJ, Tapley TL, Hoff KG, Vickery LE (2004) Regulation of the HscA ATPase reaction cycle by the co-chaperone HscB and the iron-sulfur cluster assembly protein IscU. *J Biol Chem* 279(52):53924–53931.
25. Trotter V, et al. (2009) The CsdA cysteine desulphurase promotes Fe/S biogenesis by recruiting Suf components and participates to a new sulphur transfer pathway by recruiting CsdL (ex-YgdL), a ubiquitin-modifying-like protein. *Mol Microbiol* 74(6):1527–1542.
26. Selbach BP, et al. (2014) Fe-S cluster biogenesis in Gram-positive bacteria: SufU is a zinc-dependent sulfur transfer protein. *Biochemistry* 53(1):152–160.
27. Chahal HK, Dai Y, Saini A, Ayala-Castro C, Outten FW (2009) The SufBCD Fe-S scaffold complex interacts with SufA for Fe-S cluster transfer. *Biochemistry* 48(44):10644–10653.
28. Tian T, He H, Liu XQ (2014) The SufBCD protein complex is the scaffold for iron-sulfur cluster assembly in *Thermus thermophiles* HB8. *Biochem Biophys Res Commun* 443(2):376–381.
29. Hoff KG, Ta DT, Tapley TL, Silberg JJ, Vickery LE (2002) Hsc66 substrate specificity is directed toward a discrete region of the iron-sulfur cluster template protein IscU. *J Biol Chem* 277(30):27353–27359.
30. André G, et al. (2010) Global regulation of gene expression in response to cysteine availability in *Clostridium perfringens*. *BMC Microbiol* 10:234.
31. Shen G, et al. (2007) SufR coordinates two [4Fe-4S]2+, 1+ clusters and functions as a transcriptional repressor of the sufBCDS operon and an autoregulator of sufR in cyanobacteria. *J Biol Chem* 282(44):31909–31919.
32. Wang T, et al. (2004) The sufR gene in *Synechocystis sp.* strain PCC 6803) functions as a repressor of the sufBCDS operon in iron-sulfur cluster biogenesis in cyanobacteria. *J Bacteriol* 186(4):956–967.
33. Choi YS, et al. (2007) Identification of *Pseudomonas aeruginosa* genes crucial for hydrogen peroxide resistance. *J Microbiol Biotechnol* 17(8):1344–1352.
34. Runyen-Janecky L, et al. (2008) Role and regulation of iron-sulfur cluster biosynthesis genes in *Shigella flexneri* virulence. *Infect Immun* 76(3):1083–1092.
35. Zeng J, Zhang K, Liu J, Qiu G (2008) Expression, purification, and characterization of iron-sulfur cluster assembly regulator IscR from *Acidithiobacillus ferrooxidans*. *J Microbiol Biotechnol* 18(10):1672–1677.
36. Shepard W, et al. (2011) Insights into the Rrf2 repressor family—the structure of CymR, the global cysteine regulator of *Bacillus subtilis*. *FEBS J* 278(15):2689–2701.
37. Ji Q, et al. (2012) *Staphylococcus aureus* CymR is a new thiol-based oxidation-sensing regulator of stress resistance and oxidative response. *J Biol Chem* 287(25):21102–21109.
38. Gregoret LM, Rader SD, Fletterick RJ, Cohen FE (1991) Hydrogen bonds involving sulfur atoms in proteins. *Proteins* 9(2):99–107.
39. Zhou P, Tian F, Lv F, Shang Z (2009) Geometric characteristics of hydrogen bonds involving sulfur atoms in proteins. *Proteins* 76(1):151–163.
40. Fuentes-Prior P, Salvesen GS (2004) The protein structures that shape caspase activity, specificity, activation and inhibition. *Biochem J* 384(Pt 2):201–232.
41. Turk V, et al. (2012) Cysteine cathepsins: From structure, function and regulation to new frontiers. *Biochim Biophys Acta* 1824(1):68–88.
42. Prischi F, et al. (2010) Of the vulnerability of orphan complex proteins: The case study of the *E. coli* IscU and IscS proteins. *Protein Expr Purif* 73(2):161–166.
43. Olichon A, Surrey T (2007) Selection of genetically encoded fluorescent single domain antibodies engineered for efficient expression in *Escherichia coli*. *J Biol Chem* 282(50):36314–36320.
44. Carpenter ML, Kneale GG (1994) Circular dichroism for the analysis of protein-DNA interactions. *Methods Mol Biol* 30:339–345.
45. Jerabek-Willemsen M, Wienken CJ, Braun D, Baaske P, Duhr S (2011) Molecular interaction studies using microscale thermophoresis. *Assay Drug Dev Technol* 9(4):342–353.
46. Pereira PJ, et al. (2008) Mycobacterium tuberculosis glucosyl-3-phosphoglycerate synthase: Structure of a key enzyme in methylglucose lipopolysaccharide biosynthesis. *PLoS ONE* 3(11):e3748.
47. de Sanctis D, et al. (2012) ID29: A high-intensity highly automated ESRF beamline for macromolecular crystallography experiments exploiting anomalous scattering. *J Synchrotron Radiat* 19(Pt 3):455–461.
48. Flot D, et al. (2010) The ID23-2 structural biology microfocus beamline at the ESRF. *J Synchrotron Radiat* 17(1):107–118.
49. Kabsch W (2010) XDS. *Acta Crystallogr D Biol Crystallogr* 66(Pt 2):125–132.
50. Kabsch W (2010) Integration, scaling, space-group assignment and post-refinement. *Acta Crystallogr D Biol Crystallogr* 66(Pt 2):133–144.
51. Collaborative Computational Project, Number 4 (1994) The CCP4 suite: Programs for protein crystallography. *Acta Crystallogr D Biol Crystallogr* 50(Pt 5):760–763.
52. Sheldrick GM (2010) Experimental phasing with SHELXC/D/E: Combining chain tracing with density modification. *Acta Crystallogr D Biol Crystallogr* 66(Pt 4):479–485.
53. Pape T, Schneider TR (2004) HKL2MAP: A graphical user interface for macromolecular phasing with SHELX programs. *J Appl Cryst* 37:843–844.
54. McCoy AJ, et al. (2007) Phaser crystallographic software. *J Appl Cryst* 40(Pt 4):658–674.
55. Emsley P, Cowtan K (2004) Coot: Model-building tools for molecular graphics. *Acta Crystallogr D Biol Crystallogr* 60(Pt 12 Pt 1):2126–2132.
56. Adams PD, et al. (2010) PHENIX: A comprehensive Python-based system for macromolecular structure solution. *Acta Crystallogr D Biol Crystallogr* 66(Pt 2):213–221.
57. Reboiro-Jato D, et al. (2012) ADOPS—Automatic Detection Of Positively Selected Sites. *J Integr Bioinform* 9(3):200.
58. Thompson JD, Gibson TJ, Higgins DG (2002) Multiple sequence alignment using ClustalW and ClustalX. *Curr Protoc Bioinformatics* Chapter 2: Unit 2 3.
59. Bond CS, Schüttelkopf AW (2009) ALINE: A WYSIWYG protein-sequence alignment editor for publication-quality alignments. *Acta Crystallogr D Biol Crystallogr* 65(Pt 5):510–512.
60. Holm L, Rosenström P (2010) Dali server: Conservation mapping in 3D. *Nucleic Acids Res* 38(Web Server issue):W545–W549.

Supporting Information

Santos et al. 10.1073/pnas.1322728111
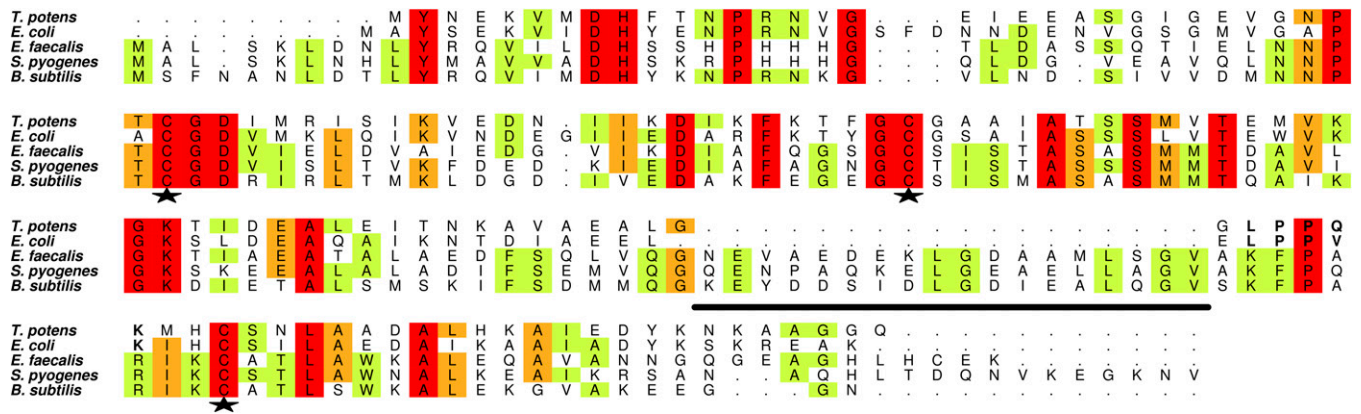
Fig. S1. *Thermincola potens* Fe/S cluster scaffold protein displays the conserved features of IscU-type scaffolds from Gram-negative bacteria. Amino acid sequence alignment of the *T. potens* TherJR_1912 gene product and homologous proteins from both Gram-positive (*Enterococcus faecalis*, *Streptococcus pyogenes*, *Bacillus subtilis*) and Gram-negative bacteria (*Escherichia coli*). Strictly conserved amino acids are highlighted in red and increasing residue conservation is represented by a color gradient from green to red. Cysteine residues known to coordinate the Fe/S cluster are denoted by a star (1), the "LPPVK" HscA-binding motif is represented in bold (2), and the characteristic Gram-positive insertion is underlined (3). Numbers above the alignment refer to the *T. potens* amino acid sequence numbering. Alignment prepared with ClustalW (4) and colored with Aline (5).

1. Mansy SS, Wu G, Surerus KK, Cowan JA (2002) Iron-sulfur cluster biosynthesis. *Thermatoga maritima* IscU is a structured iron-sulfur cluster assembly protein. *J Biol Chem* 277(24):21397–21404.
2. Hoff KG, Silberg JJ, Vickery LE (2000) Interaction of the iron-sulfur cluster assembly protein IscU with the Hsc66/Hsc20 molecular chaperone system of *Escherichia coli*. *Proc Natl Acad Sci USA* 97(14):7790–7795.
3. Riboldi GP, Verli H, Frazzon J (2009) Structural studies of the *Enterococcus faecalis* SufU [Fe-S] cluster protein. *BMC Biochem* 10:3.
4. Larkin MA, et al. (2007) Clustal W and Clustal X version 2.0. *Bioinformatics* 23(21):2947–2948.
5. Bond CS, Schüttelkopf AW (2009) ALINE: A WYSIWYG protein-sequence alignment editor for publication-quality alignments. *Acta Crystallogr D Biol Crystallogr* 65(Pt 5):510–512.
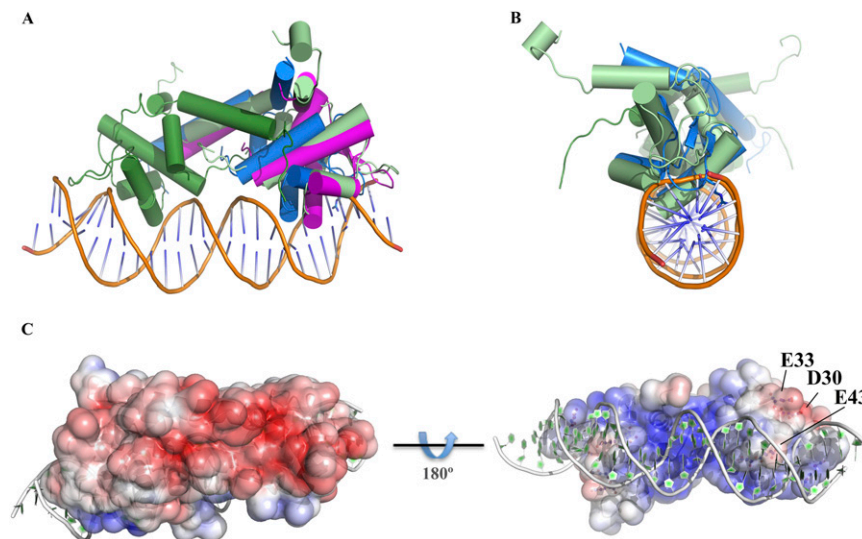
Fig. S2. The overall structure of the biologically active iron-sulfur cluster (ISC) pathway regulator (IscR) dimer is mostly unchanged upon DNA binding. (*A*) Superposition of the 3D structures of free apo-IscR^{Tp} (green), free *E. coli* apo-IscR (magenta; PDB ID code 4HF0), and *hya* promoter-bound apo-IscR^{Ec} (blue). (*B*) Superposition of the 3D structures of free apo-IscR^{Tp} and *hya* promoter-bound apo-IscR^{Ec} (colors as in *A*). The molecules were rotated ~90° around *y*, relative to the view in *A*. (*C*) An asymmetric electrostatic surface orients the functional apo-IscR^{Ec} dimer toward its *hya* DNA target. Positive surface electrostatic potential is shown in blue and negative in red. The DNA molecule backbone is depicted as a white ribbon with bases in green.
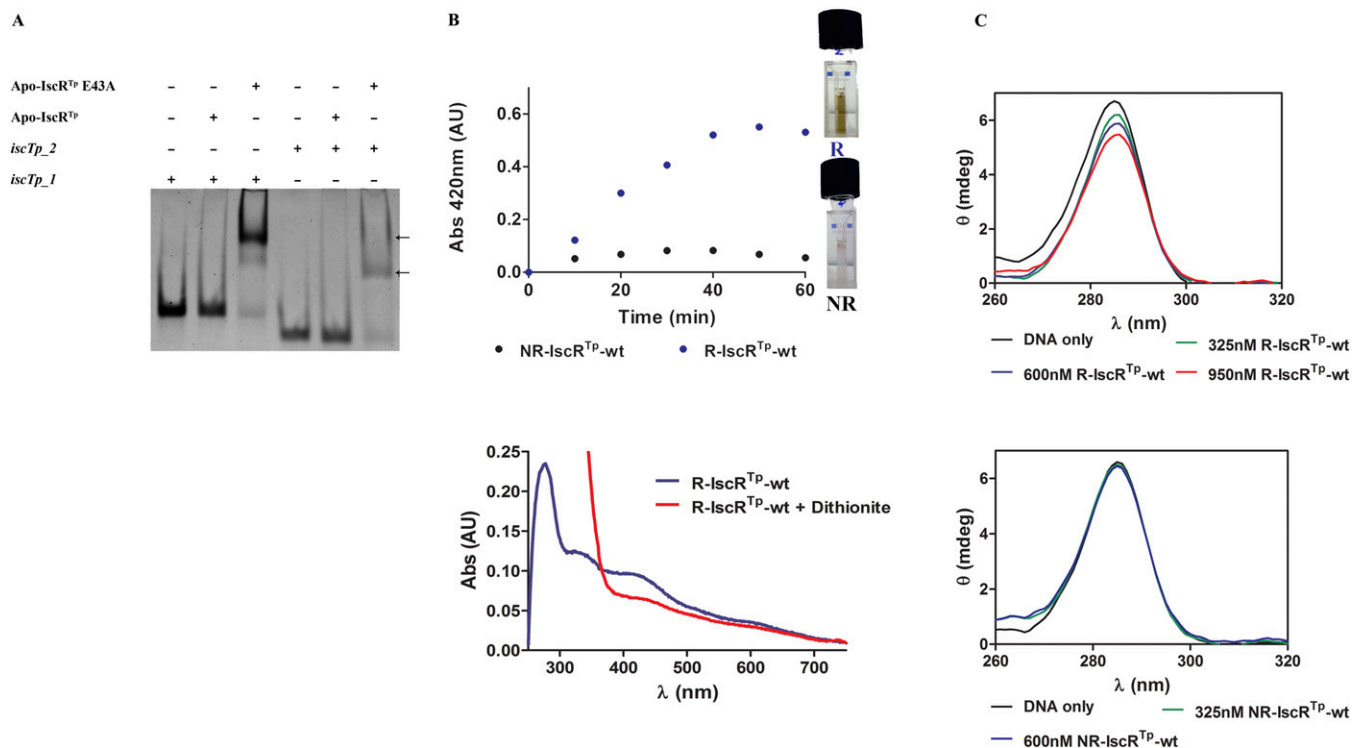
Fig. S3. The *T. potens isc* promoter region contains two binding sites for IscR[Tp]. (*A*) DNA recognition was assessed by electrophoretic mobility-shift assay of the complexes formed between apo-IscR[Tp] or apo-IscR[Tp] E43A and either the full (*iscTp_1*) or trimmed (*iscTp_2*) *isc* promoter sequence. DNA band-shifts are denoted by arrows. (*B, Upper*) Time course of Fe/S cluster assembly on apo-IscR[Tp]-wt. There is a time-dependent increase of the characteristic Fe/S cluster absorption peak at 420 nm for reconstituted apo-IscR[Tp]-wt (R-IscR[Tp]-wt; blue circles) whereas no noticeable variation could be observed for the assay performed in the absence of cysteine (NR-IscR[Tp]-wt, black circles). At the end of the assay, the reaction containing R-IscR[Tp]-wt displayed a characteristic brown color (upper cuvette; R), which was essentially absent in the control reaction (lower cuvette; NR). (*Lower*) UV/Visible absorption spectra of R-IscR[Tp]-wt. The spectrum of purified R-IscR[Tp]-wt (blue curve) displays local maxima at 420 nm and 320 nm that are characteristic of Fe/S clusters, which disappeared upon reduction with 2 mM dithionite (red curve). (*C*) Fe/S cluster binding modulates recognition of type-1 promoter DNA sequences by IscR. Circular dichroism spectra of *iscTp_1* DNA sequence (Table S1) with increasing concentrations of R-IscR[Tp]-wt (*Upper*) or NR-IscR[Tp]-wt (*Lower*). The spectra were recorded upon successive additions of each purified protein to an *iscTp_1* solution (2 μM). A significant change in ellipticity at the characteristic B-DNA peak at 285 nm (1, 2) can be observed only upon R-IscR[Tp]-wt addition, indicating that only the Fe/S cluster-containing form of IscR[Tp]-wt is able to recognize the *T. potens isc* promoter sequence and induce local DNA structural changes. Experiments were carried out at 20 °C in 40 mM Tris (pH 8), 150 mM KCl, 5% (vol/vol) glycerol, 1 mM DTT.

1. Carpenter ML, Kneale GG (1994) Circular dichroism for the analysis of protein-DNA interactions. *Methods Mol Biol* 30:339–345.
2. Carpenter ML, Kneale GG (1991) Circular dichroism and fluorescence analysis of the interaction of Pf1 gene 5 protein with poly(dT). *J Mol Biol* 217(4):681–689.

Table S1. Oligonucleotides used in binding and crystallization assays

Name	Sequence
hyaEc	5′–AAATCCACAC AGTTTGTATT GTTTTG–3′
iscbEc	5′–TAAATAGTTG ACCAATTTAC TCGGGAATGT CAGACT–3′
iscTp_1	5′–TAAAAAATCT TAGTATTTTA GTTGGAATTT TTCTTGACCA GAAAATAACT GTATGC–3′
iscTp_2	5′–TAAAAAATCT TAGTATTTTA GTTGGAATTT TTCTTGACC–3′
iscTp_3	5′–TAAAAAATCT TAGTATTTTA GTTGGAATT–3′
iscTp_4	5′–TTTTTCTTGA CCAGAAAATA ACTGTATGC–3′
iscTp_5	5′–TAAAAAATCT TAGTATTTTA GTTGGAA–3′
hya_26_OH	5′–GAAATCCACA CAGTTTGTAT TGTTTTG–3′
suf	5′–CGCTTTATAT TTAGGAAAGA TGCAGCGCCG GCTATAAAAT AGCCGGCTTT TTCTAAGCTC
	TTAATCAATA GCCGGATCCA ATTATTGTAG AATCCTGCCC AAAATTATTT GTACTTTTTT
	ATCCCGGCAG GAGGATAAAT GTGGGTGGAC AAAGAAAAAT ACCCCTGTAG TTTTTGGATT
	TAAACCAGGA ATCCGTCAGG AGGGAATATT GCGCTTTATA TTTAGGAAAG ATGCAGCGCC
	GGCTATAAAA TAGCCGGCTT TTTCTAAGCT CTTAATCAAT AGCCGGATCC AATTATTGTA
	GAATCCTGCC CAAAATTATT TGTACTTTTT TATCCCGGCA GGAGGATAAA TGTGGGTGGA
	CAAAGAAAAA TACCCCTGTA GTTTTTGGAT TTAAACCAGG AATCCGTCAG GAGGGAATAT TG–3′

Table S2. Binding affinities between IscR and type-1 and type-2 promoter sequences determined by microscale thermophoresis

DNA sequence	IscR variant	Dissociation constant K_d, nM
hyaEc	Apo-IscR^{Ec} E43A	180 ± 18
	Apo-IscR^{Tp} E43A	340 ± 52
	Apo-IscR^{Tp}	n.d.
	Apo-IscR^{Tp} P40S	11,900 ± 3,340
iscbEc	Apo-IscR^{Ec} E43A	154 ± 7
	Apo-IscR^{Tp} E43A	97 ± 6
	Apo-IscR^{Tp}	n.d.
iscTp_3	Apo-IscR^{Tp} E43A	320 ± 19
	Apo-IscR^{Tp}	n.d.
iscTp_4	Apo-IscR^{Tp} E43A	905 ± 87*
	Apo-IscR^{Tp}	n.d.
iscTp_5	Apo-IscR^{Tp} E43A	n.d.

n.d., binding not detected.

*The K_d value might be overestimated because saturation was not reached.